Lightweight Fiber Optic Gas Sensor for Monitoring Regenerative Food Production

Contract No. NAS2-13887
Period of Performance: 8/29/93 to 12/19/95

Final Report

Presented to:

NASA-Ames Research Center
Moffett Field, CA 94035

Technical Monitor:

Ann McCormack

Contractor:

Physical Optics Corporation
Research and Development Division
20600 Gramercy Place, Suite 103
Torrance, California 90501
(310) 320-3088

Principal Investigator:

Edward Schmidlin

December 18, 1995

TABLE OF CONTENTS

1.0 EXECUTIVE SUMMARY

This final report reviews the work performed between August 29, 1993 and December 18, 1995 for the SBIR Phase II contract entitled "Lightweight Fiber Optic Gas Sensors for Monitoring Regenerative Food Production." In the course of this work, sensors for oxygen, carbon dioxide, and relative humidity were demonstrated to have the detection range, dynamic range, and sensitivity required for monitoring bioregenerative life support systems.

Oxygen Sensor

POC has successfully constructed a prototype phase fluorometry-based oxygen sensor. This lightweight device can detect oxygen over the full range (0% to 100% oxygen) with a fine-tuning capability between 10% and 35% -- the range NASA is interested in. Phase-based measurement offers distinct advantages, such as immunity to source fluctuation, photobleaching, and leaching. The fluorometer is housed in a portable box, 30 cm × 25 cm × 13 cm. All optics, optoelectronics, power supply, and the printed circuit board are included in the same box; the only external connections to the fluorometer are the optical fiber sensor and a power cord. This instrument uses a pulsed light-emitting diode as the light source, and a miniature photomultiplier tube as the detector. The oxygen optrodes have undergone numerous tests, and have been specially treated for humidity resistance. This computer-controlled fluorometer has also been tested at Jet Propulsion Laboratory.

Carbon Dioxide Sensor

Physical Optics Corporation has developed an indicator-based carbon dioxide sensor. This sensor is suitable for short-term (5-day) or discrete measurements. Thorough study has led to an understanding of the challenges in developing a functional sensor for long-term monitoring needs. At the current stage of development, the CO_2 sensor has a 0% to 100% detection range. The 300 ppm to 5000 ppm dynamic range meets NASA needs. The response time is on the order of 2 minutes -- typical of indicator-based sensors in which a gas such as CO_2 penetrates a barrier and undergoes multi-step equilibrium processes.

Humidity Sensor

POC has developed a porous optical fiber-based humidity sensor. Two porous fiber designs were produced: fibers with variable-thickness porous cores, and fibers with a 10-micron thick porous cladding. The porous core fiber was chosen as the final design because it produced a direct interaction of the light beam with the porous section of the fiber. The humidity sensor has been tested over 60% to 80% relative humidity. With response time on the order of a minute, this sensor shows a long operational life. To achieve better sensitivity, POC employed chemical indicators that produce a color change on interaction with water vapor. While Reichhardt's dye appeared to be the best candidate, photobleaching argues against using this material.

2.0 OXYGEN SENSOR

The oxygen sensor developed under this program is based on the "phase fluorometry" detection method. Phase fluorometric oxygen measurement is based on the fluorescence-quenching property of oxygen, but has several advantages over intensity-based measurements of this property. The most significant improvement is that oxygen measurements using phase fluorometry are insensitive to photodegradation and therefore no photodegradation modeling or correction is needed with this method. In addition, measurements are insensitive to changes in source power and to fiber bending. Finally, the detection sensitivity of a phase fluorometry measurement is better than that of intensity-based measurements.

Phase fluorometry is a relatively new method of oxygen sensing. Its advantages are stated above, but its disadvantage is that it requires larger and more complex electronics. The major task addressed in this project was to design, fabricate, and test a compact, "no-frills" phase fluorometer. We have successfully demonstrated such a device.

Figure 2-1 shows the POC phase fluorometer. The entire optoelectronic assembly, including a miniature photomultiplier tube, is housed in a 30 cm × 25 cm × 13 cm box. Figure 2-2 shows the instrument in a field operational configuration.

Figure 2-3 shows the optrode assembly. The indicator chemistry, ruthenium-tris-1,10-phenanthroline, is entrapped in a 5 mm-long porous Vycor glass rod, illuminated through a fiber. This optrode can be placed inside a variety of housings, two of which are shown in Figure 2-3.

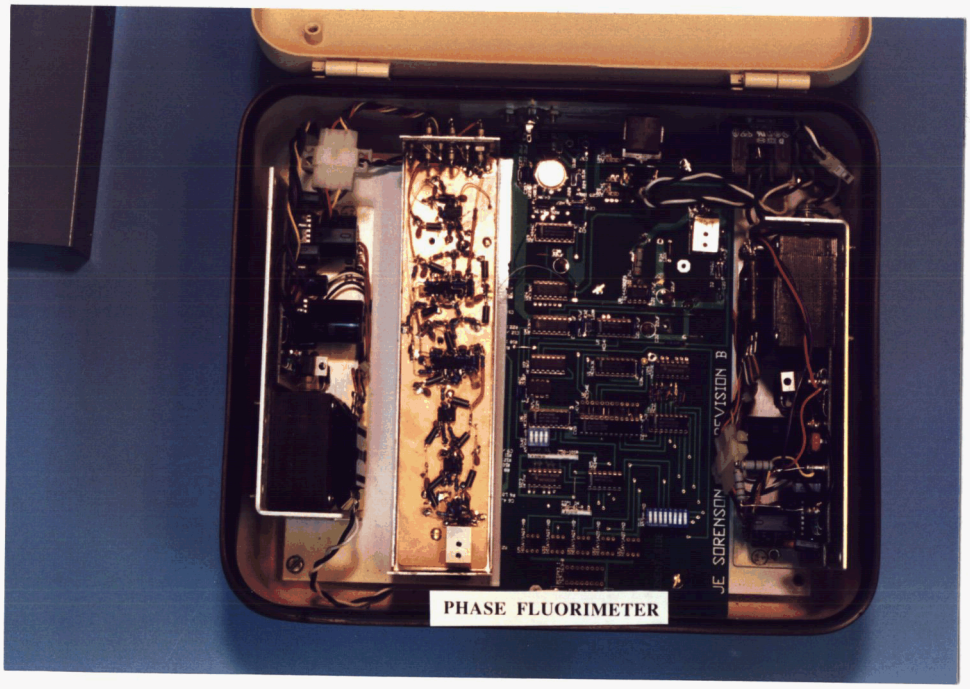

Figure 2-1
POC phase fluorometer.

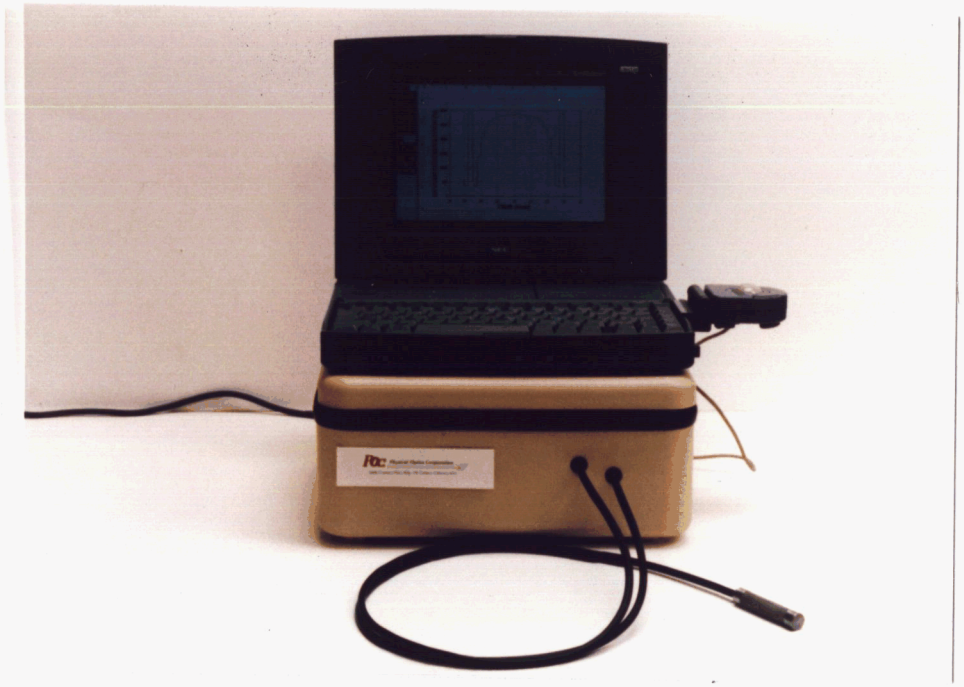

Figure 2-2
POC phase fluorometer, field-ready. The O_2 optrode/cable assembly is also shown.

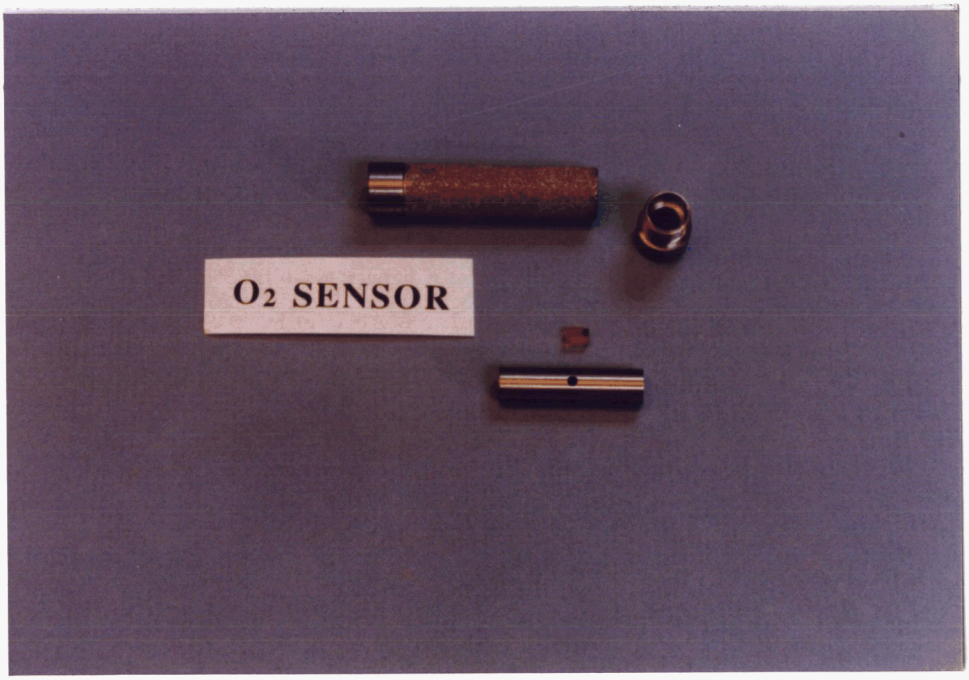

Figure 2-3
O_2 optrode assembly. Two types of housings are shown. The optrode is placed inside in such a way that it receives maximum exposure to the analyte.

The oxygen sensor system consists of three integrated components: (1) optrode, (2) light delivery fibers, and (3) phase fluorometer detector. In this system, light from a modulated blue LED (λ_{max} = 475 nm) excites the ruthenium compound. The modulated fluorescence signal (λ_{max} = 610 nm) is detected by a photomultiplier and transformed into a frequency measurement by the phase fluorometer electronics. The presence of oxygen quenches the fluorescence intensity and decreases the fluorescence lifetime. The decrease in lifetime is measured as a phase shift that is directly related to the oxygen concentration.

The oxygen-sensitive optrode consists of a 5 mm length of porous Vycor rod, impregnated with oxygen indicator by soaking in a 1.0×10^{-5} M solution of Ru-(4,7-Phenantralene)$_3$Cl$_3$ in ethanol. The optrode is fabricated in four steps: (1) prepare the ruthenium solution, (2) cut, polish, and clean the porous Vycor glass, (3) impregnate the ruthenium compound into the porous glass using an ultrasonic bath, and (4) dry and store the optrode. Typical impregnation time is 60 minutes. Once the optrode is impregnated, it is dried at 60°C for 2 hours, followed by storage in a dry atmosphere until it is ready to be tested. A mount was designed to allow the optrode to be installed and coupled to the optical fiber bundle rapidly and without the use of epoxy as shown in Figure 2-4. The optrode mount is the one shown at the bottom of Figure 2-3, a machined aluminum rod with orifices to allow the oxygen to diffuse into the optrode.

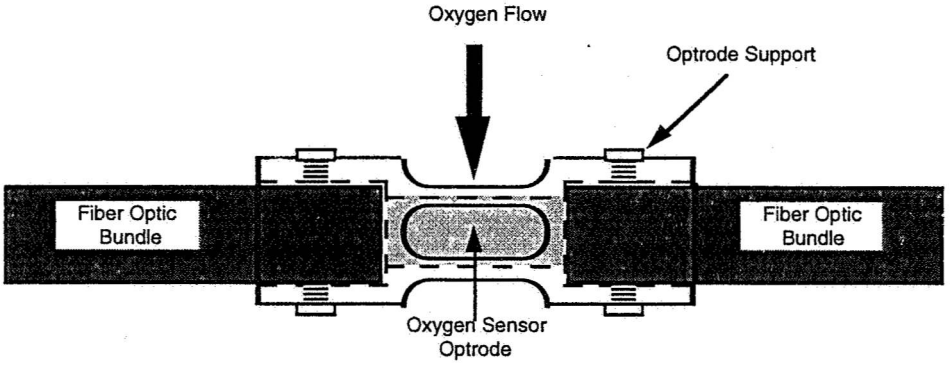

Figure 2-4
Oxygen optrode mount and optrode-to-fiber coupler.

Figure 2-5 shows the typical response of the oxygen sensor system when the ambient atmosphere inside the gas test cell was switched between 2% and 21% oxygen. The response time of the sensor for this run was 6 seconds, with a recovery time of 10 seconds. A phase angle change of 0.34° was observed every time the sensor was cycled between 2% and 21% oxygen. Furthermore, the 6-minute test showed no indication of any drift.

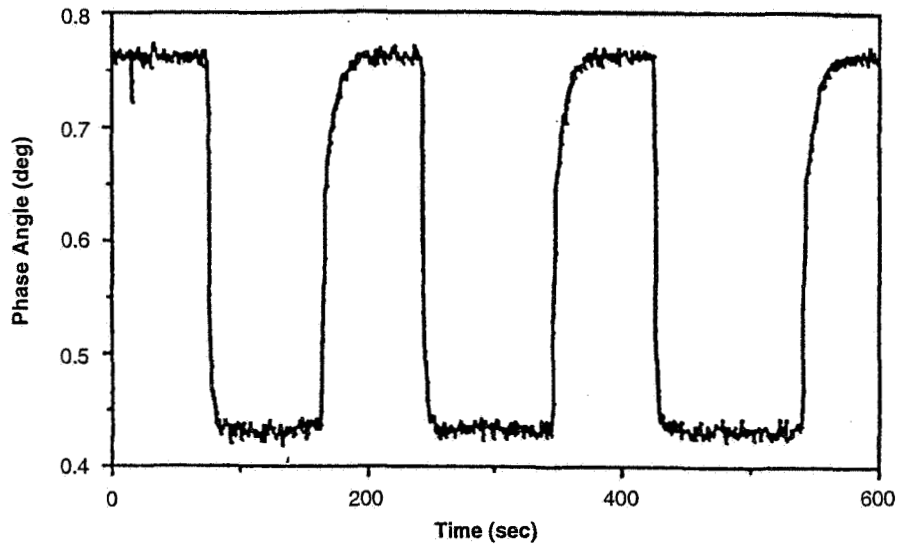

Figure 2-5
Response of oxygen sensor system to changes between 2% and 21% oxygen.

Several experimental studies were performed to fine tune the formulation. Parameters studied included: (a) concentration of the indicator, (b) etching of the porous glass, and (c) length of the porous optrode. In order to optimize each of these optrode parameters, several experimental sensors were cycled from 15% to 25% oxygen in steps of 2% for the various optrode configurations. A typical sensor response is shown as a "step plot" in Figure 2-6. The data illustrate that the sensitivity of this optrode was approximately 0.1% over the range of 15% to 25% oxygen. The sensitivity of this calculation is limited by the resolution of the A/D card. The duration of each test was 10 minutes, and the oxygen concentration was changed once per minute.

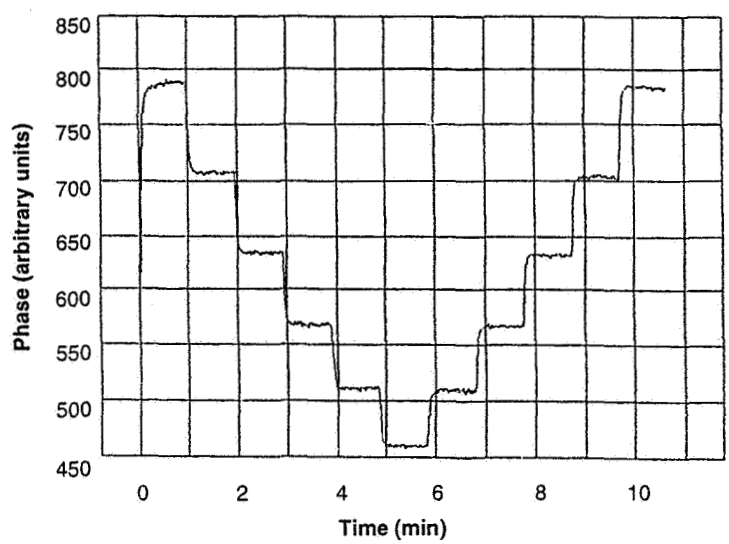

Figure 2-6
Step plot produced by cycling the oxygen concentration between 15% and 25% in 2% steps.

The first test was a study of the effect of the concentration of the solution used to immobilize the indicator in the Vycor glass. Figure 2-7 shows the results when two concentrations (10^{-5} M and 10^{-6} M) were tested. From this graph it can be seen that the 10^{-6} M sample has a greater response to oxygen. The 10^{-6} M sample had a change in phase angle equivalent to 300 mV for a 10% change in the oxygen concentration, while the 10^{-5} M sample had a change equivalent to 280 mV. These plots show some hysteresis when cycling the 10^{-5} M sample back and forth between concentrations, but reading reproducibility is good over most of the oxygen concentration range.

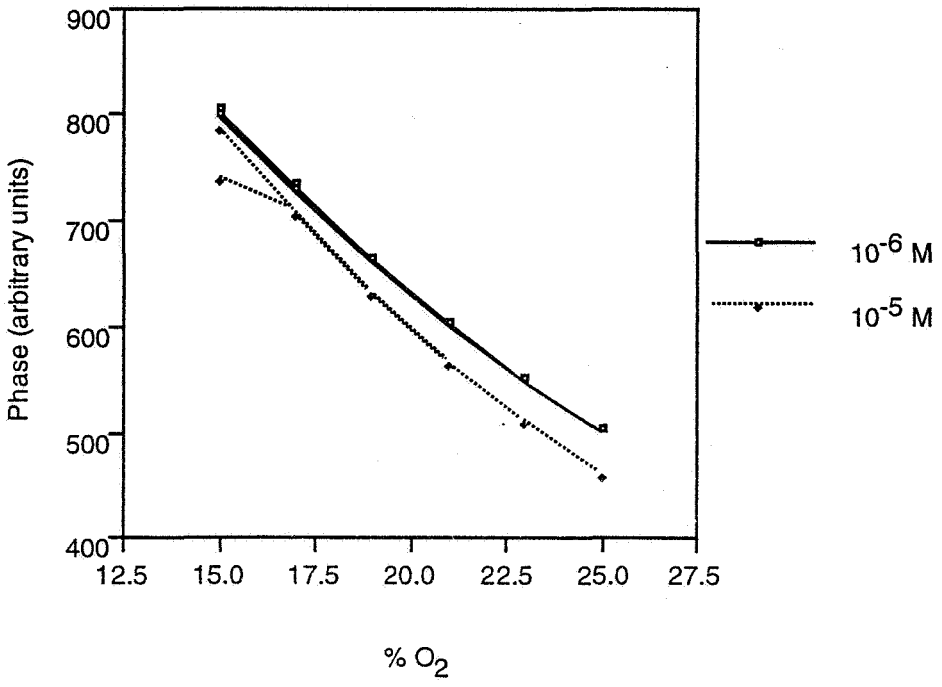

Figure 2-7
Concentration effect of the immobilized ruthenium indicator
on a Vycor glass rod (optrode length 5 mm).

The second test was performed to observe the response of the optrode to oxygen when the porous Vycor glass had been chemically etched to increase the surface area and pore size of the glass. A larger pore size results in better response time and sensitivity to oxygen. The concentration of the indicator solution selected to be used to fabricate optrodes for this study was 10^{-6} M, since this concentration produced the highest sensitivity to oxygen. Figure 2-8 shows that the optrode fabricated with the etched Vycor glass had a much better response to oxygen both in terms of sensitivity and reproducibility. The regular Vycor glass produced a phase change of 122 mV for changes in the oxygen concentration between 15% and 25%, while the etched Vycor produced a change of 300 mV for the same conditions.

The last set of experiments was performed to determine the effect of optrode length on the response to changes in the oxygen concentration. Two lengths were tested: a 5 mm optrode and a 15 mm

optrode. The concentration of the indicator in solution used to make the optrodes was 10^{-6} M, and un-etched Vycor glass was used. Results from this test, shown in Figure 2-9, illustrate that the 5 mm optrode has a larger phase shift response to changes in oxygen between 15% and 25%. The 5 mm optrode showed a change of 122 mV, while the 15-mm optrode showed a change of only 40 mV. This occurs because the fluorescence is absorbed by the indicator before it reaches the detector.

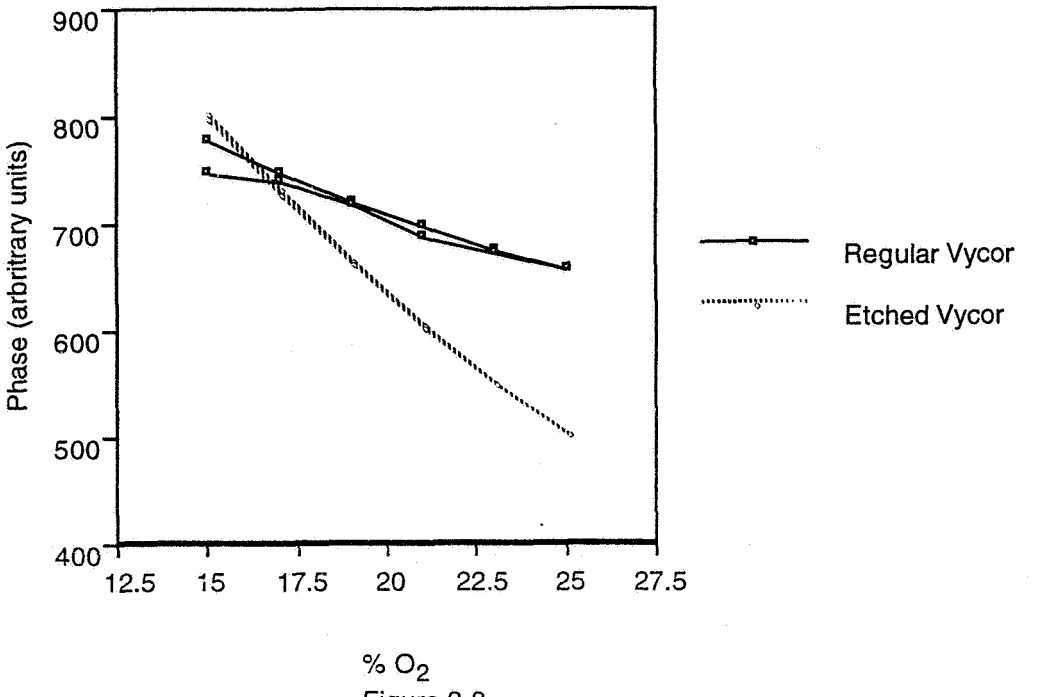

Figure 2-8
Oxygen response using regular vs. etched porous Vycor glass. Two sets of data for each type of sensor (optrode length 5 mm, indicator concentration 10^{-6} M).

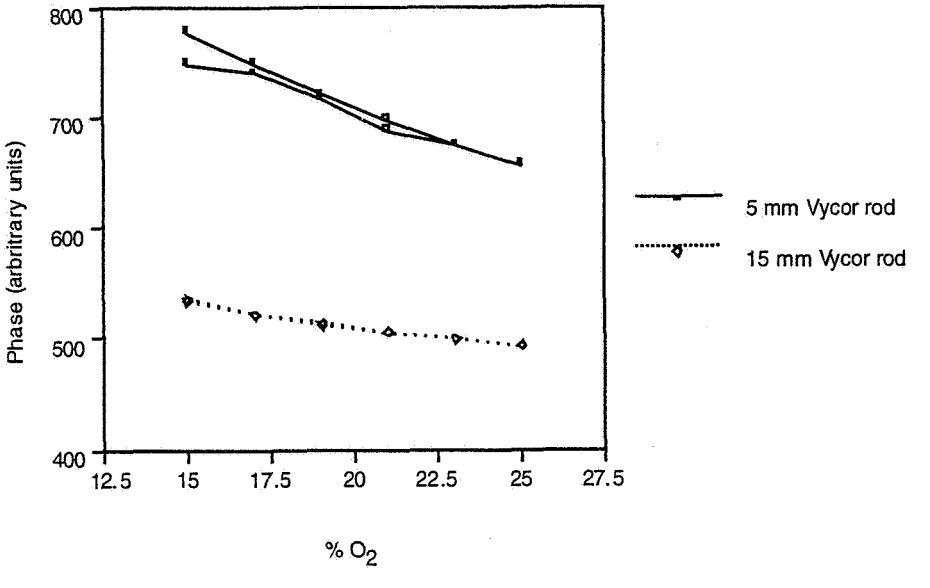

Figure 2-9
Effect of optrode length (10^{-6} M, regular Vycor glass) on oxygen response.

Thus, the experimental results have demonstrated that a ruthenium-based oxygen optrode using a 5 mm chemically treated etched Vycor glass produced the best results. This sensor demonstrated a response time of 6 seconds with a recovery time of 10 seconds for changes in oxygen concentration between 2% and 21%. Furthermore, the results demonstrated no hysteresis and almost no drift when the sensor was cycled between 15% and 25% oxygen.

The repeatability of oxygen measurements using a phase fluorometer is shown in Figure 2-10. Measurements were performed over six cycles between 0% and 48% oxygen in 3% increments. Figure 2-11 shows the first cycle in expanded scale.

Figure 2-12 shows the results of using a mathematical model to "fit" to the data. Although literally thousands of distinct fits can be obtained, our goal was to perform a fit based upon the equations that govern the O_2 optrode's behavior. These equations are:

$$\tan\varphi = \omega\tau \ , \tag{2-1}$$

$$\tau_0 / \tau = 1 + K_{sv} \cdot P_{O_2}, \tag{2-2}$$

where φ is the phase shift, ω is the source modulation frequency, τ is the fluorescence lifetime, τ_0 is the lifetime in the presence of 0% O_2, K_{sv} is the Stern-Volmer constant, and P_{O2} is the partial pressure of O_2. For our application we are interested in relating the variables φ and P_{O2}. This is easily accomplished by some simple manipulations, which lead to the following equation:

$$\varphi = \tan^{-1}\left(\omega\tau_0 /(1 + K_{sv} \cdot \ P_{O_2})\right). \tag{2-3}$$

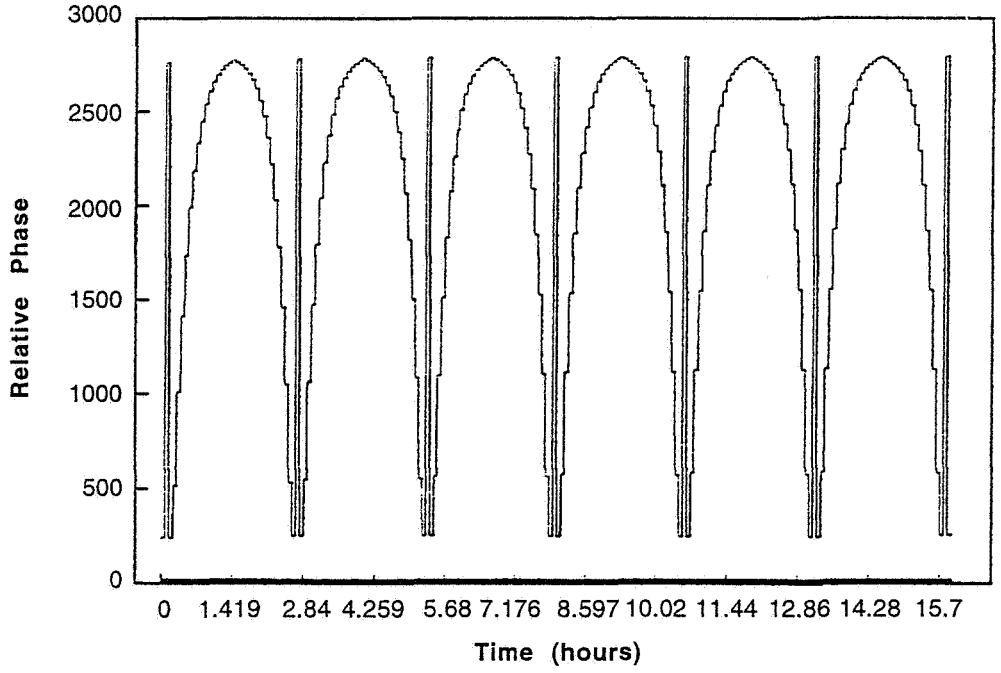

Figure 2-10
Repeated performance of an O_2 optrode cycled between 0% and 48% O_2 in 3% increments. The incremental response curves are bracketed by the response curve over 0%-48%-0% O_2.

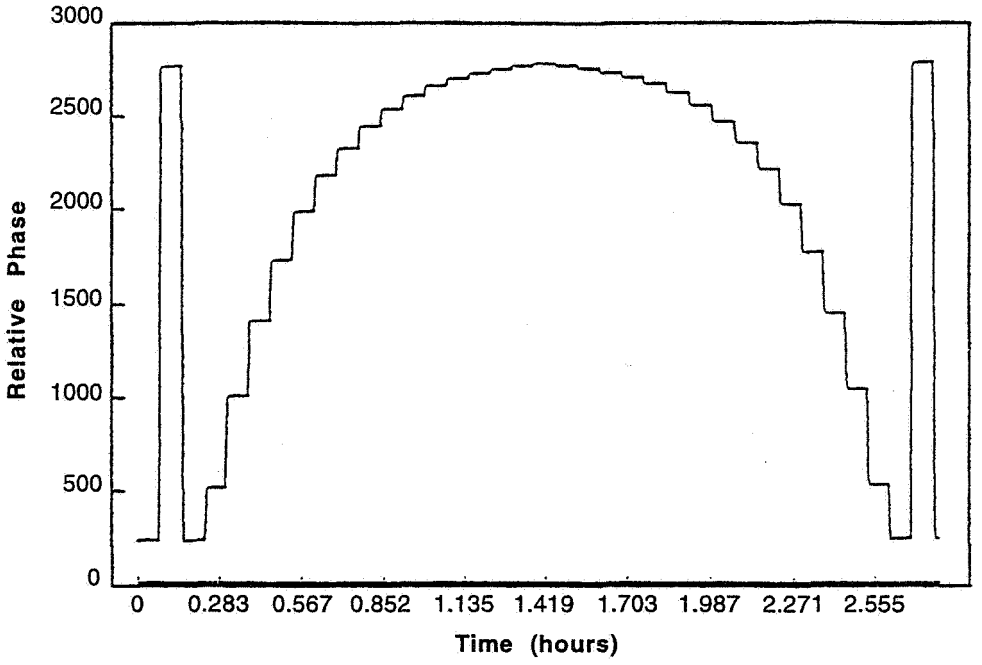

Figure 2-11
Expanded view of the first cycle in Figure 2-6, showing a symmetrical response pattern of the O_2 optrode cycled between 0% and 48% O_2 in 3% increments. The incremental response curve is again bracketed by the response curve over 0%-48%-0% O_2.

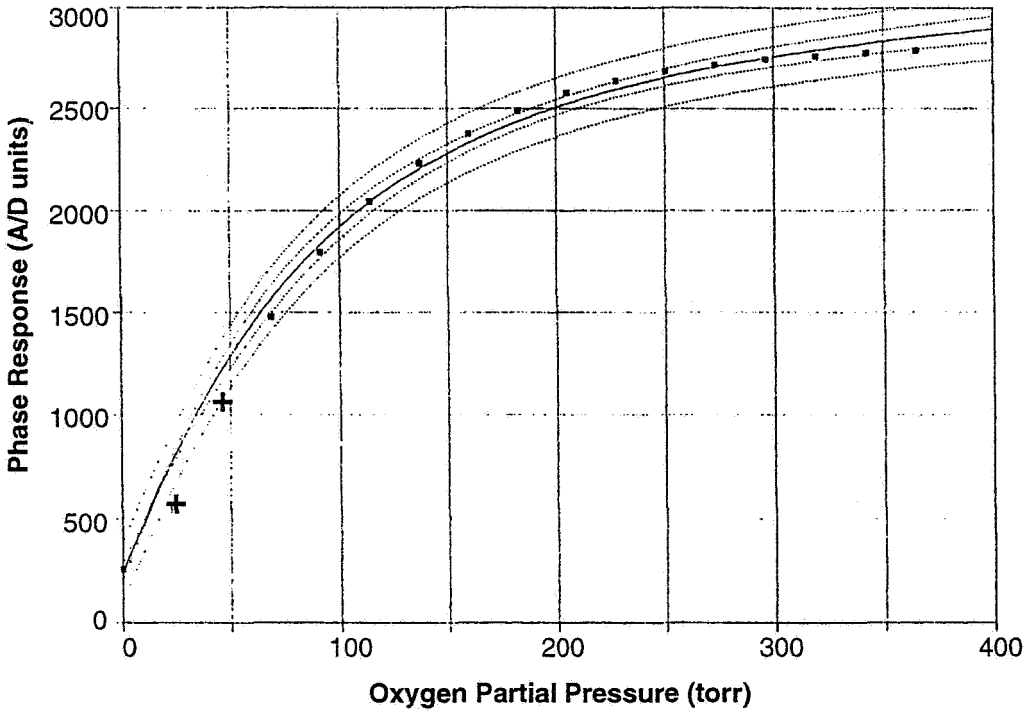

Figure 2-12
Mathematical fit of the O_2 response data (1 torr = 0.13% oxygen).

Using TableCurve 2D, a curve-fitting software package from Jandel Scientific, we programmed a "user-defined function" (UDF) based upon Eq. (2-3) to fit the data obtained empirically. Initially, the UDF included three optimizable parameters, τ_0, K_{sv}, and A (an amplitude parameter), while holding ω constant at 2.5 π MHz. Although the initial results appeared promising, the actual fitting process yielded predicted values for τ_0 and K_{sv} that were several orders of magnitude too large. We determined that these errors were caused by the fact that the model was over-specified (i.e., one or more of the optimizable parameters was unnecessary). Specifically, when the product $K_{sv} \cdot P_{O2}$ grows large, the utility of the term $(1+K_{sv} \cdot P_{O2})$ is lost because the 1 becomes insignificant. To correct this problem, the parameter τ_0 was fixed at a value of 10^{-6} second -- as determined by Eq. (2-1) -- while A and K_{sv} were still allowed to vary. This correction yielded both a good curve-fit and meaningful values for the variable parameters A and K_{sv}. In particular, the value of the coefficient of determination r^2 is very close to one (~0.9959). This parameter, which ranges from zero to one, is an indicator of the reliability of the regression. As the value of r^2 increases, so does the reliability of the statistical fit. Moreover, the parameter K_{sv} equals approximately 0.0908, which is in a range consistent with the value of 0.133 from Eq. (2-2).

In Figure 2-12, the solid black line represents the actual curve-fit. The two dotted lines closer to the solid fit line show the 99% confidence limit, while the outer dotted lines are 99% prediction limits. The best fit encompasses fifteen experimental data points, shown in solid rectangles. Two data points (plus signs) fall outside the 99% confidence limit. This trend has been consistent in multiple data sets, and may indicate the presence of a second fluorophore in the optrode. To achieve a total fit, we investigated the response behavior in the partial pressure range between 0 torr and 30 torr.

2.1 Moisture Sensitivity of Oxygen Optrode

The principle of operation of our oxygen sensor involves de-excitation of the upper excited state of tris-ruthenium (III) phenanthroline through the formation of singlet oxygen:

$$Ru(phen)_3^{2+} + h\upsilon \rightarrow Ru(phen)_3^{2+*} \qquad (2\text{-}4)$$

$$Ru(phen)_3^{2+*} + {}^3O_2 \rightarrow Ru(phen)_3^{2+} + {}^1O_2 \,. \qquad (2\text{-}5)$$

However, other molecules such as water may compete with oxygen in quenching the excited state. This competition can only lead to a higher oxygen reading than is actually present.

As Figure 2-13 shows, the response of an oxygen optrode is strongly affected by changes in relative humidity (RH) between 50% and 100%. Below 50% RH, the humidity effect is less pronounced.

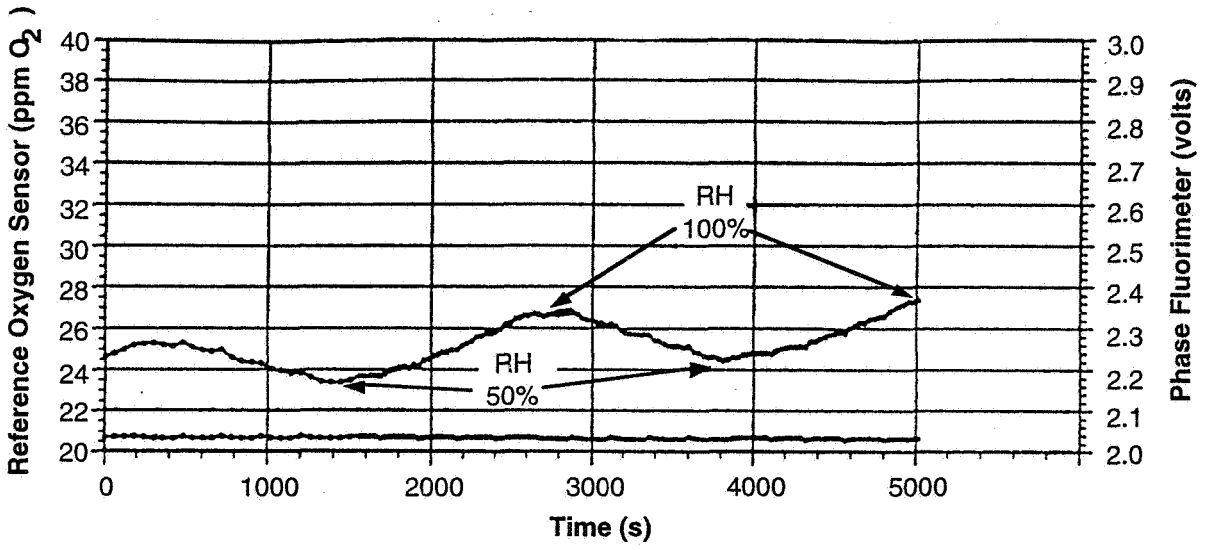

Figure 2-13
Response of POC's untreated fiber optic oxygen sensor (top trace) and a reference oxygen sensor (bottom trace) under constant 20% oxygen. While maintaining steady 20% oxygen, the RH was varied between 50% and 100% over 2400 sec (40 min) cycles.

2.2 Desensitizing the Oxygen Optrodes to Humidity

One solution to the moisture sensitivity problem is to apply a thin water-repellent overcoating on the indicator chemistry. In order to test this solution, two multifunctional silanes were purchased from Pierce: Aquasil and Surfasil. These siliconizing fluids are specifically designed to chemically bond microscopically thin, water repellent films to glass. The coated surface is neutral, hydrophobic, non-oily, has increased water resistance, and is neither affected by organic solvents nor readily hydrolyzed.

2.3 Application of Aquasil™ Siliconizing Fluid

The active ingredient in Pierce's Aquasil formulation is octadecyltrialkoxy silane. A 1% aqueous solution of this ingredient was prepared starting from a commercially available 20% solution in a mixture of alcohols. When mixed with water, octadecyltrialkoxy silane hydrolyzes to a silanol (≡Si-OH). When the oxygen optrode is dipped into this 1% solution for five minutes, the silanol groups condense with available hydroxyl groups on the surface of the porous glass that forms the substrate of POC's oxygen optrode, and with other silanol monomers. This forms a film on the surface of the glass, making the optrode water-repellent. The optrode is then baked for two hours at 60°C.

2.4 Application of Surfasil™ Siliconizing Fluid

Surfasil is a clear polymeric (short chain) silicone fluid consisting of dichlorooctamethyltetrasiloxane. For coating, a 1% Surfasil solution was prepared in toluene. The

oxygen optrode was dipped into this solution for five minutes and then baked at 60°C for two hours.

When applied to glass, the unhydrolyzed chlorines in dichlorooctamethyltetrasiloxane react with surface silanols, and form a neutral hydrophobic and tightly bonded film over the entire surface.

2.5 Performance of Waterproof Optrodes

Figure 2-14 shows the performance of an Aquasil-coated oxygen optrode over 50% to 100% RH. Note the improvement in moisture resistance over an uncoated optrode. Surfasil-coated optrodes show similar improvements. Note that the pronounced sinusoidal pattern seen in Figure 2-13 has been sharply reduced.

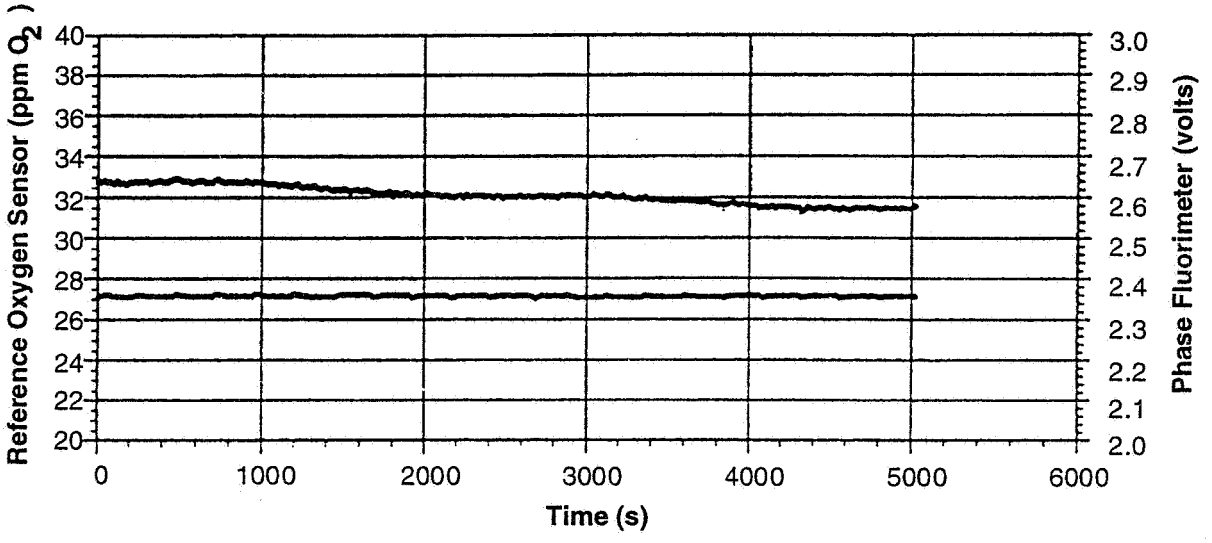

Figure 2-14
When the oxygen optrode is overcoated with a water repellent film, its sensitivity to moisture diminishes drastically (compare top trace with the corresponding trace in Figure 2-13). The bottom trace represents the performance of the reference sensor. Experiments were carried out at room temperature (20°C), in 80% nitrogen, and 20% oxygen. The relative humidity was cycled between 50% and 100% in 40 min (2400 sec) cycles.

Figure 2-15 shows that the oxygen optrode remains sensitive to oxygen after treatment with Aquasil. The oxygen concentration was varied stepwise between 0% and 50% in 5% increments. Figure 2-16 shows similar behavior when Surfasil was used as the water-repellent material.

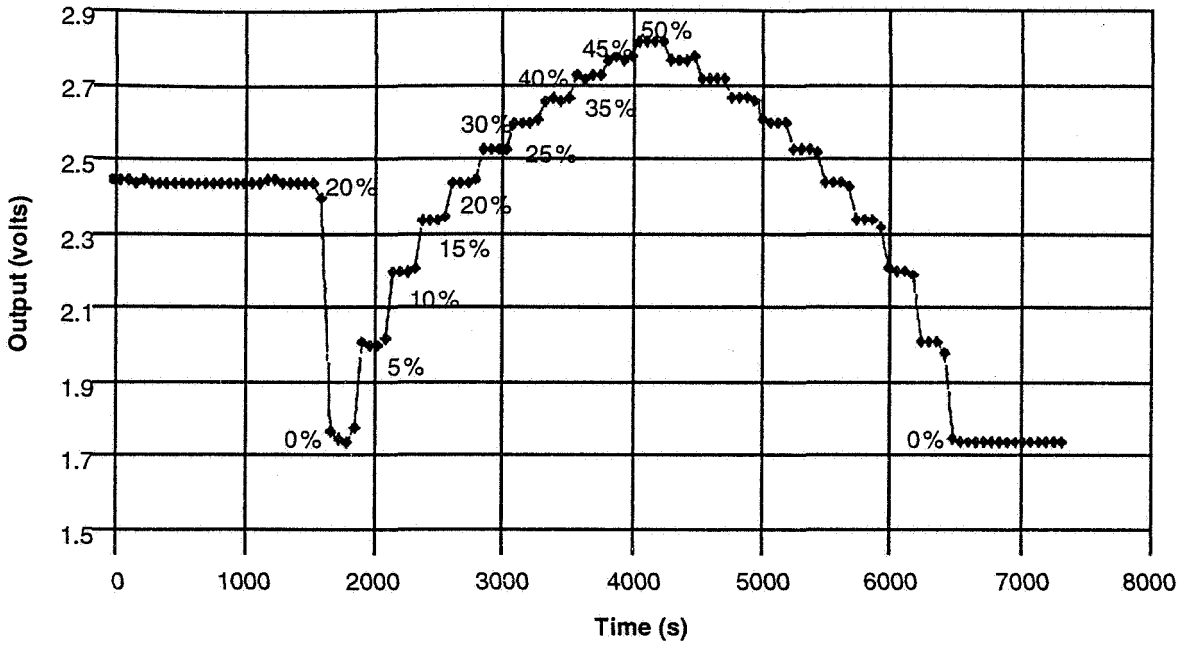

Figure 2-15
Response of oxygen optrode after coating with a hydrophobic membrane of Aquasil. Note that the oxygen optrode ***remains sensitive*** to oxygen. Flat areas of the response curve reflect constant oxygen levels.

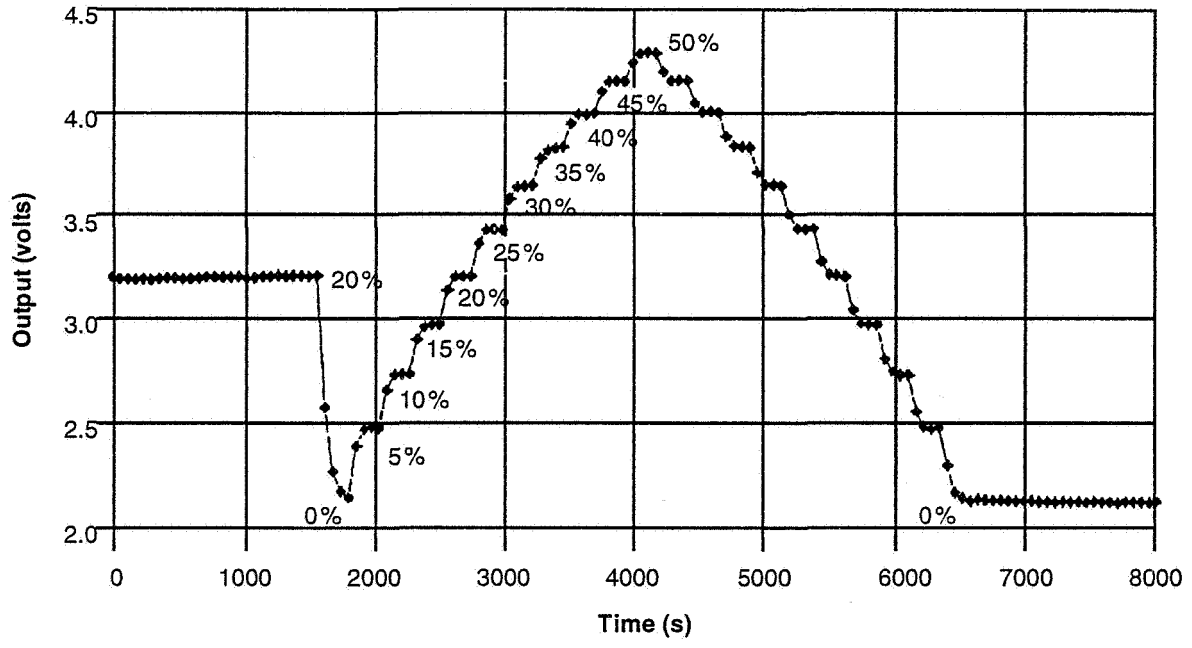

Figure 2-16
The oxygen optrode also remains sensitive to oxygen when an overcoat of Surfasil is applied. The concentration of oxygen was varied between 0% and 50% stepwise in 5% increments.

Figures 2-17 and 2-18 show the prolonged moisture resistance of Aquasil- and Surfasil-coated optrodes, respectively. Here, measurements were made for more than 20 hours. The spikes immediately preceding and following the bold horizontal line were in response to oxygen concentration adjustments in the moisture chamber.

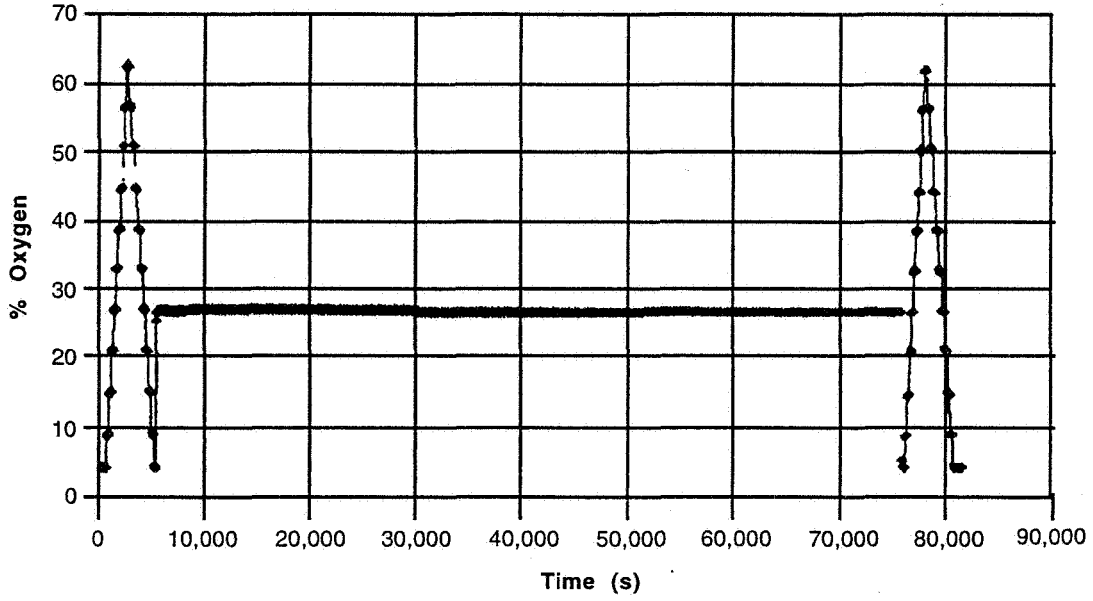

Figure 2-17
The Aquasil-treated optrode shows moisture insensitivity from 50% to 100% RH over 20 hours. Throughout this test the RH was cycled between 50% and 100% in 2400 sec cycles.

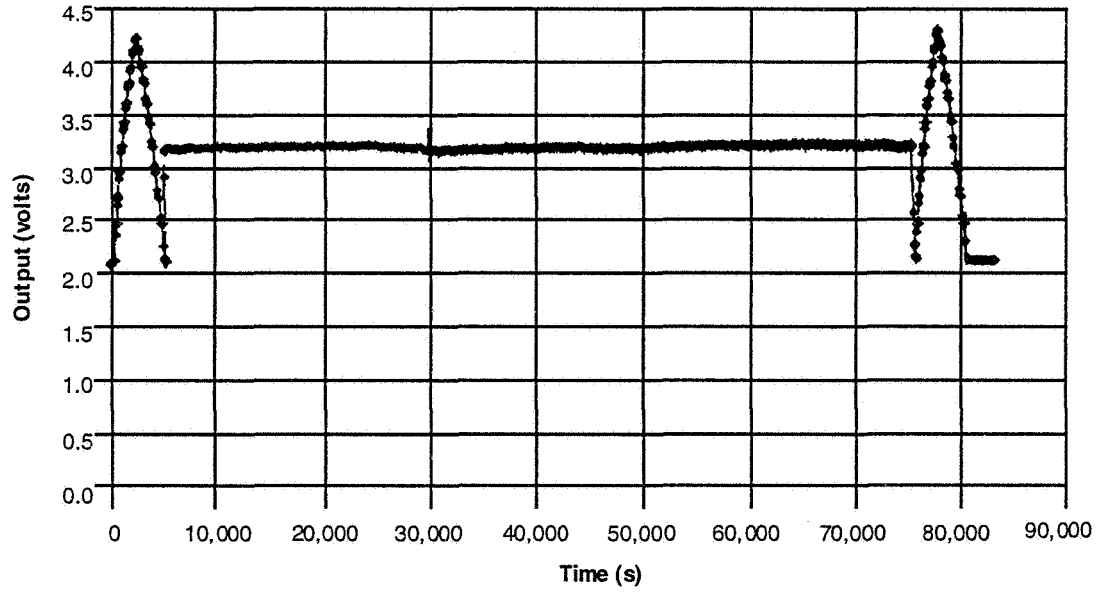

Figure 2-18
The long-term performance of a Surfasil-treated oxygen optrode under exposure to RH from 50% to 100%. Throughout this test RH was varied between 0% and 100% in 2400 sec cycles.

In summary, we have developed an oxygen sensor that exhibits the following performance characteristics.

Table 2-1 Performance Features of the Oxygen Optrode

Detection Range	0% to 100%
Quantification Range	5% to 35%
Temperature Range	5°C to 35°C
Humidity Range	20% to 95% RH
Response Time	5 Seconds
Drift	<2% over 24 hours
Resolution	0.01%
Operational Life	>1 year

3.0 CARBON DIOXIDE SENSOR

POC's fiber optic carbon dioxide (CO_2) sensor is based on the diffusion of CO_2 through a porous membrane containing a pH-sensitive indicator and a pH-maintaining buffer. The chemistry of the sensor is based on the following acid-base equilibrium reactions:

$$CO_2\,(g) + H_2O \quad <\!\!\longrightarrow\!\!> \quad H_2CO_3\,(aq) \qquad K_a = 3.4 \times 10^{-2} \qquad (3\text{-}1)$$

$$H_2CO_3\,(aq) + H_2O \quad <\!\!\longrightarrow\!\!> \quad HCO_3^-\,(aq) + H_3O^+ \qquad K_a = 3.5 \times 10^{-7} \qquad (3\text{-}2)$$

$$HCO_3^-\,(aq) + H_2O \quad <\!\!\longrightarrow\!\!> \quad CO_3^{=}\,(aq) + H_3O^+ \qquad K_a = 6.0 \times 10^{-11} \qquad (3\text{-}3)$$

where K_a is the acid dissociation constant. As CO_2 diffuses through the porous water-rich membrane, it induces a pH change in the membrane. This change in pH is measured by the pH indicator through a characteristic colorimetric change. The extent of color change is directly proportional to the CO_2 concentration.

POC's CO_2 optrode development began with an investigation to select the best CO_2 permeable matrix. Since the CO_2 sensor depends on the presence of water, the matrix must be able to retain water for extended periods of time while allowing gaseous CO_2 to pass through the matrix freely. An extended library search narrowed the choices of CO_2 permeable matrices with a high degree of water content to: (1) hydrogel polymers; (2) water adsorbent polymers, e.g., Nafion; and (3) porous sol-gel silica glasses. Of these, the third option is being independently investigated by POC under other funding (NASA SBIR Contract NAS9-19526, "Integrated Optic Spacesuit Atmospheric Quality Monitor"), albeit in an integrated-optic, rather than a fiber-optrode configuration.

3.1 Hydrogels

Preliminary laboratory experiments were conducted in the polymerization of water soluble polymers (hydrogels). Several types of hydrogels were investigated with the goal of producing an optical-quality porous membrane with a high percent-by-weight of water. In addition to the hydrogel study, preliminary experiments were conducted on water-rich Nafion thin films

impregnated with a CO_2 sensitive pH indicator. These films were deposited on glass slides and evaluated for their response to CO_2, and for their possible degradation under prolonged exposure to ambient atmospheric conditions. Hydrogel impregnation led to a response time on the order of minutes.

3.2 Nafion CO_2 Sensitive Films

Another water-rich polymer with potential applications as a CO_2 permeable matrix appeared to be Nafion. Nafion is the DuPont trademark for perfluorosulfonic acid polymer, a cationic polymer that contains approximately 15% (by weight) water. It is commonly used for the deposition of thin polymer films in which a high degree of water content must be maintained.

Preliminary experiments were conducted to observe the water retention ability of Nafion films containing a pH indicator (bromo cresol blue; pH range 5.2 to 6.8) and tetra-octyl-ammonium hydroxide base, under prolonged exposure to ambient room air. The base was added to the Nafion film in order to maintain the color of the pH indicator in its basic state (purple color). When it adsorbed CO_2, the pH indicator changed color from purple (basic state) to yellow (acidic state). Figure 3-1 shows the spectral absorbance response of the Nafion films to CO_2. These films showed a fast color change from purple to yellow upon exposure to 100% CO_2.

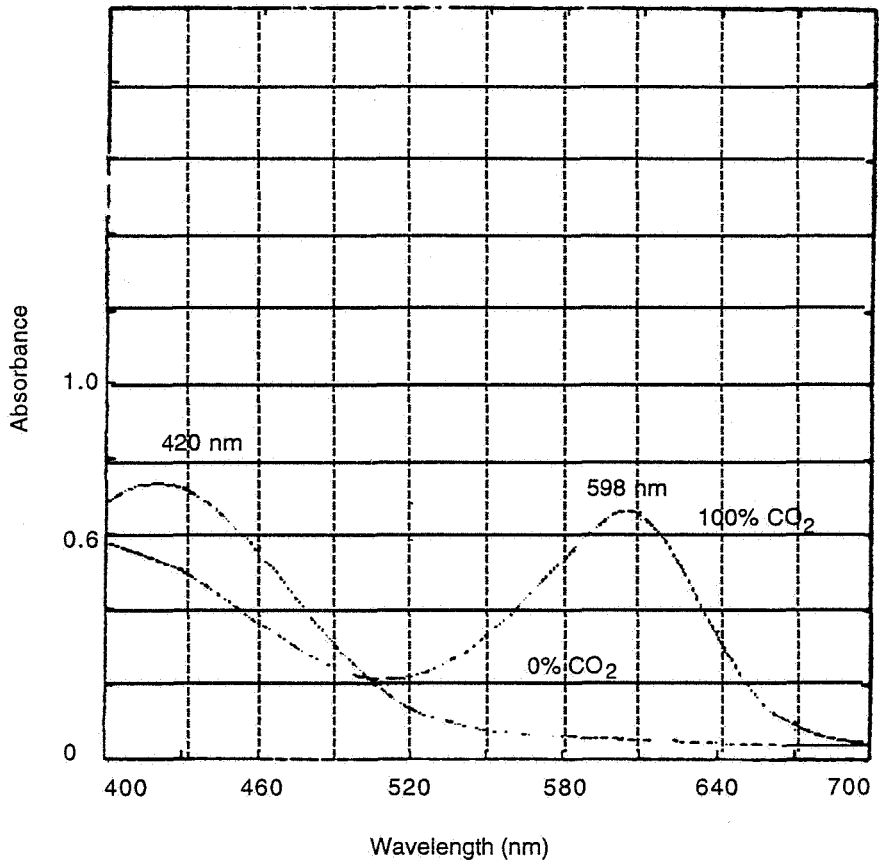

Figure 3-1
Change in optical absorbance of a Nafion CO_2 sensitive film.

Several CO_2 sensitive Nafion films were prepared in order to compare and optimize the sensor film chemistry. Nafion and meta-cresol purple (MCP) pH indicator (pH range 1.2 to 2.6) were mixed, using various water-soluble solvents. Once the polymeric solution was prepared, thin films were deposited on glass slides and allowed to dry in room air. Once the films dried, they were tested for their response to CO_2, as shown in Figure 3-1 above. The films were then left in room air for a prolonged time to test for room air stability, with the results shown in Table 3-1.

Table 3-1 Nafion CO_2 Sensitive Film Compositions

No	Composition	Room Air Stability (hours)
1	Nafion + CH_3OH + MCP	~ 12
2	Nafion + MCP	~ 300
3	Nafion + C_2H_5OH + MCP	~12
4	Nafion + H_2O + MCP	~ 96
5	Nafion + THF + MCP	~ 24

The degradation of the films was monitored by observing a change in color from blue to yellow. Of all of the films prepared and tested, only film No. 2 responded to CO_2 after 20 days. Three of the remaining films (Nos. 1, 3, and 5) did not respond to CO_2 after exposure to room air for 24 hours. Film No. 4 respond to 100% CO_2 after 4 days.

Once a stable film base was formulated, the next step was to choose the pH sensitive indicators and buffering system. In order to make an analytical decision, we produced a preliminary model to analyze the effect of CO_2 concentration on pH. The initial model assumed an aqueous environment with an initial pH of 7. Based on the H_2O-CO_2 equilibrium chemistry, a direct relationship between the partial pressure of carbon dioxide (P_{CO_2}) and pH was determined:

$$pH = - \log \left\{ (A + B) \cdot P_{CO_2} \right\}^{1/2} \qquad (3\text{-}4)$$

where $A = K_1K_2K_3$ and $B = K_1K_2K_4$.

The results obtained with this model are shown in Figure 3-2. From this figure we predicted, to a first approximation, the change in the pH environment of a neutral film (pH = 7) as a function of CO_2 concentration. Figure 3-2 indicates that for a polymer film with an initial pH of 7, the maximum pH change the film will experience on exposure to 0.5 atm of CO_2 will be approximately 1.7 pH units.

This information and the results from the model were used to select three possible indicators as shown in Table 3-2. These indicators were selected to cover the pH range from acidic to neutral.

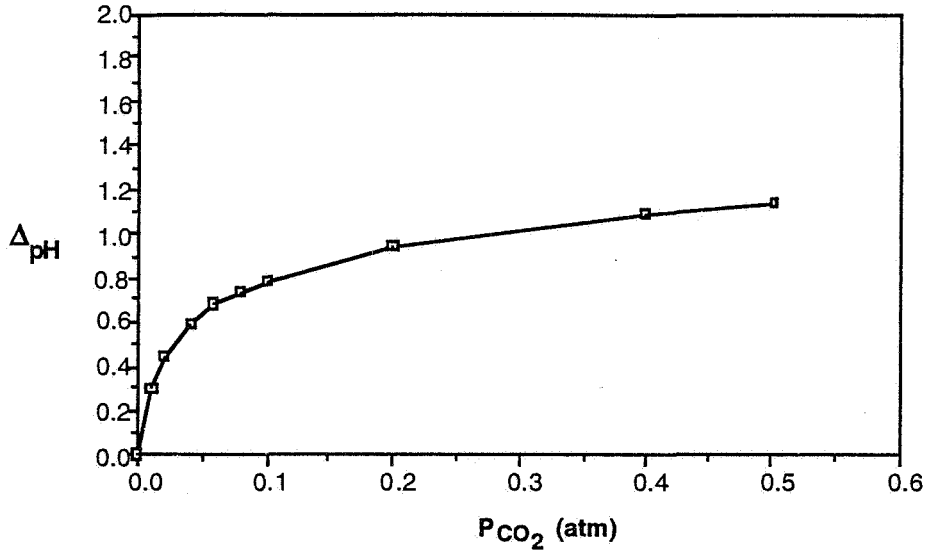

Figure 3-2
Change in pH as a function of CO_2 pressure.

Table 3-2 Selected pH Sensitive Indicators

Indicator	pH Range	Colorimetric Range
m-Cresol Purple	7.0 to 9.0	371 nm to 579 nm
Phenol Red	6.8 to 8.2	360 nm to 557 nm
Chlorophenol Red	4.8 to 6.4	435 nm to 572 nm

3.3 Preliminary Test Results

Because meta-cresol purple (MCP) is better suited to pH modulation around 7, development of the carbon dioxide sensor proceeded by evaluating the response of a Nafion/MCP mixture to changes in the CO_2 concentration from 0 ppm to 3000 ppm. Figure 3-3 shows the response of the MCP sensor for the changes in the CO_2 concentration between 300 ppm and 3000 ppm. The 90% response time for an increase in CO_2 is 30 seconds, and for a decrease in CO_2 is 60 seconds. The sensor was cycled four times for a total test time of 20 minutes. Over this period, a drift of 2.6% was observed, related to the drift (~0.7%) in the RH environment.

To study cross-response effects, humidity and temperature sensors were added inside the gas cell while the sensor was in operation. Figure 3-4 diagrams the modified CO_2 sensor test setup. In this setup, the carbon dioxide/air gas flow circulated through a water bath kept at a constant temperature (~65°C) prior to entering the gas cell. Keeping the water bath temperature constant allowed us to maintain a constant humidity (65±5% RH) inside the gas test cell. The temperature and humidity in the gas cell were monitored by a thermocouple and a Survivor II hygrometer from HY CAL Engineering. The MCP/Nafion polymeric mixture was coated on the surface of a silicon PIN detector. Output from the thermocouple, hygrometer and CO_2 sensor were recorded simultaneously throughout each test. Figure 3-5(a) shows the PIN detector coated with a thin film of the MCP/Nafion polymeric mixture, and Figure 3-5(b) shows the test cell.

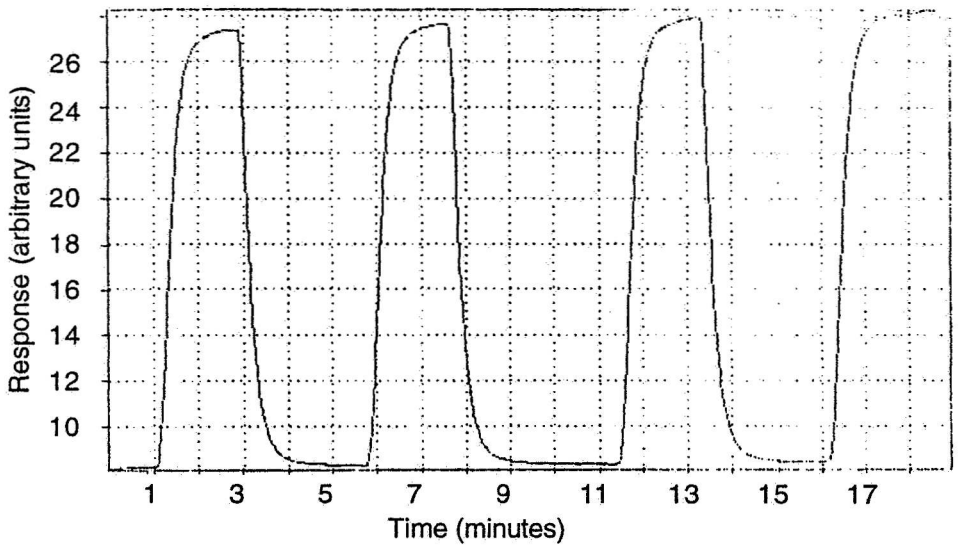

Figure 3-3
Optical response of MCP sensor to changes in the CO_2 concentration from 330 ppm to 3000 ppm.

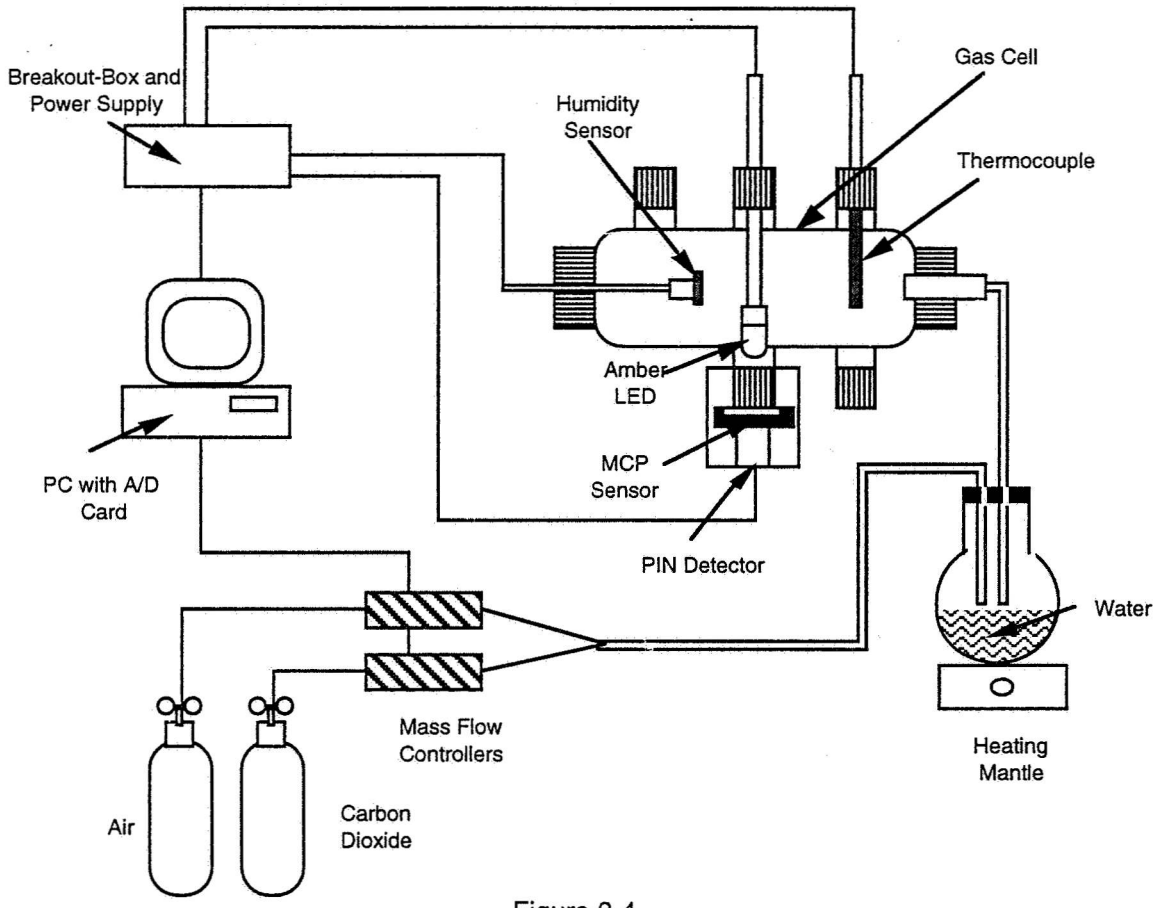

Figure 3-4
Carbon dioxide sensor test setup.

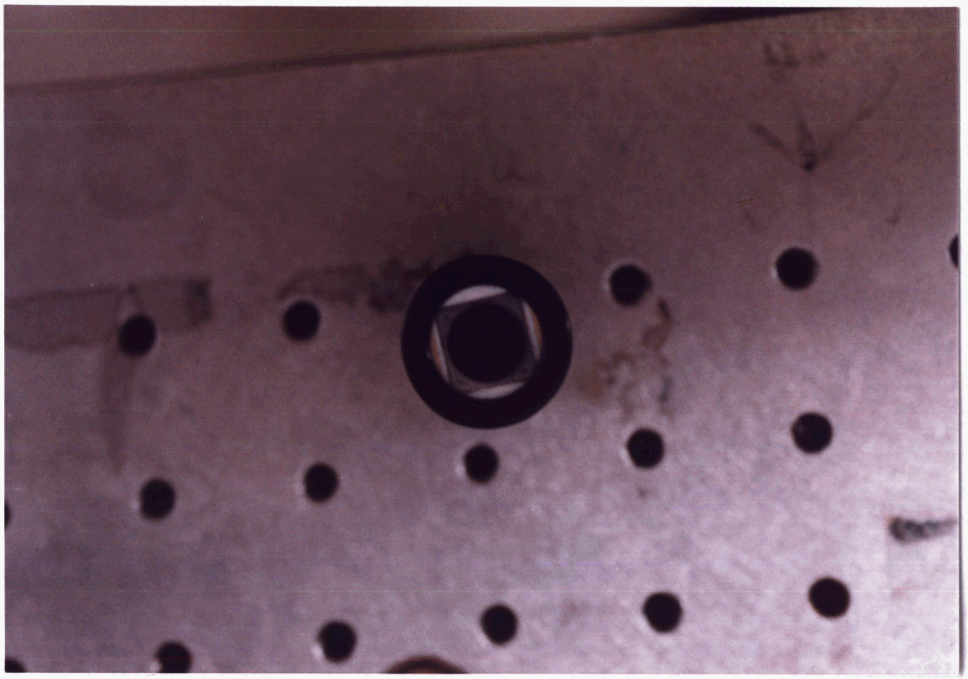

(a) MCP/Nafion film coated on a silicon PIN detector.

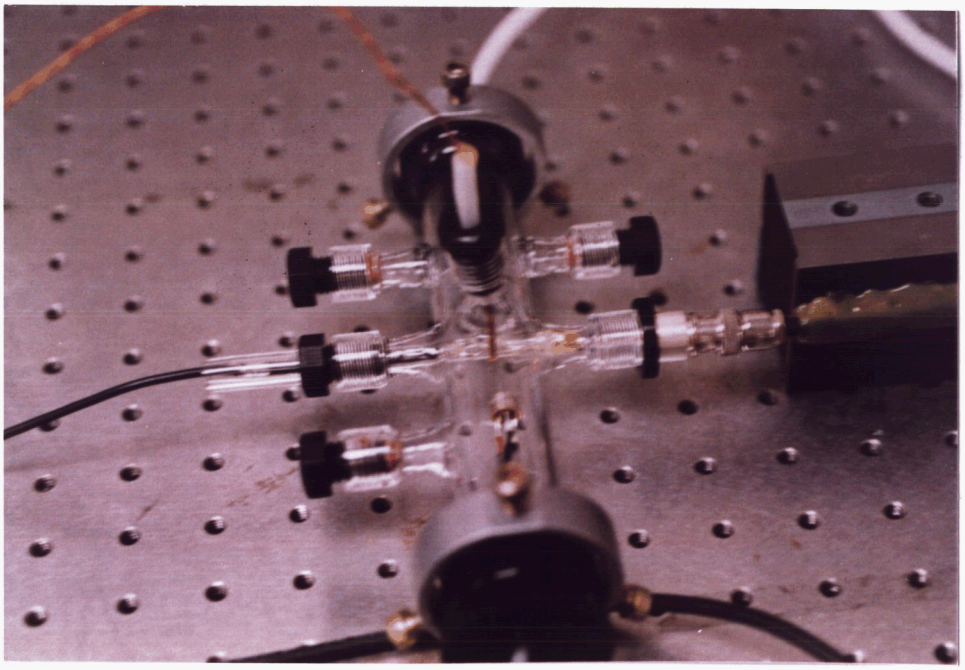

(b) Gas test cell with thermocouple, hygrometer, and MCP sensor system.

Figure 3-5
Details of CO_2 sensor setup.

Figure 3-6 shows the output of the preliminary long-term test performed with this experimental setup. For this test, a 1 μm thick MCP/Nafion film was coated onto the detector and allowed to dry at room temperature for 12 hours. The dried film was then placed in the test setup and exposed to alternating concentrations of 330 ppm and 10,000 ppm of CO_2 in 30 minute cycles for a total period of 22 hours. The data were plotted along with the relative humidity inside the gas cell. The data display a large increase in sensitivity of the sensor over the first 10 hours of the run. After this period the sensor output stabilizes. A similar signature is observed for the relative humidity signal. Over the first 10 hours, the relative humidity in the gas cell increases from 60% to 70%. After this period, the humidity stabilizes in the gas cell. The similarity in the sensor signatures for CO_2 and relative humidity seems to indicate a direct correlation between the two.

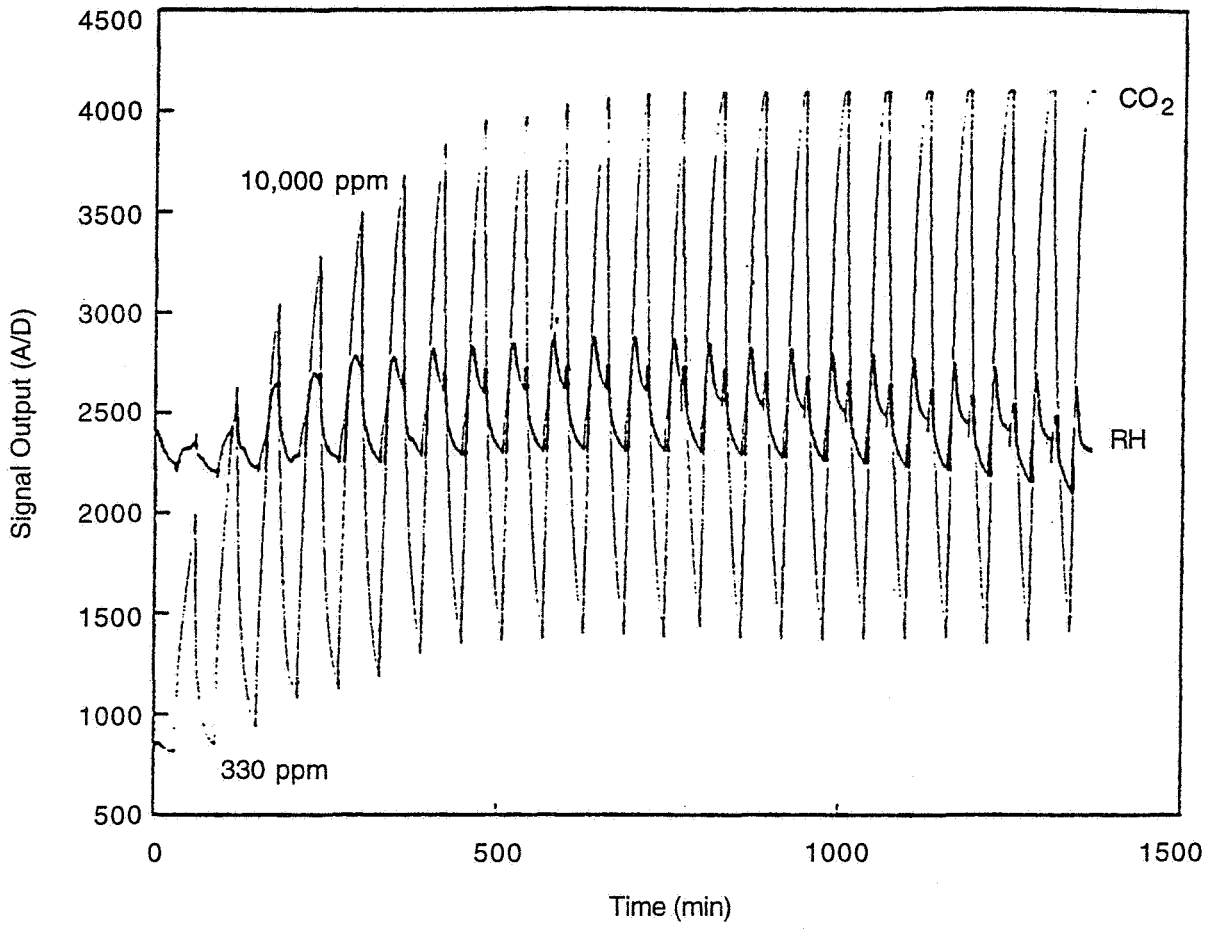

Figure 3-6
Preliminary long term response of CO_2 sensor, showing CO_2 and relative humidity signals.

From previous experiments it was known that the CO_2 sensitive films remained moist during testing, probably as a result of incomplete removal of the solvent base-rich phase. Consequently, it was decided to modify the film preparation procedure to produce solvent-free films in an attempt

to improve the humidity and/or temperature independence of the CO_2 sensor. The new procedure was aimed at producing films with large quantities of the Nafion/indicator phase present, and to reduce the amount of solvent-base (alcohol/tetrahexyl ammonium hydroxide) left in the dry film.

In the new procedure, the chemical components -- MCP, Nafion, and tetra-hexylammonium hydroxyde (THAH) -- of the sensor system remained the same, and only the mixing and separation procedures were changed. In the mixing procedure, 0.1 mg of MCP was dissolved in 4 ml of Nafion and mixed for 10 minutes. At the same time, another 0.1 mg of MCP was dissolved in 4 ml of tetraoctylammoniumhydroxide (TOAH) and mixed for 10 minutes. These two solutions were then mixed in an ultrasonic bath for 10 minutes. The resulting solution was centrifuged at 3000 rpm for one hour. This separated two phases: a polymer-rich phase at the bottom of the vial, and a solvent-rich phase at the top of the vial. The solvent-rich phase was removed from the vial with a syringe, leaving behind the thick polymer-rich phase, which was rinsed with 5 ml of ethanol and centrifuged for one more hour. After centrifuging, the solvent was removed, leaving behind an MCP/Nafion polymeric paste. This paste was slightly dissolved with 1 ml of ethanol to produce a mixture that could be readily used for coating the PIN detector. The detector coated with the MCP/Nafion composition was dried in an oven at 70°C for two hours.

This new sensor was tested for 24 hours under the same conditions as in the test shown in Figure 3-6. The results of this test, shown in Figure 3-7(a), demonstrate that the new sensor composition is much more stable over a 24 hour run. A drift of only ~2.1% over the 24-hour period is observed -- a substantial improvement over the drift observed in the preliminary test run shown in Figure 3-6. Also, the optical response of the new sensor is far less subject to variations in humidity and temperature in the test cell, as shown in Figure 3-7(b).

Figure 3-8(a) shows further experimental results. The CO_2 sensor used in this test was the same sensor that produced the results shown in Figure 3-7. This graph shows that the sensor is responding consistently to changes in the CO_2 concentration from 330 ppm to 10,000 ppm, and that it exhibits greatest sensitivity in the range from 330 ppm to 1000 ppm. The relative humidity in this run varied from 70% to 58%, and the sensor showed very little sensitivity to these humidity changes. Relative humidity and temperature inside the test cell for this run are plotted in Figure 3-8(b).

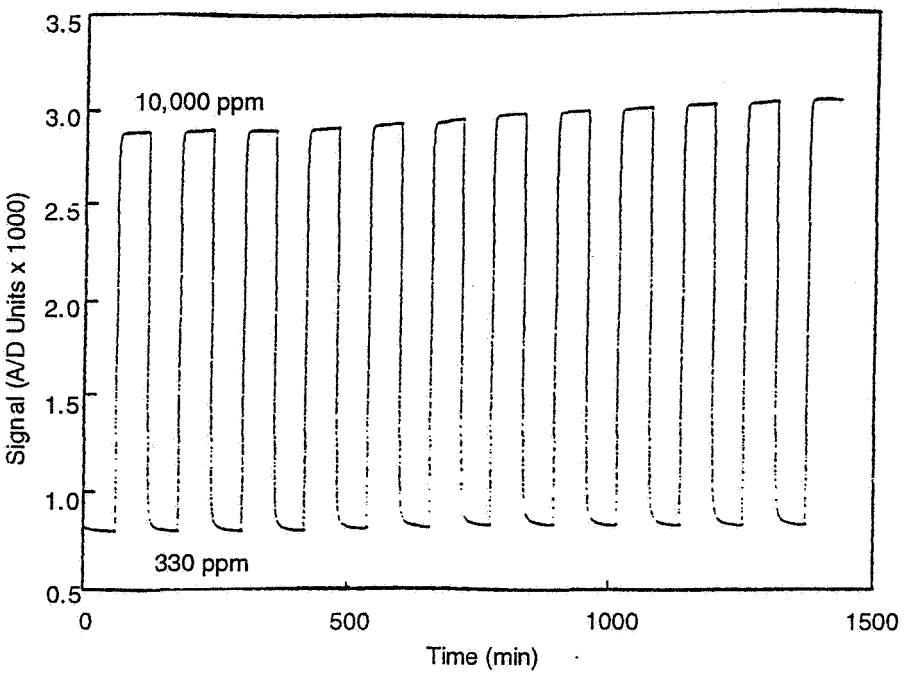

(a) Response to CO_2

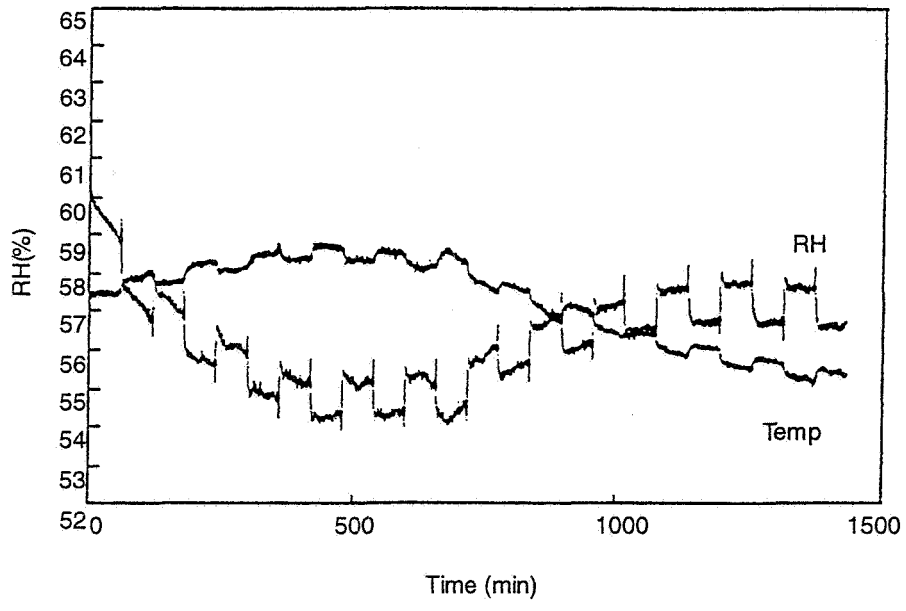

(b) Relative humidity and temperature inside test cell.

Figure 3-7
24-hour run using improved sensor chemistry.

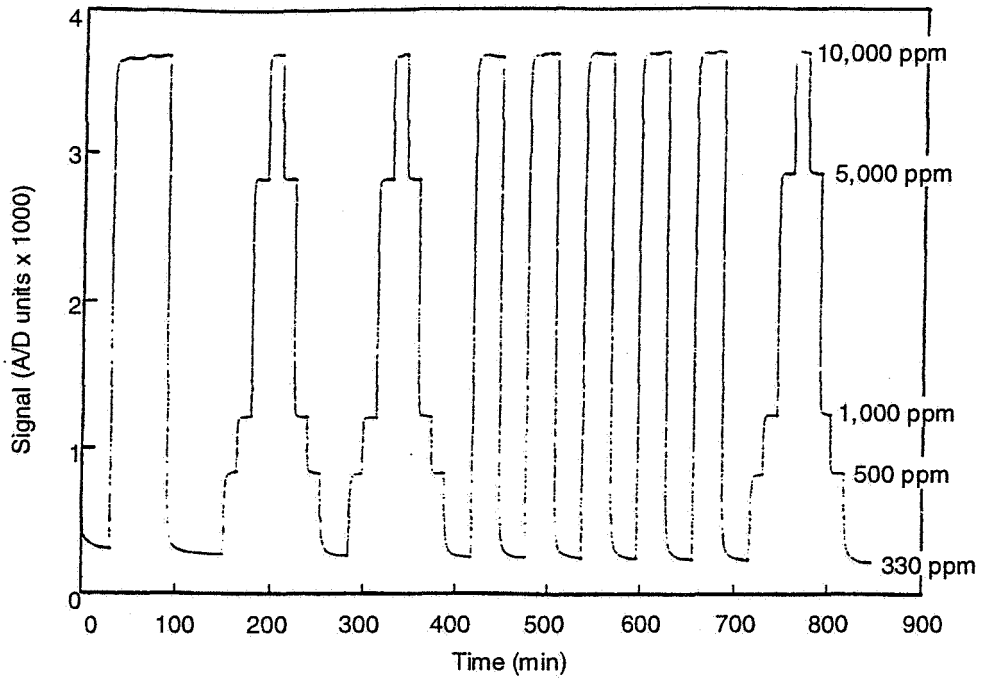

(a) Response to CO_2

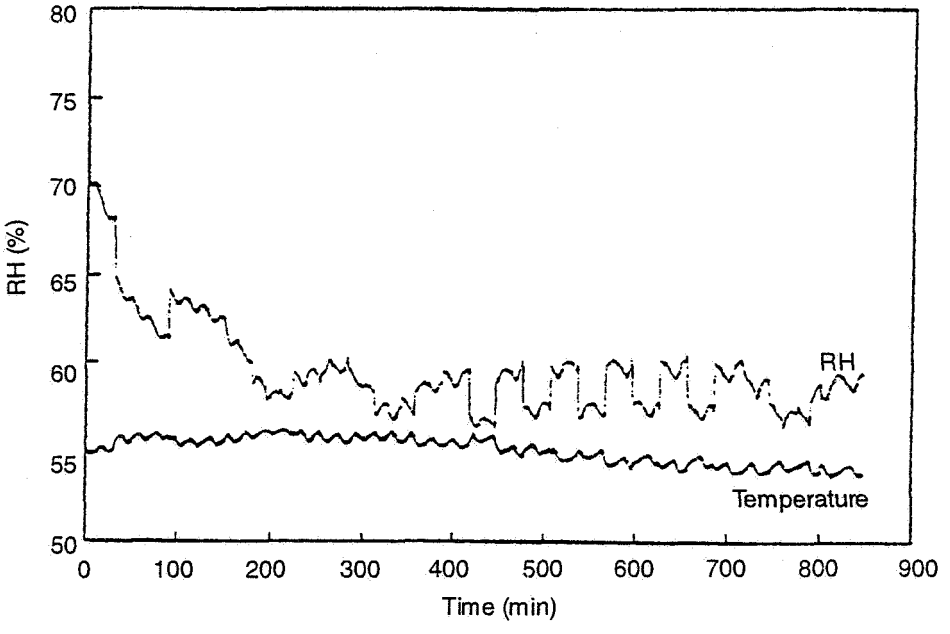

(b) Relative humidity and temperature.

Figure 3-8
Fourteen hour test using advanced test protocol.

Figure 3-9 plots the sensor output vs. CO_2 concentration, computed by averaging the CO_2 sensor output signals corresponding to all measurements made at a particular concentration value. For example, for each of the nine intervals during which the CO_2 concentration was held at 10,000 ppm (see Figure 3-8(a)), numerous measurements of CO_2 sensor output were made. Thus, the data point at 10,000 ppm in Figure 3-9 actually represents the average of 1,200 values, taken during the aggregate time of 200 minutes for which the test chamber contained 10,000 ppm CO_2. Error bars corresponding to the standard error of each of the five points in Figure 3-9 are too small to see on the graph. The geometrical average of the standard errors was computed to be 2.84 %.

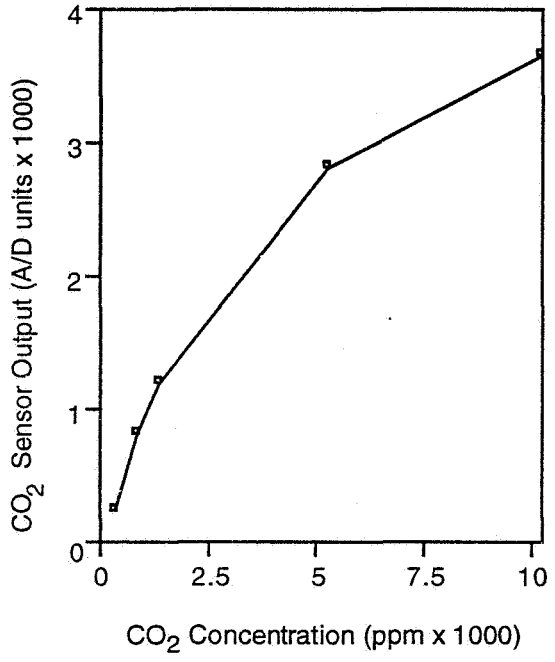

Figure 3-9
Raw CO_2 sensor output vs. CO_2 concentration.

With these encouraging results, we decided to increase the duration of the test. Figure 3-10 shows the results obtained for a five-day test. The experimental conditions were identical to those of the previous run. The same sensor unit was used for this experiment.

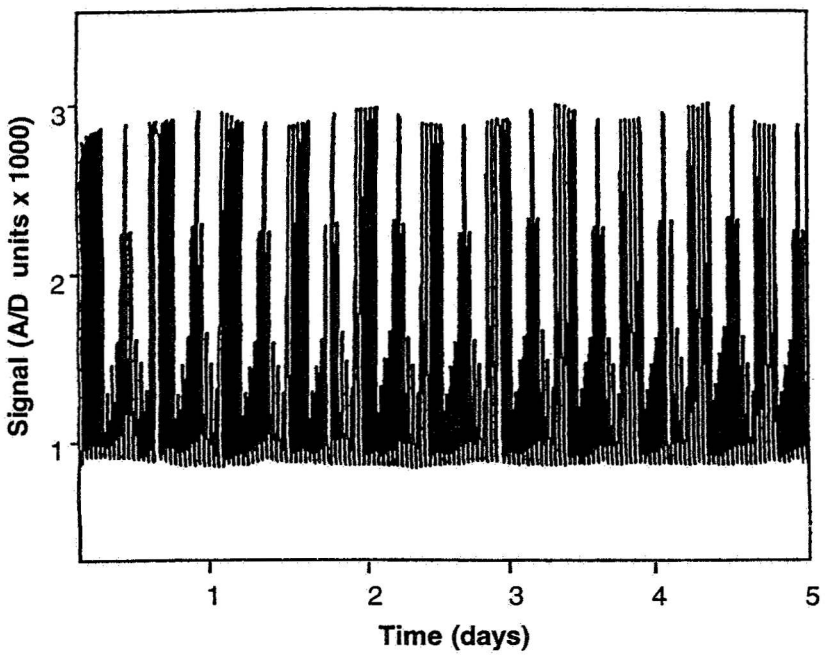

Figure 3-10
Five day duration test. The fluctuations in the signal are caused by changes in temperature, and relative humidity. The CO_2 concentrations in ppm were 330, 824, 1071, 1319, 2800, and 5265.

The results in Figure 3-10 show a very reproducible response to changes in the CO_2 concentration. However, detailed examination of the data shows a cyclic undulation. This effect is quite pronounced when the sensor is exposed to 5000 ppm of CO_2, but it is also observed to a lesser extent when the sensor is exposed other CO_2 concentrations. The undulation of the data occurred on a 24-hour cycle (see Figure 3-11). A similar 24-hour cyclic undulatory effect is observed for both RH and temperature. These cyclic changes are due to the air conditioning in the building, which cools a few degrees at night and warms up again in the morning. Figure 3-12 plots average response of the sensor to changes between 330 ppm and 5000 ppm of CO_2 over the five-day period. The data points and error calculation for this calibration curve were arrived at using the same method as for Figure 3-9. The geometrical average of the percent standard error was found to be 1.8%. Using an algorithm described in Appendix A, the data of Figures 3-10 and 3-12 was corrected for this spurious temperature/humidity response and calibrated. The results (Figures 3-13 and 3-14) clearly show improvement of the performance of the sensor by temperature compensation. In Figure 3-13 the cyclic variation in CO_2 response of Figure 3-10 has been virtually eliminated, leaving only random variations in sensor response. In Figure 3-14, which displays the final response characteristics of the sensor, the geometrical average of the standard errors is 1.3%, significantly better than for the uncompensated data of Figure 3-12. ***With this signal processing algorithm, optrodes could be used in practical sensor systems whose performance is considerably better than competitive CO_2 sensors.***

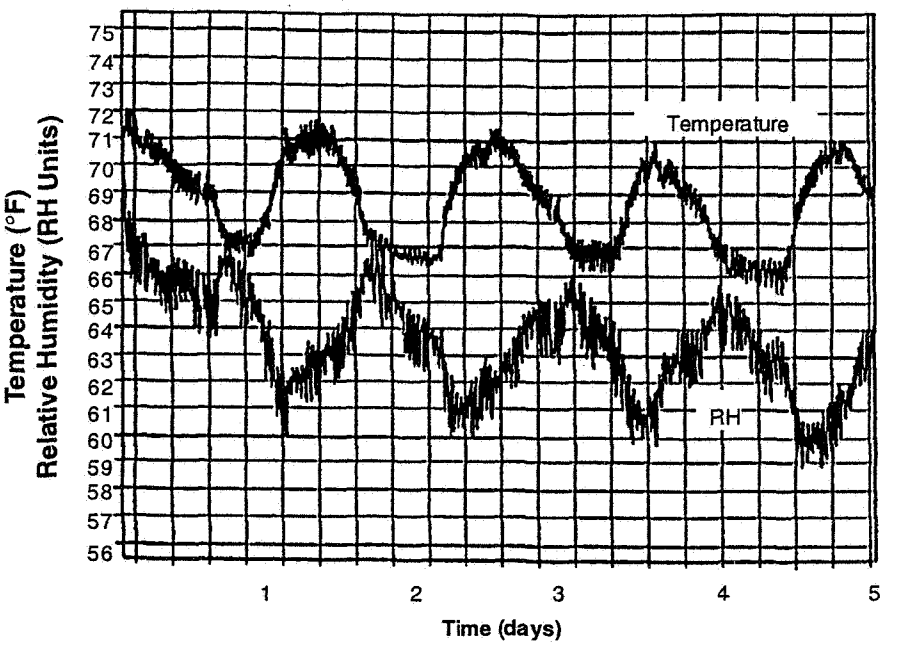

Figure 3-11
Relative humidity and temperature inside test setup during five day duration test.

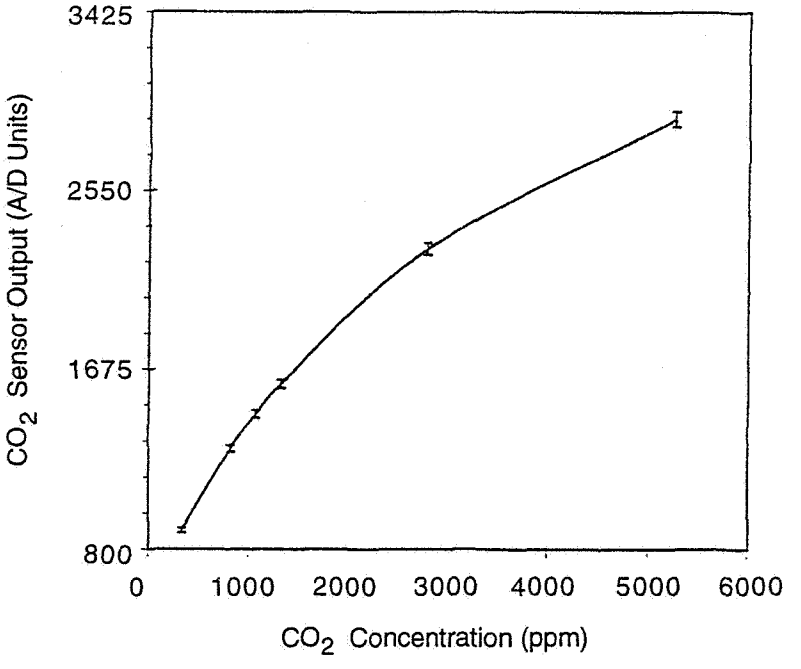

Figure 3-12
Average sensor signal vs. CO_2 concentration for a five day duration test. The range of interest is from 0 to 5,000 ppm.

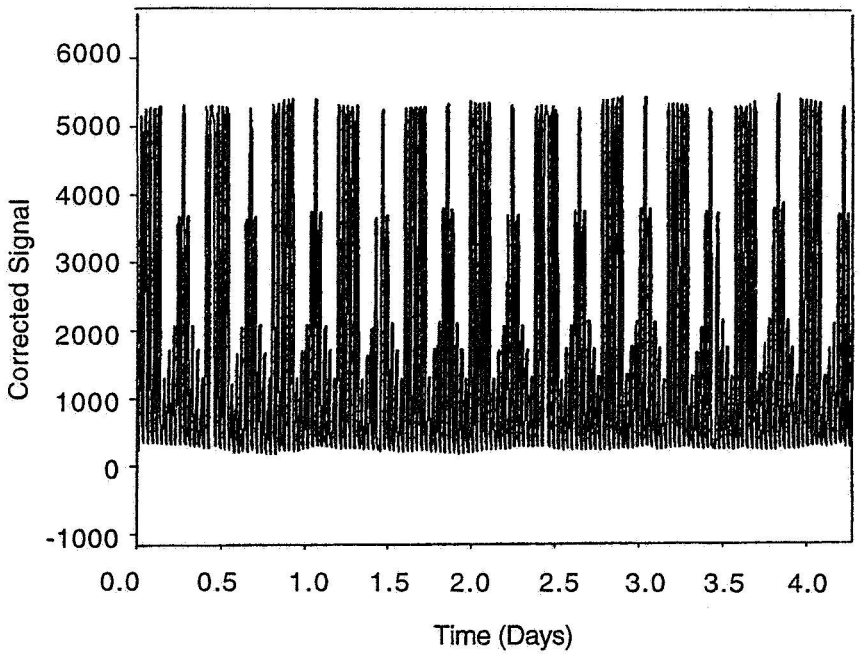

Figure 3-13
Calibrated and corrected CO_2 sensor response for a five-day test.

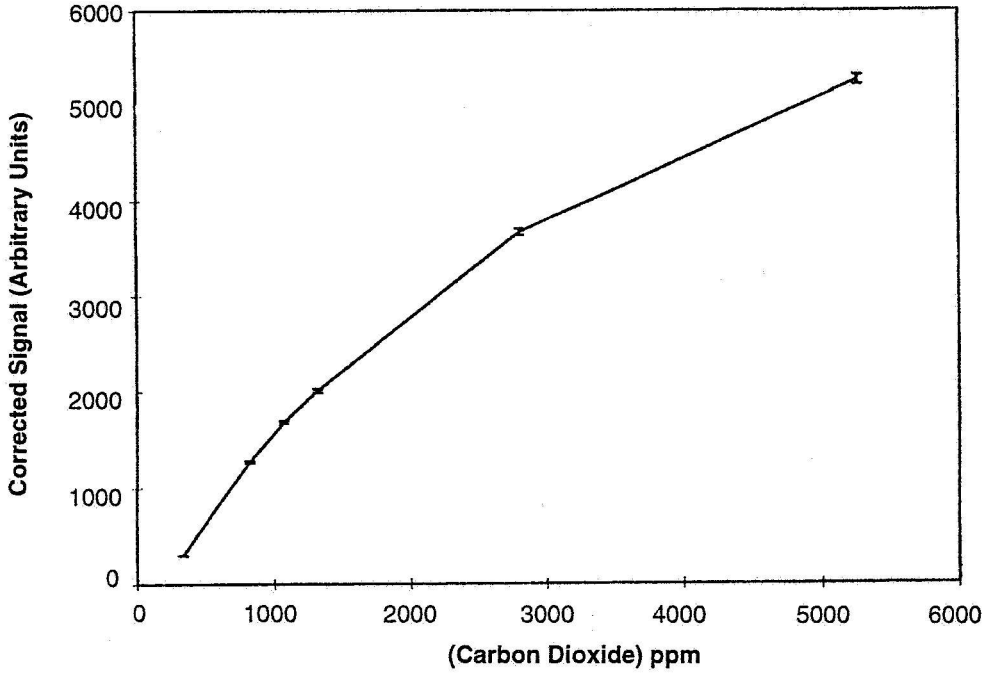

Figure 3-14
Corrected CO_2 sensor response (see Appendix A) vs. actual CO_2 concentration for a five-day test.

3.4 Sensor Reproducibility

Before the CO_2 sensors were tested for reproducibility, the sensor design and experimental setup were modified. Figure 3-15 pictorially shows the CO_2 sensor assembly. The Nafion/MCP indicator mixture was spin-coated on a mirror, fixed at the end of a threaded nut that was fitted to a hollow porous metal housing. Measurements were made in reflection mode in the test cell shown in Figure 3-5(b) above. A 640 nm light emitting diode (LED) was used as the light source, driven by a power supply/signal generator, Model 3011B from BK Precision. Light was transmitted to the indicator through a bifurcated optical fiber bundle 1 mm in diameter. The reflected light was coupled back into the fiber and directed to a preamplifier (Stanford Research Systems, Model SR 570). The signal from the preamplifier was fed to a lock-in amplifier (Stanford Research Systems, Model SR510) for further processing. Figure 3-16 is a schematic of the carbon dioxide test setup.

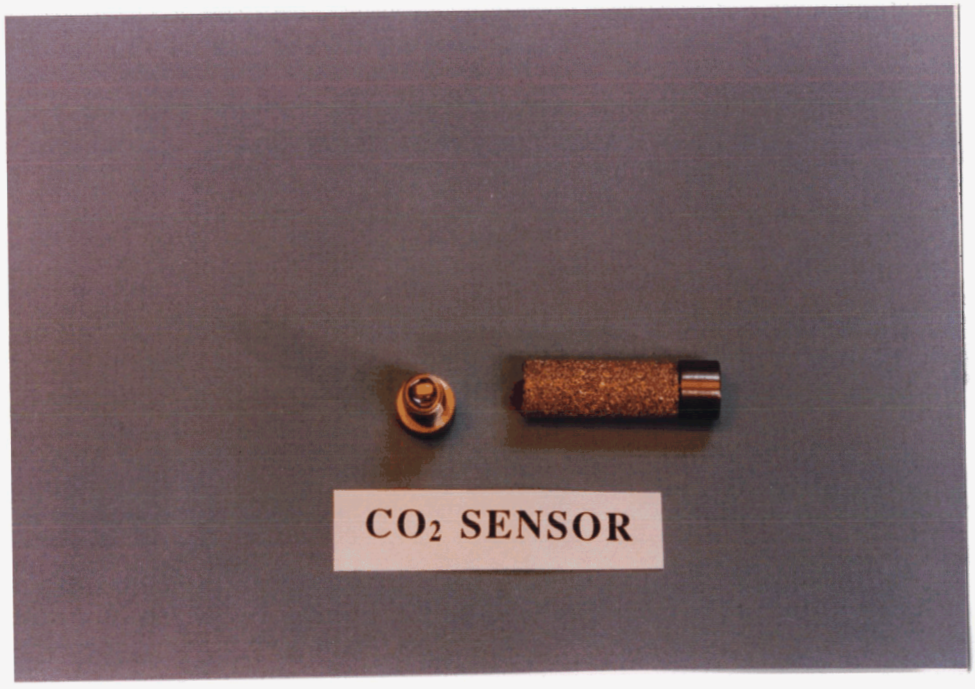

Figure 3-15
Carbon dioxide optrode assembly. A mirror was mounted on a threaded nut (left). The indicator chemistry was spin-coated on the mirror. The threaded nut along with mirror is fitted to the porous metal housing.

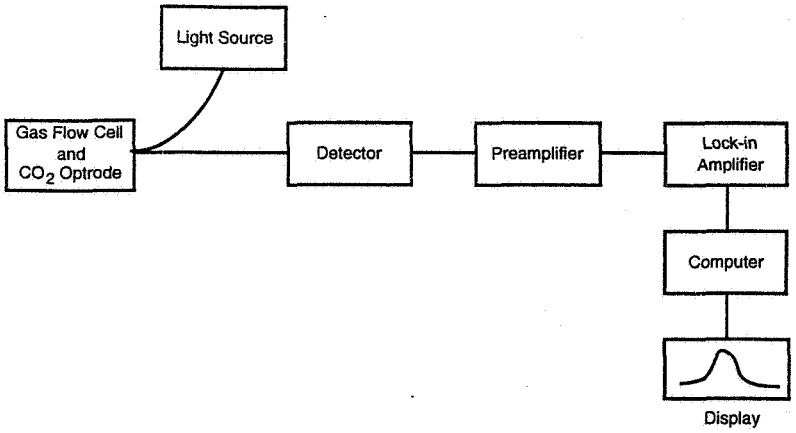

Figure 3-16
Carbon dioxide modified test setup.

3.4.1 Test Results

Six carbon dioxide optrodes were tested to evaluate the sensor-to-sensor reproducibility. Figure 3-17 shows the response curve of a typical sensor that was exposed to 0, 250, 500, 1000, 2500, and 5000 ppm of carbon dioxide vapor at 0% ambient relative humidity (RH). All of the optrodes show a strong response to carbon dioxide.

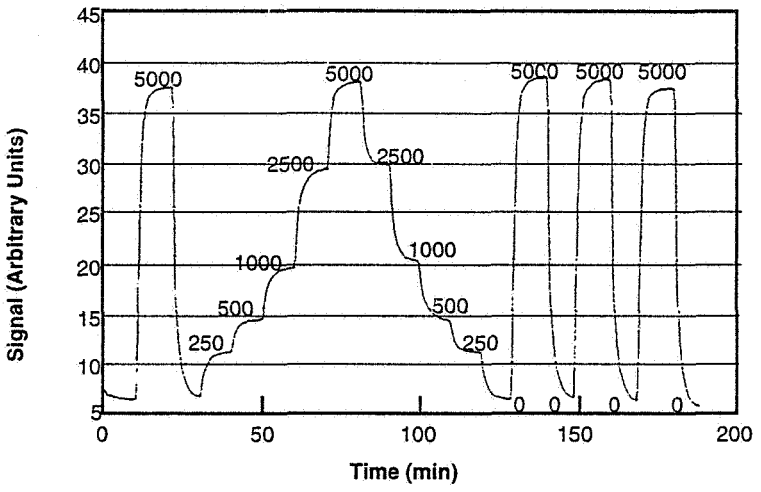

Figure 3-17
Response of CO_2 optrode 1A to six concentrations of CO_2 vapor.

Figure 3-18 presents an expanded view of the response time of the optrode when the CO_2 concentration is changed from 0 ppm to 5000 ppm. This concentration range (0 to 5,000 ppm) was selected as the range of interest early in the project. The response time (90% of full scale) is approximately 1.3 minutes for this sensor. Figure 3-19 shows the response time when switching the CO_2 concentration back from 5000 ppm to 0 ppm.

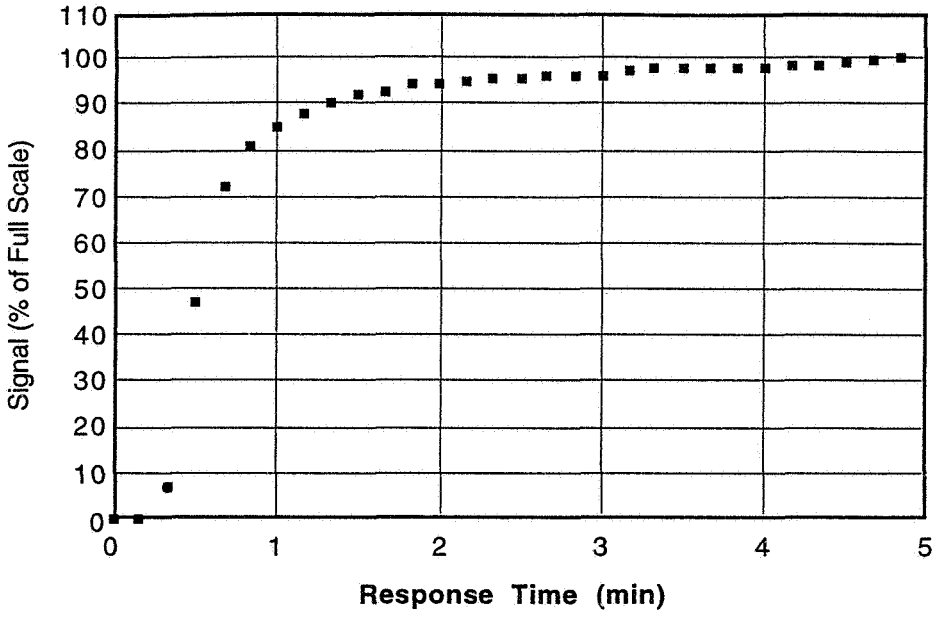

Figure 3-18
Forward response curve of CO_2 optrode 1A from 0 ppm to 5000 ppm CO_2.

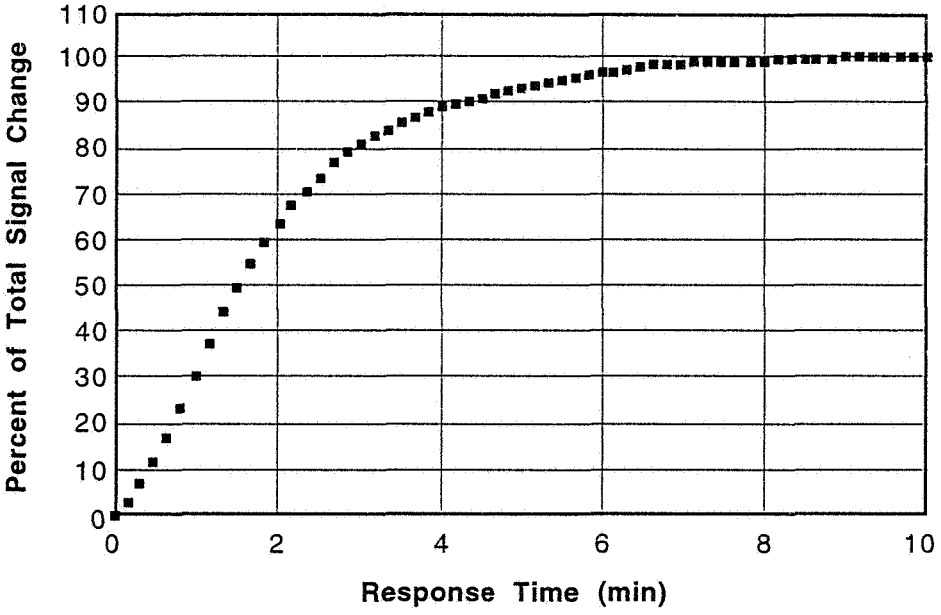

Figure 3-19
Response time of CO_2 optrode 1A from 5000 ppm to 0 ppm CO_2.

The "reverse" response time was approximately four minutes to 90% of full scale. This longer response time is due to complex kinetic factors, one of which may be that the dissolution of CO_2 in an aqueous medium is roughly 30 times faster than the evacuation. Table 3-3 lists the "forward" and "reverse" response times for all six CO_2 optrodes. Visual inspection of sensors indicated that variations in the thickness of the CO_2-sensitive films may be the cause of the response-time variations.

Table 3-3 Forward and Reverse Response Curves of the CO_2 Optrode

Sensor ID	Forward Response (min.)	Reverse Response (min.)
1A	1.3	4.0
2A	2.4	6.1
3A	0.9	2.1
3B	0.7	1.4
4A	0.8	1.4
4B	0.8	1.2

Table 3-3 clearly shows sensor-to-sensor differences in response-time, possibly attributable to film thickness variations.

3.5 Operational Lifetime

Emphasis was placed on extending the operational life and shelf life of the CO_2 sensors. Nafion/MCP-based CO_2 sensors exhibit a shelf life of more than a year when the indicator chemistry is kept isolated from the ambient environment. Under operational conditions, however, the indicator chemistry slowly and irreversibly turns from blue to yellow. This degradation of the indicator chemistry can be ascribed to the insufficient buffering capacity of the indicator matrix. We took a closer look at the functional characteristics of the individual components, and altered the indicator matrix to improve our understanding of this phenomenon.

An alkaline material is used in the indicator matrix to maintain MCP in the deprotonated form before and after reaction with CO_2. Typically, the alkaline material is a tetraalkylammonium hydroxide (e.g., tetrahexylammonium hydroxide, THAH). A properly functioning CO_2 sensing chemistry requires both water and a deprotonating agent in the matrix. If the matrix dries out, performance of the sensor deteriorates. Because the atmosphere is a large reservoir for CO_2, protons are continuously being generated within the matrix on exposure to the ambient environment. These protons, in turn, are being neutralized by the quaternary bases in the indicator matrix. Thus, the deprotonating agent is continuously being depleted under operational conditions, leading eventually to a nonfunctional sensing chemistry. When the chemistry is kept isolated from the atmosphere, CO_2-induced degradation of the base is substantially retarded, and the chemistry stays functional.

In addition to tetrahexylammonium hydroxide, we investigated tetrabutylammonium hydroxide (TBAH) as a deprotonating agent. The base strength of TBAH is less than that of THAH because of the shorter alkyl chain length. It was anticipated that TBAH would prolong the sensor's operational lifetime. However, when the indicator chemistry (coated on a glass slide) with TBAH was exposed to the ambient atmosphere, the color of the slide turned from blue to yellow within two weeks, a time comparable with that for slides containing THAH.

Next, the role of water-retaining agents was explored. Two hygroscopic chemicals were used separately: calcium chloride and magnesium chloride. The concentration of these agents in the indicator matrix was about 25%. Again the indicator matrix was cast on microscope slides and left under ambient atmospheric conditions. The blue meta-cresol purple again turned yellow within two weeks. Thus, the use of hygroscopic agents did not appear to influence the operational life of the sensing chemistry.

We also turned our attention to a publication by Andrew Mills [1], which describes the use of ethyl cellulose as a film-forming matrix. Results in that paper led us to believe that a longer-lived CO_2 sensor may be achievable. Following the published recipe, we prepared an indicator chemistry utilizing the following components:

- meta-cresol purple — indicator
- tetraoctylammonium hydroxide — deprotonating agent
- ethyl cellulose — film-forming polymer
- tributyl phosphate — plasticizer
- glass slide — substrate

The plasticizer, tributyl phosphate, is used to lower the glass transition temperature (T_g) of the film and to facilitate the permeation of CO_2. Use of this recipe, however, did not lead to an operational life of more than two weeks. Our efforts have led to a reversible CO_2 sensor with 100 hours of continuous operational life.

3.6 Lifetime-Based CO_2 Indicator

The experimental results discussed above led us to two operational difficulties:

1. Indicators lose sensitivity over time because they dry out.
2. Thicker films last longer but have slower response times.

We attempted another approach to solving these performance problems using a fluorescence lifetime-based pH indicator. The use of a lifetime-based system appeared to be advantageous because intensity variations due to film aging should have no effect on such a system, and because POC's oxygen sensor uses a lifetime-based fluorescence readout device. For these reasons, we redirected our sensor development efforts to work on fluorescence lifetime-based CO_2-sensitive chemistry. A brief discussion of lifetime-based CO_2 detection follows.

The lifetime-based carbon dioxide optrode incorporates a fluorescence-based organometallic indicator adsorbed into a porous (glass or polymer) support. The pH-dependent organometallic indicator detects CO_2 gas at ppm levels. CO_2 detection is based on lifetime quenching induced by proton transfer in the excited state. The advantages of this principle over existing luminescence-based chemistries are:

- Excitation (460 nm) and emission (650 nm) wavelengths fall in the visible region of the electromagnetic spectrum.
- The large Stokes shift (460 nm to 650 nm) allows easy separation of the fluorescence signal from scattered excitation light.
- No referencing is required.
- Fiber bending or microbending has no effect on the optrode signal.
- Leaching or photobleaching of the sensing chemistry does not affect measurements.

We focused on the ruthenium-based organometallic complexes listed in Table 3-4. These compounds were synthesized by Dr. Steven Tysoe of Saint Mary's College of Maryland. These complexes are well known redox reagents that readily undergo spectroscopic changes as a function of pH.

Table 3-4 Ruthenium(II) Complexes

Ru(II)-Complex	Ligand	Absorption (nm)	Emission (nm)	Lifetime (ns)
tris[2-(2-pyrazinyl)thiazole[1]	(pzth)	460	652	320
4,7-phenanthrolino-5,5,6,6-pyrazine	(ppz)	474	690	200
2,3-bis(2-pyridyl)-5,6--dihydropyrazine[2]	(dhp)	475	675	140

The ruthenium complexes readily undergo protonation in the excited state when exposed to low concentrations of CO_2. Figure 3-20(a) shows the UV-vis absorption spectra of Ru-$(pzth)_3^{2+}$ in aqueous solutions with varying pH. Similarly, Figures 3-18(b) and (c) show the effect of pH on the fluorescence emission of Ru-$(ppz)_3^{2+}$ and Ru-$(dpp)_3^{2+}$, respectively.

Figure 3-21 shows the fluorescence intensity change when an aqueous solution (10^{-4} M) of $Rd(pzth)_3^{2+}$ was purged with 100% nitrogen and carbon dioxide, respectively. This 4 dB signal change is barely sufficient to meet NASA needs (300 ppm to 5000 ppm). $Ru(pzth)_3^{2+}$ was impregnated into porous glass, and tested with a phase fluorometer. No discernible signal change was observed. This indicates that $Ru(pzth)_3^{2+}$ also requires a pH-maintaining buffer for CO_2 detection. However, the use of a buffer leads to the sensor having only a short (5 to 10 day) operational lifetime, as we have seen with meta-cresol purple.

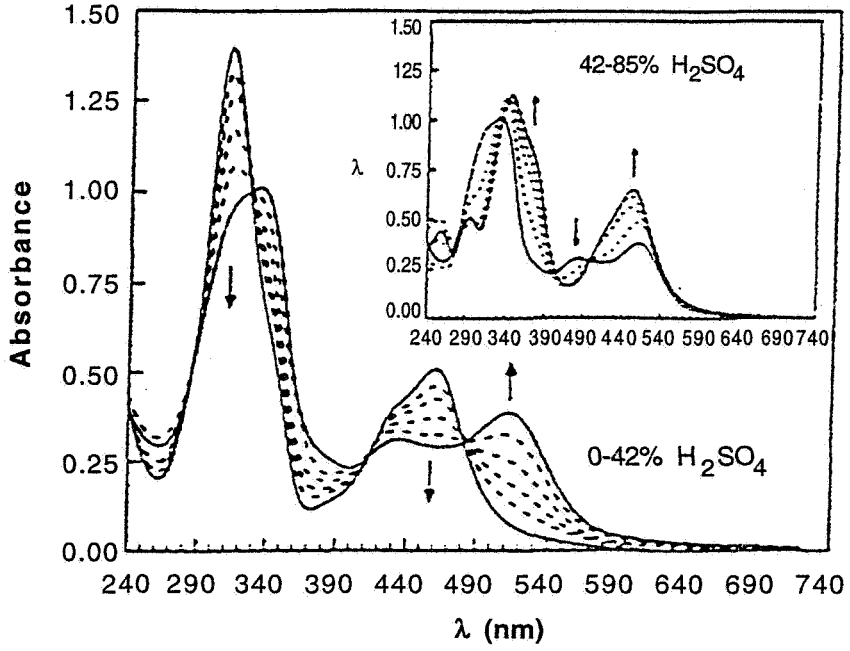

(a) UV-vis absorption spectra of $Ru(pzth)_3^{2+}$ in aqueous solutions for varying pH (up arrows indicate higher concentration of H_2SO_4, down arrows lower).

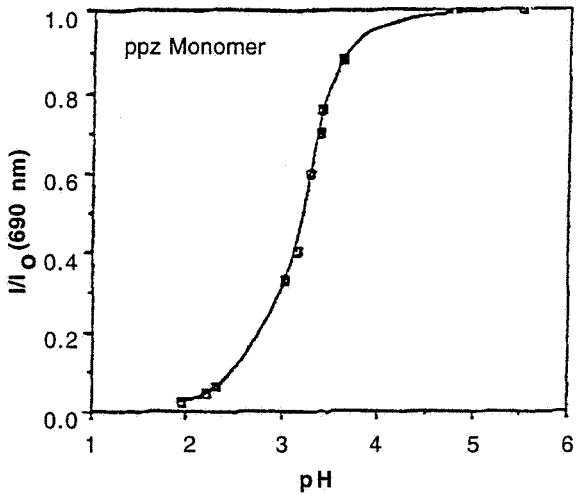

(b) Relative emission vs. pH for $Ru(ppz)_3^{2+}$

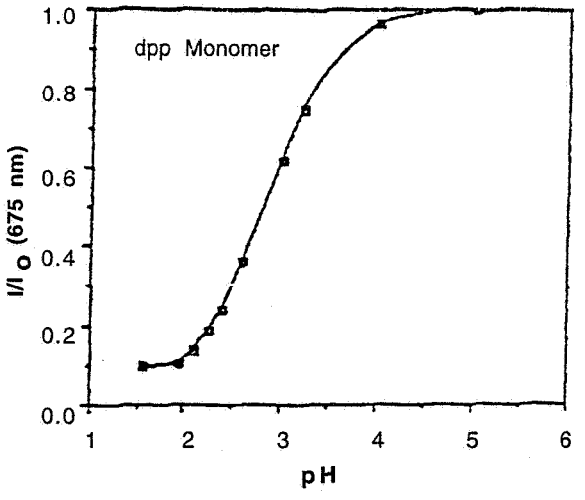

(c) Relative emission vs. pH for $Ru(dpp)_3^{2+}$

Figure 3-20
Spectroscopic properties of ruthenium complexes for CO_2 detection.

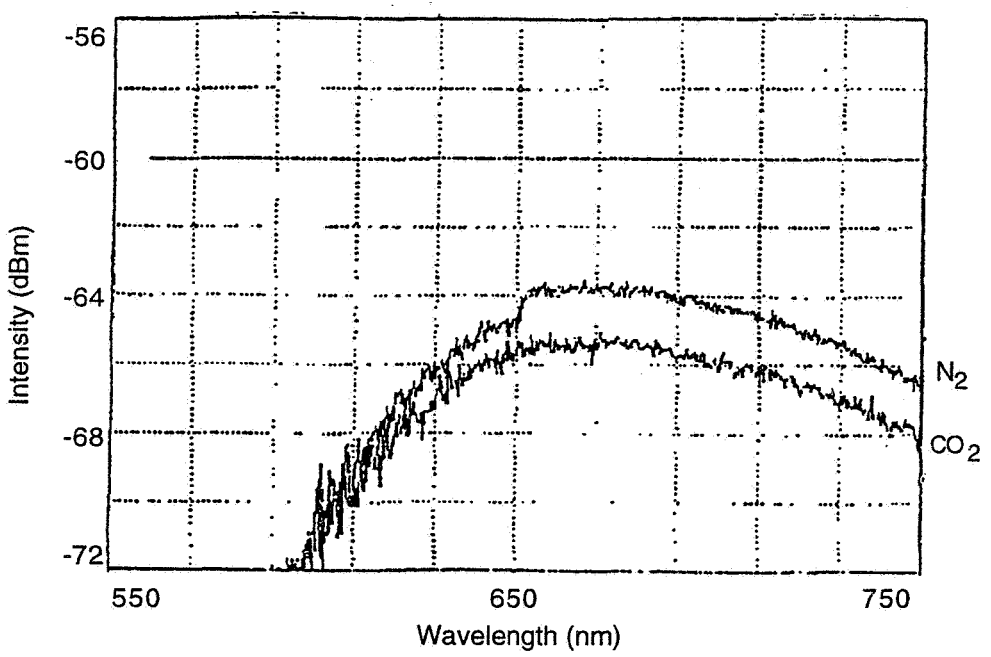

Figure 3-21
Luminescence intensity changes of $Ru(pzth)_3^{2+}$ in aqueous medium. A 10^{-4} M solution was excited at 470 nm. For one million ppm CO_2, the intensity is changed by 4 dB.

3.7 Conclusion

POC's carbon dioxide sensor appears to be suitable for a short-term measurements (<5 days). Although this sensor will not meet long-term monitoring needs, the experience gained here establishes a necessary groundwork for future development efforts. The meta-cresol purple-based sensor will detect CO_2 for a short time. Table 3-5 shows the tentative specifications of our CO_2 sensor.

Table 3-5 Specifications for CO_2 Sensor

Detection Range	0% to 100%
Dynamic Range	0 - 5000 ppm
Temperature Range	15°C to 25°C
Humidity Range	60% to 95% RH
Response Time	<2 min
Drift	5% over 200 min
Operational Life	5 days
Storage Life	>1 year under nitrogen

4.0 RELATIVE HUMIDITY DETECTOR

4.1 Vycor Glass as an Intrinsic Moisture Sensor

An experimental test station was constructed for evaluating several types of fiber optic humidity sensors. The test station includes a compact capacitive-type humidity sensor (Survivor II relative humidity sensor, HY CAL Engineering) mounted inside the gas cell to be used for calibration of the fiber optic humidity sensors. The HY CAL sensor has a linear response, and was calibrated between 0% and 80% relative humidity (RH). The response time of the sensor was tested by passing wet and dry gas through the gas cell. The sensor's response time was approximately one minute when the relative humidity varied between 60% and 80%.

The first task toward developing an optical humidity sensor involved the characterization of porous Vycor glass. The Vycor we tested is commercially available from Corning, Inc. in 0.125 in. diameter rods. Initially, samples of Vycor were cleaned by placing them in a solution of methanol in an ultrasonic bath, rinsing them in water, and drying them under a nitrogen purge. Several of these sensors were then evaluated by exposing them to 60% and 80% RH. Broadband optical transmission spectra were measured through the sensors under both 60% and 80% RH. These sensors all showed response to changes in RH, but the results were inconsistent from sensor to sensor. In order to obtain repeatable results, we changed the sample preparation. First, the Vycor rods were placed in a hot hydrogen peroxide bath (H_2O_2) for one hour, and a then in hot distilled water for one hour. After cleaning, the rods were rinsed in boiling distilled water for one hour. Once the rods were cleaned, they were dried in an oven at 300°C. The samples were stored at 300°C until they were ready for testing.

The samples stored at 300°C showed much better repeatability in their RH response than earlier (unheated) samples. These samples showed an average maximum response of 3.9 dB from 60% to 80% RH at wavelengths between 430 nm and 445 nm. However, initial tests of the response time indicated that these sensors are very slow, taking ~28 minutes to get to 90% of full response.

Figure 4-1 shows a typical spectral change for a cleaned Vycor sensor exposed to 60% and 80% RH. From these results we concluded that: (1) storing the Vycor samples in a furnace at 300°C until they are used improves reproducibility from sample to sample; (2) untreated Vycor glass responds to 60% to 80% relative humidity; and (3) chemical treatment improves Vycor glass response time when exposed to RH.

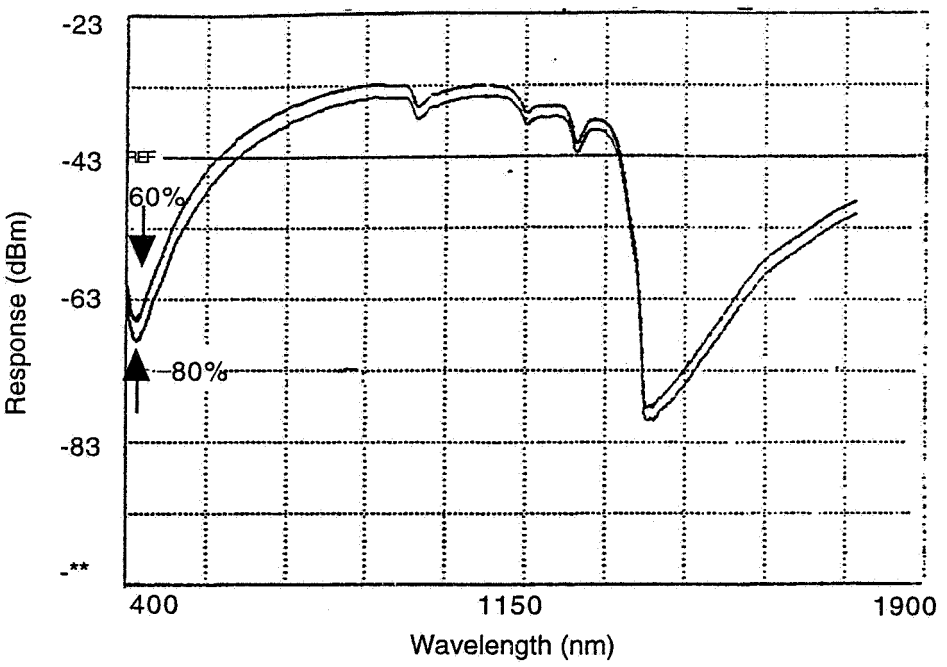

Figure 4-1
Change in optical transmission spectrum through a Vycor sensor at RH of 60% and 80%.

4.2 Etched Vycor Glass

In order to reduce the response time of these sensors, the Vycor samples were etched before cleaning. Three types of etching treatments were tested: (1) concentrated hydrofluoric acid (HF); (2) concentrated ammonia (NH_3); and (3) ammonium fluoride (NH_4F). HF is a strong acid and NH_3 is a strong base, while NH_4F is a weak acid. The procedure for etching consisted of immersing the glass rods in the etchant for a certain period of time, followed by extensive rinsing in hot water, followed by the cleaning procedure described in Section 4.1 above. HF reduced the outside diameter of the Vycor rods from 0.125 in. (3.1 mm) to ~0.025 in. (1 mm) in 5 to 10 minutes. The other two etchants, NH_3 and NH_4F, mildly etched the surface of the glass without noticeable loss in the diameter of the glass rods. All three of the etchants increased the diameter of the pores, allowing gases to pass more freely into the porous structure.

Each of the etched Vycor samples was tested for its response to RH changes between 60% and 80%. The results demonstrated that neither NH_3 nor NH_4F decreased the response time below 28 minutes. However, the samples etched with HF demonstrated a reduction in response time from ~28 minutes to ~4 minutes. This improved response time is attributed to the reduced diameter of the glass rod. The sensitivity of the HF-etched glass to RH was of the same order of magnitude as the untreated glass. Figure 4-2 illustrates the change in optical transmission for the HF-etched Vycor sensor. Note that the wavelength of maximum sensitivity shifted from ~430 nm for the untreated Vycor to ~530 nm for the etched Vycor. The conclusions drawn from these tests are: (1) HF can be used to reduce the diameter of porous Vycor glass rods, (2) smaller diameter Vycor rods produce faster response times, and (3) increasing the diameter of the pores does not improve the response time.

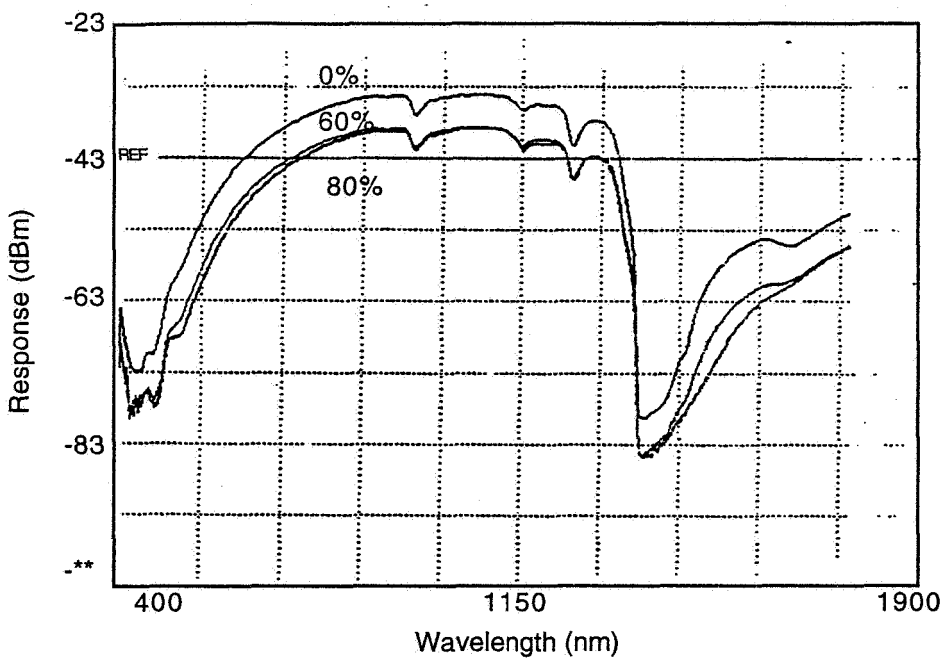

Figure 4-2
Optical transmission spectra through an HF etched Vycor sensor with 0%, 60%, and 80% RH.

Results of the Vycor sample tests indicate that the response time of the sensor mainly depends on the distance the water vapor must travel in the porous silica medium. In order to reduce the response time below four minutes, we tested porous optical fibers (~250 μm diameter) and thin films of porous sol-gel (~1.0 μm thickness) in a planar waveguide structure. Figures 4-3 and 4-4 illustrate the changes in optical transmission for the porous fiber and sol-gel sensors, respectively. The porous fiber showed a response time of approximately 1.0 minute, while the sol-gel film showed a response time of only six seconds. While these new sensors demonstrated improved response time, they also demonstrated decreased sensitivity. The maximum change in optical transmission was ~1.6 dB for the porous fiber and ~0.2 dB for the sol-gel sensors.

These results indicate that the response time of porous glass humidity sensors increased with the thickness of the porous material. Sol-gel films with a porous layer approximately 1.0 μm thick showed the best response, and therefore our investigation of the sol-gel approach was expanded.

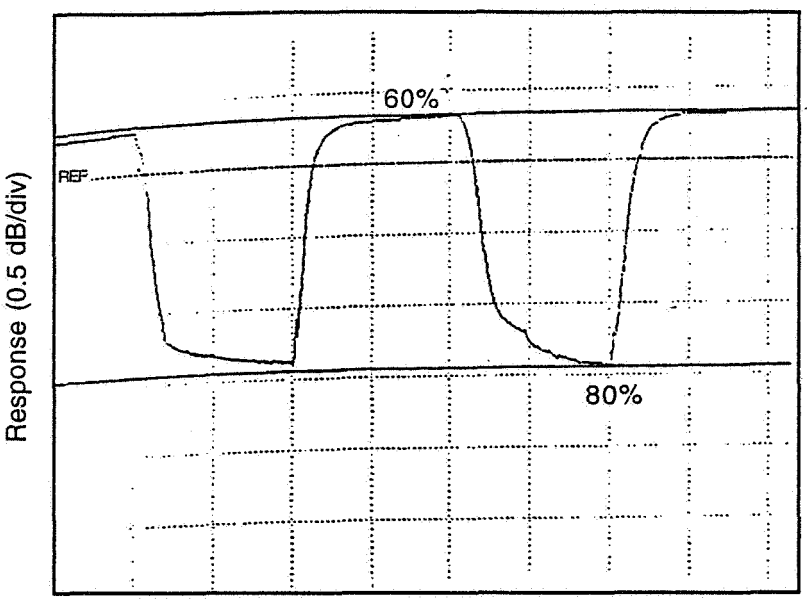

Figure 4-3
Optical transmission at 678 nm through a porous fiber sensor exposed to 60% RH and 80% RH.

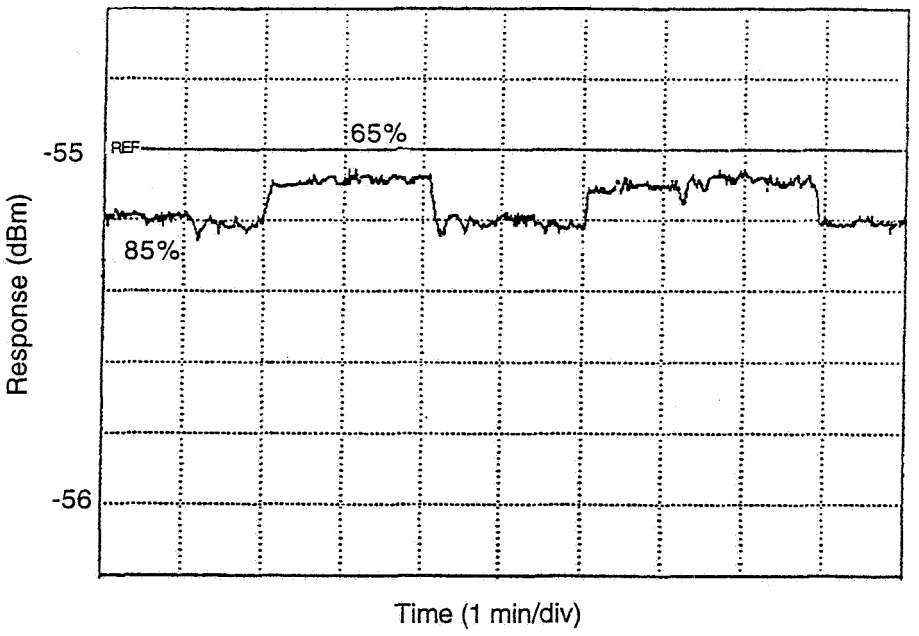

Figure 4-4
Optical transmission at 420 nm through a thin film sol-gel sensor exposed to 65% and 85% RH.

4.3 Sol-Gel Rod Relative Humidity Sensor

The sol-gel process for fabricating porous silica glasses involves mixing a silicon alkoxide [$Si(OR)_4$], water, and alcohol according to the following hydrolyzation reaction:

$$Si(OR)_4 + n\ H_2O \longrightarrow Si(OR)_{4-n}(OH)_n + n\ ROH. \quad (4\text{-}1)$$

R represents either a hydrogen atom or a ligand, and ROH is an alcohol. Soon after the hydrolysis reaction, condensation polymerization of the silica network begins. This is represented by the reactions:

$$Si(OR)_{4-n}(OH)_n + Si(OR)_4 \longrightarrow Si(OR)_{4-n}(OH)_{n-1}\text{-}O\text{-}Si(OR)_3 + ROH \quad (4\text{-}2)$$

and

$$2\ Si(OR)_3(OH) \longrightarrow (RO)_3Si\text{-}O\text{-}Si(OR)_3 + H_2O. \quad (4\text{-}3)$$

Once the gel silica network has been formed, the gel glass is heat-treated to remove the unwanted organics, yielding a porous silica glass network

$$(RO)_3Si\text{-}O\text{-}Si(OR)_3 \longrightarrow Si\text{-}O\text{-}Si + ROH. \quad (4\text{-}4)$$

Sol-gel porous fibers approximately 1.0 mm in diameter were fabricated according to the following experimental procedure: a sol-gel solution of a metal alkoxide, tetraethyl-ortho-silicate (TEOS), ethanol, and water was prepared using the following stoichiometric proportions:

Reagents	Mole %
TEOS	13.86
ETOH	51.85
H_2O	34.28

The sol-gel solution was mixed for 12 hours in order to complete the hydroxylation reaction. The solution was then transferred into plastic molds 2 mm in diameter × 10 cm long and allowed to polymerize and gel for two weeks, yielding solid porous glass rods ~2 mm in diameter. The glass rods were then transferred into heating crucibles and heat-treated using the heating cycle shown in Figure 4-5. This shrank the porous rods (or fibers) to ~1.0 mm in diameter × 5 cm in length.

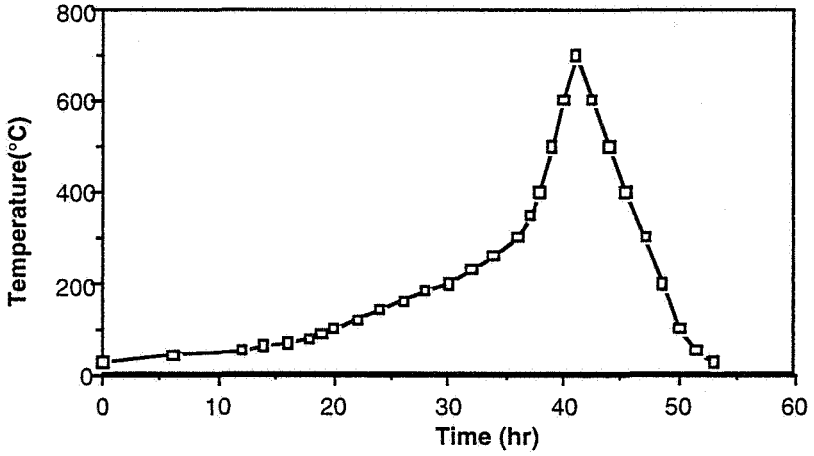

Figure 4-5
Sol-gel heating cycle.

The sol-gel solution described above was also deposited as a thin-film porous sol-gel cladding on a silica fiber. The fabrication procedure was as follows: a short segment (~3 cm to 5 cm) of a 400 μm silica core, plastic clad fiber was declad, using a torch to burn off the polymer cladding. The declad section of the fiber was then cleaned and coated with a thin sol-gel film using the apparatus shown in Figure 4-6. The sol-gel solution is placed inside the plastic cylinder, in which the bottom orifice is approximately the same dimension as the clad fiber (~400 μm). The fiber is then pulled, using a weight at the end. As the declad section of the fiber passes through the sol-gel solution, it is coated with a thin film, which is then rapidly dried with hot air guns. The sol-gel cladding did not bond well with the optical fiber.

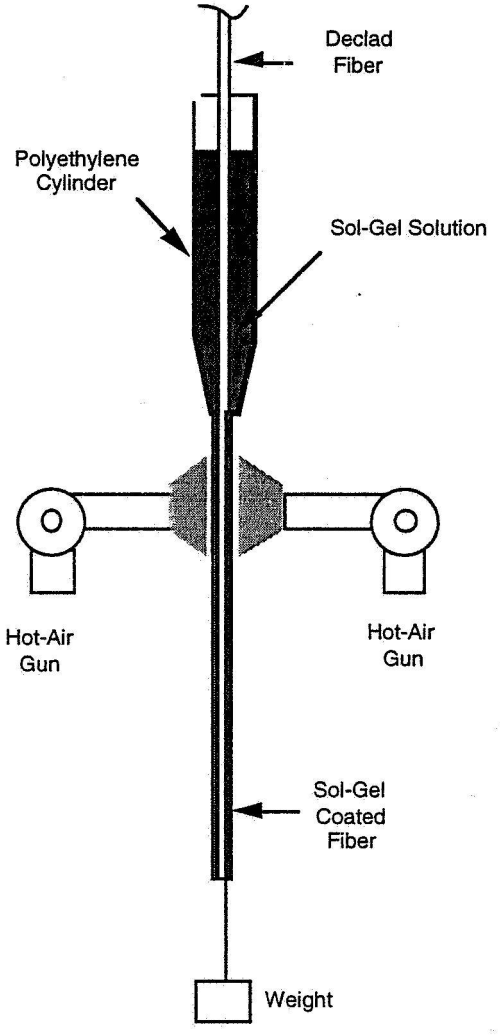

Figure 4-6
Sol-gel fiber cladding apparatus.

4.4 Indicator-Based Humidity Sensor

Because humidity changes the color of certain indicators, we selected four potential dyes: (1) cobalt chloride ($CoCl_2$), (2) Reichardt's dye (2-6-diphenyl-4-(2-4-6-triphenyl-N-pyridino)phenolate), (3) merocyanine 540, and (4) rhodamine 6G. These dyes were selected on the basis of literature describing their spectroscopic properties in the presence of humidity.

Polymeric films of the dyes were dispersed in polyvinyl acetate (PVAc). A typical film was prepared by dissolving the polymer (PVAc) in acetone and adding the indicator to the polymer solution. Typically, a 0.1 M solution of the dye in a 5% solution of PVAc in acetone was prepared. This solution was stirred for approximately 12 hours on a hot plate at 40°C in order to produce a homogeneous solution. Films were prepared by dispersing 1.0 ml of the polymer mixture on a glass microscope slide and then evaporating the acetone from the film.

Once the films were prepared, they were tested for their response to relative humidity using the experimental apparatus shown in Figure 4-7. Preliminary tests on films containing $CoCl_2$ and merocyanine 540 showed no optical response to changes in humidity from 0% to 100% RH. However, films containing both the Reichardt's dye and rhodamine 6G (R6G) showed optical changes on exposure to changes in humidity from 0% to 100% RH. Because the R6G films showed the largest optical absorption changes, we characterize this dye first.

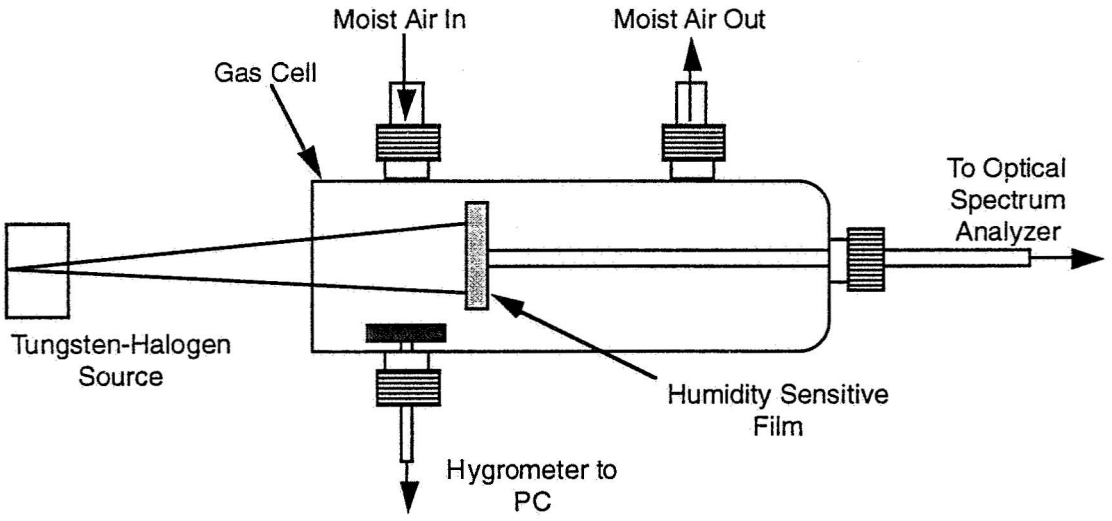

Figure 4-7
Experimental apparatus for RH testing.

Figure 4-8 shows the optical spectrum of an R6G/PVAc film on exposure to changes in RH from 0% to 60% and 80%. From these data, it was determined that the maximum optical absorbance change occurs at 531 nm. Several experiments were performed with films prepared from the same solution. Each of these films responded in a manner similar to the film shown in Figure 4-8. Furthermore, these films were cycled back and forth between 60% and 80% RH to determine the response time and sensitivity, as shown in Figure 4-9. From this figure, it can be seen that a

change in optical power of 0.6 dBm with a response time of approximately 2 minutes was measured.

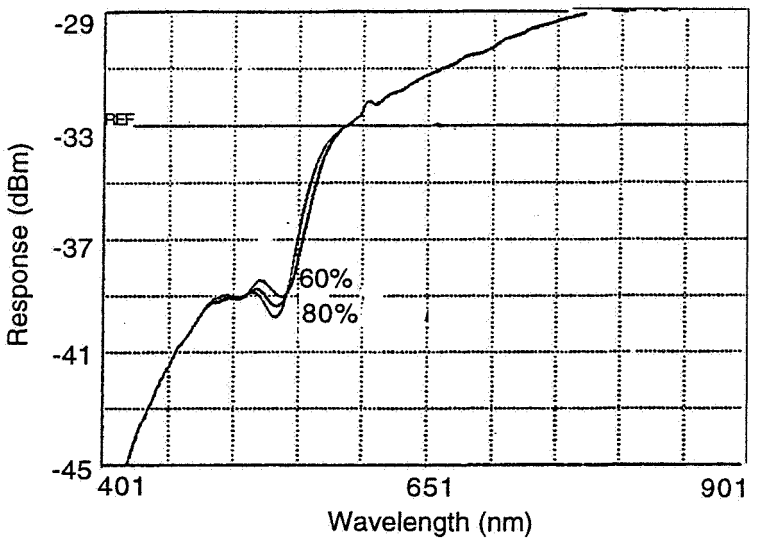

Figure 4-8
Optical spectrum of a rhodamine 6G/PVAc film as a function of changes in the relative humidity of the test cell.

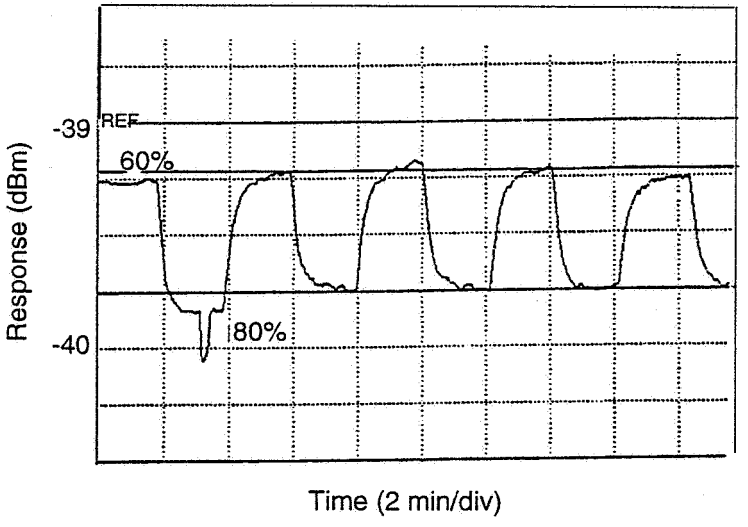

Figure 4-9
Step plot of a rhodamine 6G/PVAc film subjected to changes in relative humidity from 60% to 80% RH (measured at 530 nm).

4.4.1 Rhodamine 6G as an Indicator

In order to increase the sensitivity and response time of the R6G RH sensor, a multilayer sensor approach was developed. A stack of thin glass slides, each coated with a humidity-sensitive thin film of the indicator-doped polymer 5 μm to 10 μm thick, was mounted to an optical fiber and analyzed for its response to relative humidity. The experimental set-up is shown schematically in Figure 4-10.

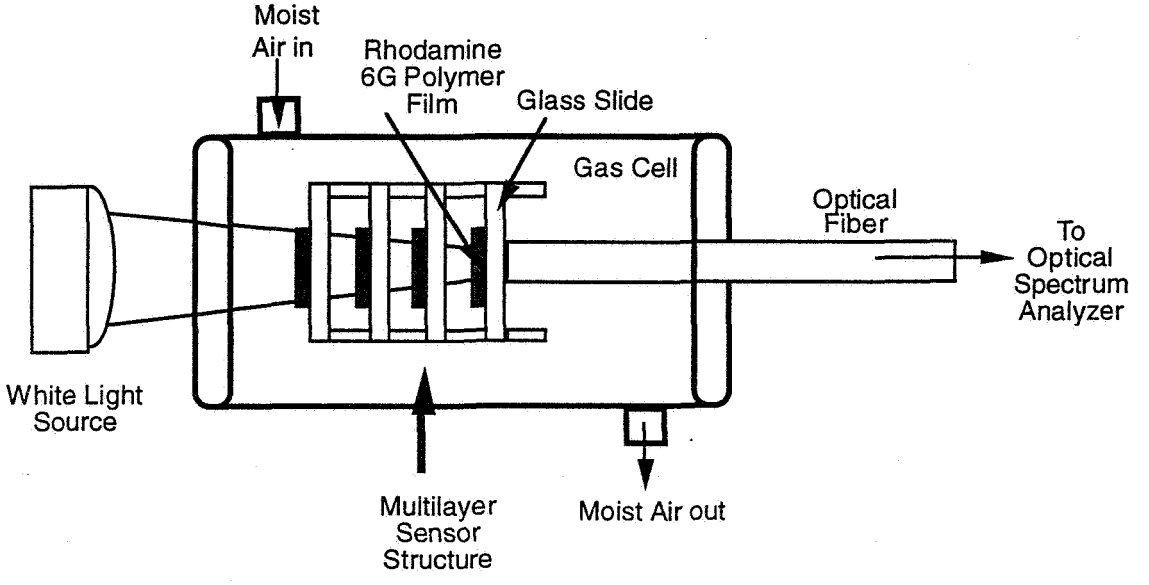

Figure 4-10
Schematic diagram of multilayer RH sensor structure.

Once the thin films were fabricated, they were stacked in a multilayer array with a typical spacing between layers of 1 mm to 2 mm. Then the sensor array was mounted at the tip of a 600 μm diameter optical fiber. Several multilayer sensors similar to the one shown in Figure 4-10 were then tested for their response to relative humidity. The results of these experiments are shown in Figures 4-11 and 4-12.

From these results it was observed that the sensitivity and response speed of the sensor increased as the number of layers increased. For example, in the four-layer sample the optical sensitivity to humidity for changes between 60% and 80% RH was 1.3 dB, while the response time was 1.5 minutes. For the eight-layer sensor structure, the sensitivity was 6.5 dB, with a response time of 18 seconds. From these results it was concluded that a highly sensitive, fast-responding humidity sensor could be produced using R6G as the indicator.

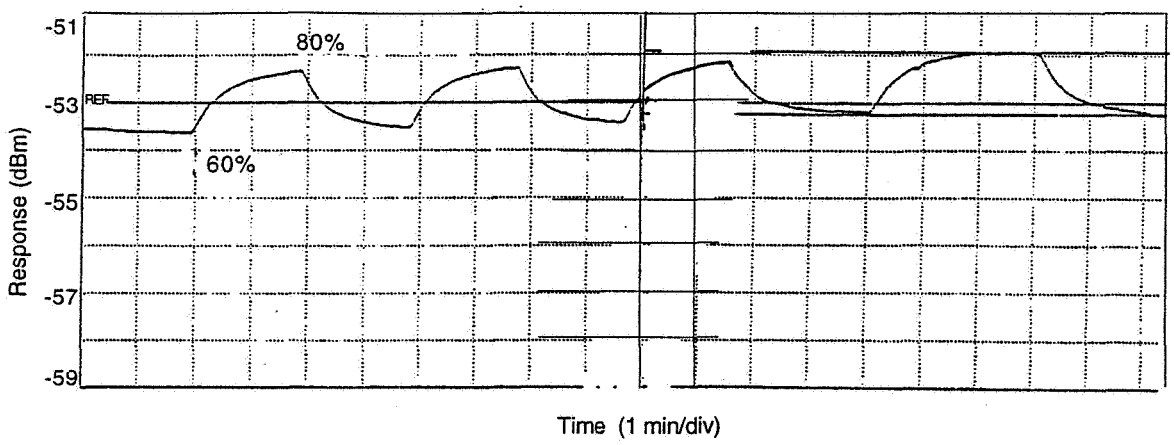

Figure 4-11
Response at 530 nm of a four-layer sensor structure to changes in humidity between 60% and 80% RH.

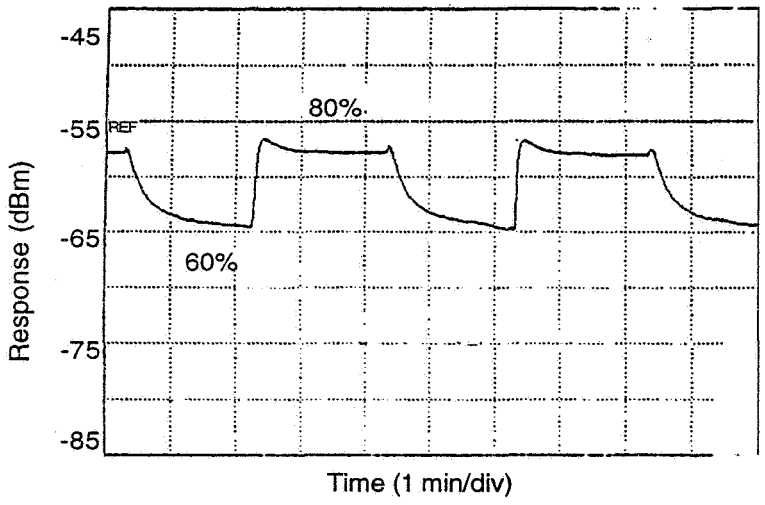

Figure 4-12
Response at 410 nm of an eight-layer sensor structure to changes in humidity between 60% and 80% RH.

Further characterization of this sensor, however, has shown unsatisfactory long-term behavior. Long-term testing was performed by exposing the sensor to repeated changes between 60% and 80% RH for a period of 3.8 hours. The relative humidity was cycled back and forth approximately every 6 minutes. Results from this experiment are shown in Figure 4-13.

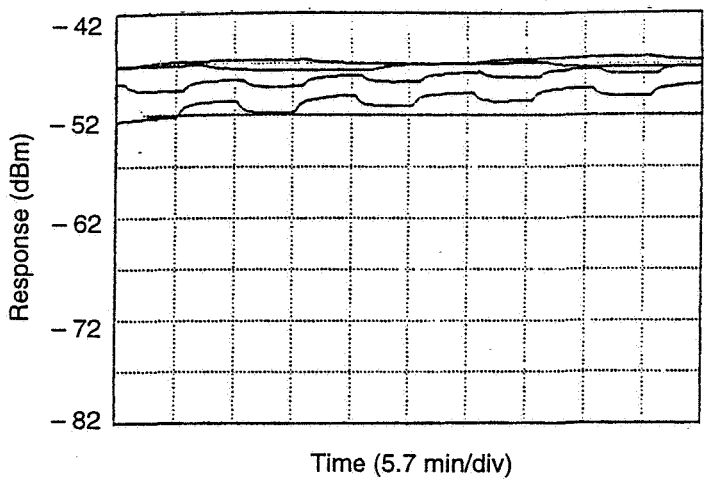

Figure 4-13
Long-term response at 556 nm to changes in relative humidity between 60% and 80% of a rhodamine 6G multi-layer humidity sensor (5.7 min/div; 4 traces totaling 3.8 hours).

These four traces illustrate that the sensor loses its sensitivity to humidity after a period of approximately 2 hours. It also shows that total signal strength increased over the same period. Both of these effects can be attributed to photobleaching of the R6G. In order to reduce the amount of photobleaching, an experiment was conducted using a low-power, narrow-bandwidth source (previous experiments had been conducted using a broadband tungsten-halogen source). The source was an LED with peak power at 556 nm and a full width at half maximum output of 40 nm. The sensor was illuminated for 24 hours. This experiment demonstrated that the photodegradation was reduced, but not eliminated. Over the 24-hour test, the absorption peak of R6G again decreased by ~10 dB as shown in Figure 4-14. These experiments led to the conclusion that photobleaching of R6G by the analyzing light source severely affects the response of the sensor. Consequently, this sensor was not selected for further development.

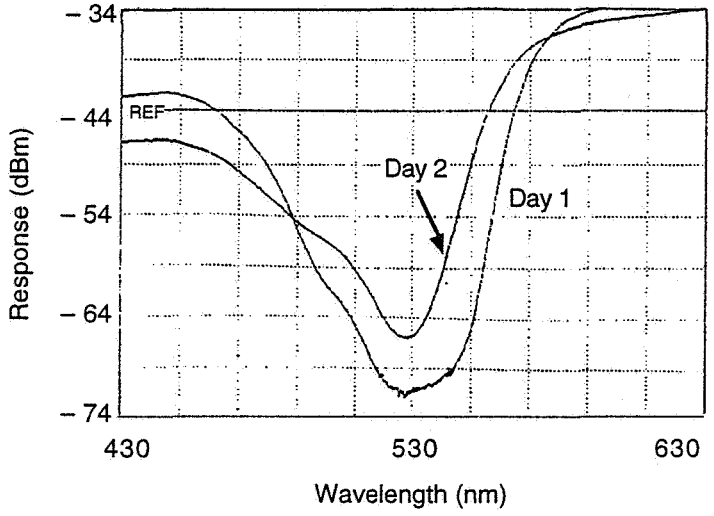

Figure 4-14
Optical spectrum of Rhodamine 6G multilayer humidity sensor before and after 24 hour exposure to a low intensity light source.

4.4.2 Reichardt's Dye Sensor

Another humidity indicator, Reichardt's dye, was evaluated for its response to changes in relative humidity. Reichardt's dye is a solvatochromic indicator that exhibits a reversible bathochromic shift in its absorption spectrum in the presence of humidity. The wavelength of maximum sensitivity to humidity for this indicator was determined to be 700 nm. A Reichardt's dye sensor was prepared by dissolving 100 mg of the indicator in a PVA/acetone mixture, made by dissolving 5 gr of PVA in 100 ml of acetone. The indicator/polymer mixture was stirred for 12 hours to produce a homogeneous mixture. Once the polymeric mixture was ready, a multi-layer sensor was fabricated. The Reichardt's dye sensor demonstrated an optical response of 2.8 dB (compared to the 8.5 dB for the R6G sensor) to changes in RH between 60% and 80% as shown in Figure 4-15.

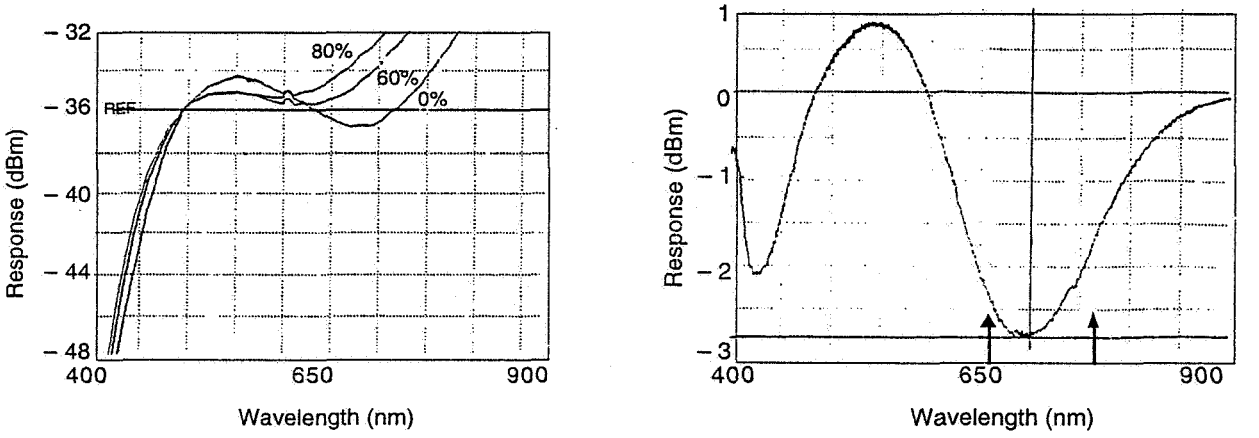

(a) 0%, 60%, and 80% RH

(b) Difference between response at 60% RH and 80% RH

Figure 4-15
Spectral changes of Reichardt's dye upon exposure to humidity.

A 48 hour experiment was then conducted to observe the long term response of the Reichardt's dye sensor. Results are shown in Figures 4-16 and 4-17. This experiment determined that, like the R6G, the Reichardt's dye photodegraded over time. The absorption peak of the indicator was completely photobleached after the 48-hour test. Once again, in order to further characterize the photobleaching effect of the indicator, a narrowband light source -- a 678 nm laser diode -- was used to analyze the sensor. In addition, a red polyester filter was used to attenuate the laser diode emission before it reached the optrode. Results of this experiment demonstrated that after a 12-hour exposure the absorption peak of Reichardt's dye was completely photobleached. Hence, like the R6G indicator, the Reichardt's dye indicator was not selected for further sensor development.

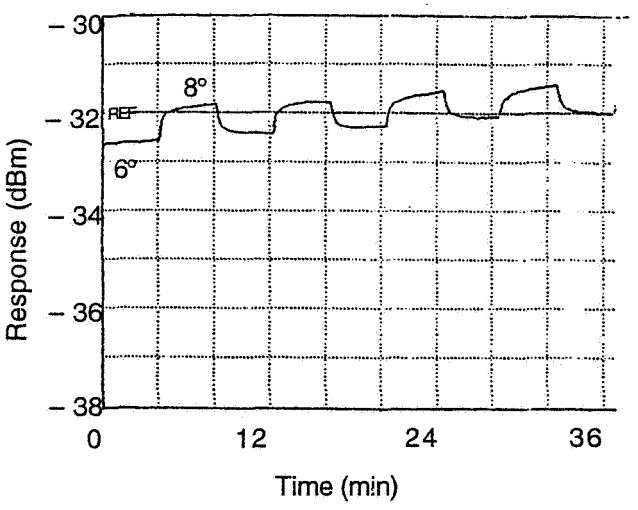

Figure 4-16
Long term response to changes in relative humidity between 60% and 80%
of Reichardt's dye sensor (four layers; x-axis: 4.0 min/div)

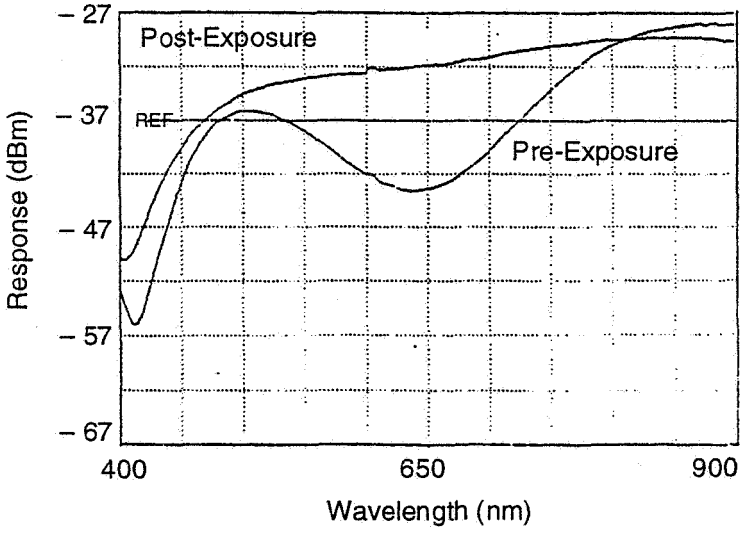

Figure 4-17
Long term light exposure of Reichardt's Dye sensor
(48 hour exposure to a low intensity laser diode; $\lambda = 678$ nm).

4.5 Redesigned Porous Glass Sensor

4.5.1 Sol-Gel Porous Glass Sensor

We completed our long-term stability characterization of all of the humidity sensors fabricated, (porous glass and indicator-based) by returning to the porous fiber sensor and analyzing its long-

term response. A 250 μm diameter porous fiber, 4.5 cm long, was mounted in line as shown in Figure 4-18 and tested for repeated changes in relative humidity between 60% and 80%.

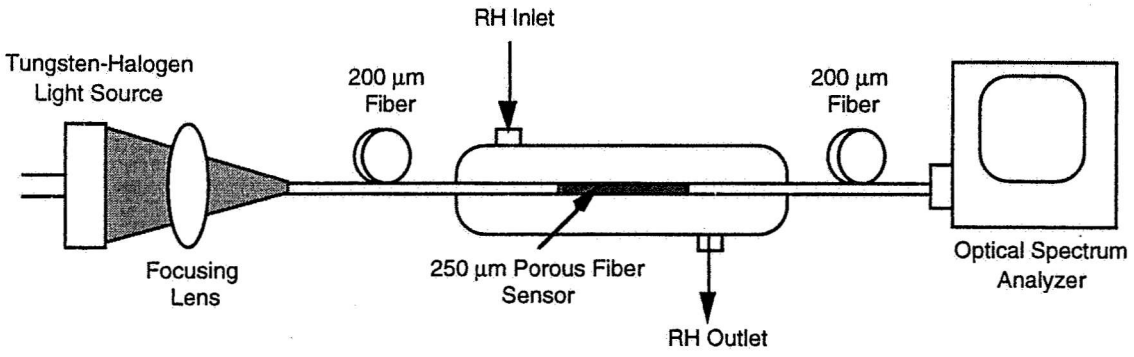

Figure 4-18
Experimental setup for measuring the relative humidity response of an in-line porous fiber sensor.

Preliminary experiments determined that 410 nm was the wavelength at which the fiber was most responsive to changes in RH between 60% and 80%. A 16-hour experiment was conducted to determine the long-term stability of the fiber, with the results shown in Figure 4-19. In that test, the RH was switched between 60% and 80% every 16 minutes. These tests show some drift in signal strength, but no photodegradation.

Before testing, the fiber showed a response of 12.7 dB to changes between 60% and 80% RH. At the end of the 16 hour run, the fiber still showed a response of ~12.0 dB. In the course of the 16 hour run, the change in signal varied from a minimum of 6.2 dB to a maximum of 14.1 dB. The average response was calculated to be 8.05 ± 1.79 dB. The standard deviation was calculated to be 22%.

From all the experiments carried out to date with several types of porous glasses, (i.e., porous fiber, Vycor glass, and sol-gel glasses), and with several different colorimetric indicators (i.e., cobalt chloride, Rhodamine 6G, and Reichardt's dye), it has been determined that the porous fiber sensors produced the best results in terms of long-term stability and reproducible response to changes in relative humidity between 60% and 80%.

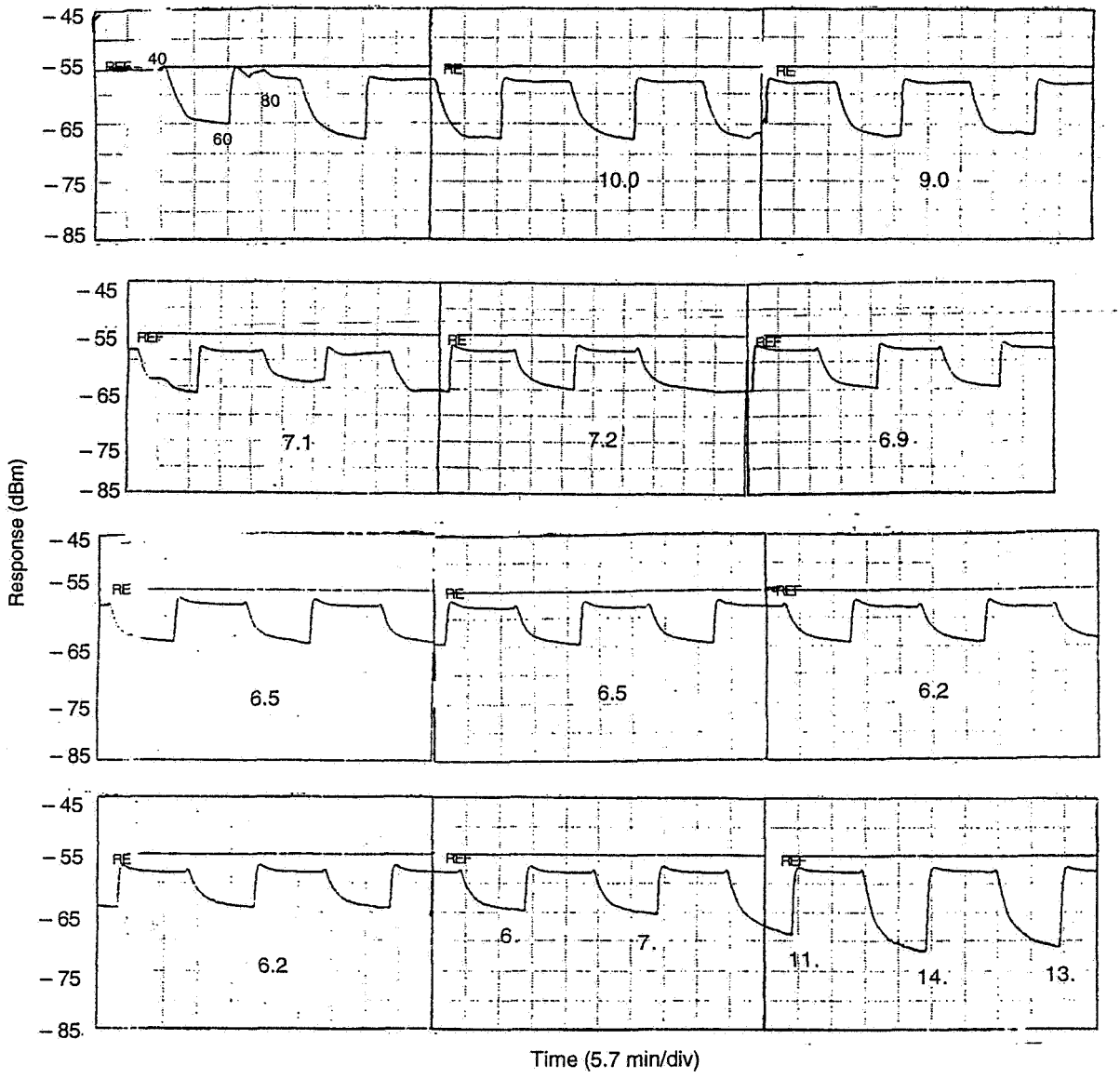

Figure 4-19
Long-term response at 410 nm to changes in relative humidity between 60% and 80% of a 250 μm diameter porous fiber. The entire duration of the 16 hour test is represented by the four frames. The topmost frame shows the first segment.

4.5.2 Porous-Coating Fiber Humidity Sensor

Work next focused on the design and fabrication of several types of porous optical fibers. Previous experimental results had shown that thinner porous silica films have much faster response times (see Table 4-1). These results indicated that both the response time and the sensitivity of the sensor were highly dependent on the thickness of the porous region. Consequently, it was decided to design a new fiber sensor with an active porous region having a thickness somewhere between 1 μm and 200 μm.

Table 4-1 Porous Silica Sensor Response to Changes in Relative Humidity between 60% and 80%

	Sol-Gel Thin Film (<1 μm)	200 μm Porous Fiber
Intensity change from 60% to 80% RH (dB/m)	0.2	~8
Response time (sec)	6	60

Several porous fiber designs were developed and sent for evaluation to our consultant, Dr. Shahriari of Rutgers University. Two porous fiber designs were produced: fibers with variable thickness porous cores (Figure 4-20(a)); and fibers with a 10 μm thick porous cladding (Figure 4-20(b)).

The advantage of the design shown in Figure 4-20(a) is that the porous section of the fiber is directly in the optical path. This direct interaction ensures ample sensitivity to changes in relative humidity. This design is a modification of the previously used 200 μm porous fiber (Table 4-1), in which the entire core diameter was porous. Reducing the thickness of the porous section of the core shortens response times.

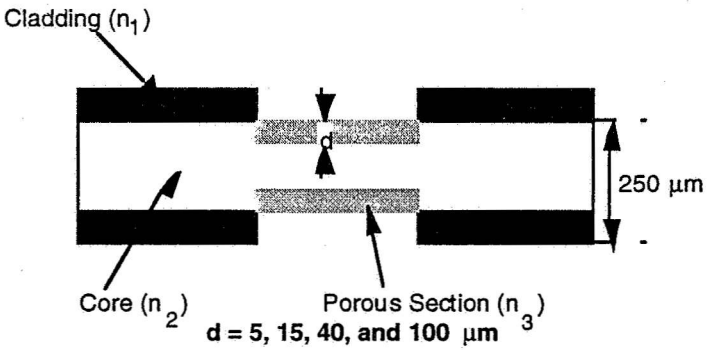

(a) Partially porous core

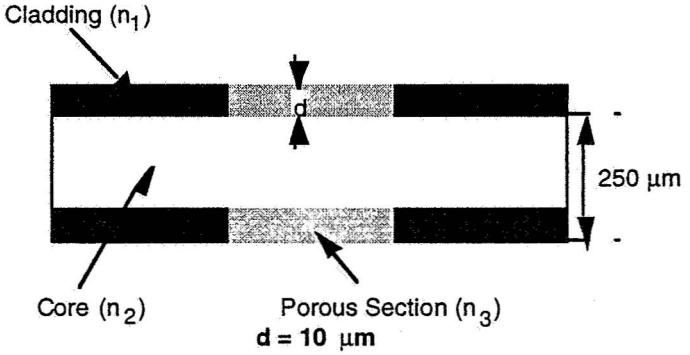

(b) Porous cladding

Figure 4-20
Porous fiber designs.

In the second fiber design, (Figure 4-20(b)), the active porous region is the cladding of the fiber. In this design we wanted a fiber with ≤10 μm porous cladding, since thicker claddings did not increase sensitivity to moisture and did slow response time. Mathematical modeling of this optrode design showed that the optical interaction with the cladding was solely due to evanescent fields in the cladding (Figure 4-20(b)). From a previously developed mathematical model, we knew that light in the evanescent field of an optical fiber typically penetrates less than 1 μm into the cladding. In summary, we designed four fibers of type (a), with pore thicknesses of 5, 15, 40, and 100 μm.

Dr. Shahriari evaluated our designs and concluded that with his existing facilities he is only able to fabricate the porous cladding fiber (Figure 4-20(b)), and he did produce fibers with a 10 μm porous cladding. He supplied the new fibers in a brass housing, as shown in Figure 4-21 with SMA fiber optic connectors that allow the sensor element to be coupled rapidly through fiber optic cables to light sources and detectors. Furthermore, the porous fiber was protected from the environment by the porous brass housing. This housing was highly permeable to moisture, while potentially preventing biofouling accumulation in the porous region of the fiber sensor.

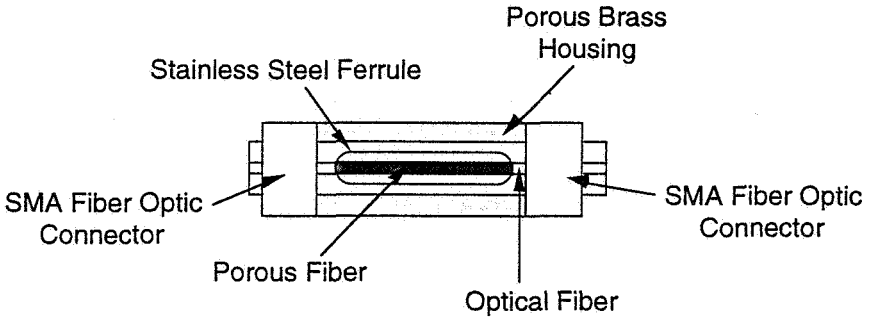

Figure 4-21
Porous fiber packaging.

POC assembled a dip-coating apparatus (Figure 4-22), which allowed us to coat sol-gel porous films onto unclad glass fibers. With this apparatus we expected to clad optical fibers with porous silica ranging in thickness from 0.5 μm to 5 μm. Unclad optical fibers with a high index of refraction (n = 1.58) were obtained from Cuda Products Corporation. These fibers were coated by spooling the fiber through a sol-gel solution and then heating them rapidly. The thickness of the cladding was controlled by using a variable speed motor. These fibers and the new Rutgers porous fibers were evaluated for their response to humidity, and the results were compared. Tests with these fibers did not show any improvement in performance over Vycor glass.

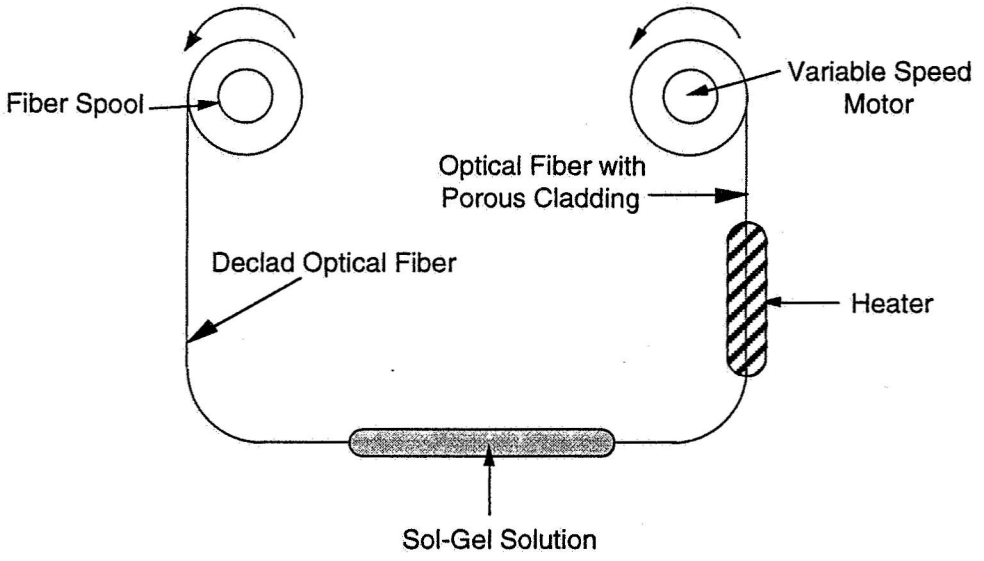

Figure 4-22
In-line sol-gel dip coating apparatus.

While an indicator-based relative humidity sensor has the potential to be a sensitive device, porous glass optrodes were found to have faster response times, wider dynamic range, and less drift. Based on our findings, the specifications in Table 4-2 were arrived at tentatively for the humidity sensor.

Table 4-2 Performance Specifications for the Humidity Sensor

Detection Range	10% to 100% RH
Dynamic Range	60% to 80% RH
Temperature Range	15°C to 25°C
Response Time	<5 minutes
Drift	22% drift in 16 hours
Operational Life	~1 year

4.6 Biofouling Tests

A report on biofouling tests performed at POC and NASA Ames Research Center is included as an Addendum to this report.

5.0 COMMERCIALIZATION

Over the course of the project, POC has been in contact with several companies, discussing the application of the oxygen and carbon dioxide sensors in various fields. From our research, it is

apparent that rugged and reliable oxygen and carbon dioxide sensors that withstand temperatures as high as 100°C are needed in the field of bioremediation.

We are in the process of developing manufacturing and distribution relationships with companies that are recognized as reliable suppliers in the bioremediation field. Completion of these arrangements will give POC access to the market, and will establish our credentials as a supplier of reliable and cost effective oxygen and carbon dioxide sensors.

In addition to the activity in the bioremediation field, we have been seriously pursuing other applications, including the regenerative food production field.

6.0 REFERENCE

1. Mills, A.; Chang, Q.; McMurray, N. Equilibrium Studies on Colorimetric Plastic Film Sensors for Carbon Dioxide, Anal. Chem. 1992, *64*, pp. 1383-1389.

APPENDIX A
CO_2 Sensor Calibration

In order to improve our ability to predict CO_2 concentration from the raw data (in "A/D units") collected during optrode testing, a simple calibration/temperature compensation algorithm was developed. This algorithm is embodied in Eq. (A-1).

$$C = kTR - B \qquad \text{(A-1)}$$

where

C = computed CO_2 concentration
R = "raw" A/D data
T = temperature inside test cell
k = calibration constant
B = baseline correction factor.

To implement this algorithm, and to determine the values of the calibration constant and baseline correction factor, the following four operations were performed on the data:

1. Baseline subtraction
2. Temperature Compensation
3. Scaling
4. Final Baseline Correction

A.1 Baseline Subtraction

During the data collection process, a constant value, arbitrarily set to move the A/D values to the center of the range of the A/D board, was added to all data. The precise value of this additive constant was not recorded. Thus, it was necessary to compensate for an unknown, fixed, offset. The first step in this process was to subtract M, the global minimum value of the data set, from each point within the data set. This had the effect of resetting the baseline of the data from approximately 800 "A/D units" to zero.

A.2 Temperature Compensation

Careful inspection of Figures 3-10 and 3-11 shows that the periodic variation in CO_2 response is almost perfectly anticorrelated with the temperature variation. Furthermore, the humidity variation in the test chamber was also anticorrelated with the temperature variation, with the introduction of a slight time lag. We therefore decided to use test cell temperature as the independent variable in compensating CO_2 sensor response for environmental effects.

Temperature compensation was accomplished using the following steps:

(1) The temperature variation data was smoothed by using a 15-point running average. This was necessary to avoid introduction of thermocouple "noise" into the temperature-compensated data.

(2) After the first stage of baseline correction (Baseline Subtraction, Step 1 above), each point of the baseline-subtracted CO_2 sensor data was multiplied by its corresponding average temperature value.

A.3 Scaling

To determine the scaling factor, a very simple process was used:

(1) The average value of the temperature-corrected data for all signals corresponding to 5265 ppm CO_2 was computed.

(2) The average value of the temperature-corrected data for all signals corresponding to 330 ppm CO_2 was computed.

(3) The scaling factor was computed as follows:

$$k = (k_1 - k_2) / (5265 - 330) \qquad \text{(A-2)}$$

where

k_1 = average value computed in step (1) above
k_2 = average value computed in step (2) above.

A.4 Final Baseline Correction

Final baseline correction was accomplished by adding 330 - k_2 to all data points. This process had the effect of bringing to 330 the average value of the corrected data points corresponding to 330 ppm CO_2, and bringing to 5265 the average value of the corrected data points corresponding to 5265 ppm CO_2. It can be shown that, with this final adjustment, the baseline correction factor, B, in (A-1), is given by

$$B = kM + k_2 - 330 \ . \qquad \text{(A-3)}$$

A.5 Final Sensor Calibration

It should be noted that, while the above process has the effect of correcting the baseline of the data and bringing the range of the data into agreement with the range of carbon dioxide concentrations measured, it does not result in a complete mathematical procedure for the calibration of the optrode response. This could be accomplished by fitting an empirically derived mathematical expression to the corrected calibration curve shown in Figure 3-14. This is more convenient, but essentially equivalent, to simply using the individual values in the spline-fit smoothed curve shown in

Figure 3-14 in a "look-up" table relating actual carbon dioxide concentrations to the corrected data values obtained by following the procedure outlined in Sections A-1 through A-4.

Lightweight Fiber Optic Gas Sensor for Monitoring Regenerative Food Production

Contract No. NAS2-13887
Period of Performance: 8/29/93 to 12/19/95

Addendum to Final Report:
Biofouling Study

Presented to:

NASA-Ames Research Center
Moffett Field, CA 94035

Technical Monitor:

Ann McCormack

Contractor:

Physical Optics Corporation
Research and Development Division
20600 Gramercy Place, Suite 103
Torrance, California 90501
(310) 320-3088

Principal Investigator:

Edward Schmidlin

December 18, 1995

1.0 EXECUTIVE SUMMARY

Because of potential interference from microbes in the plant growth chamber, steps were taken to evaluate the degree of biofouling on five optrodes, and how it affects their light transmission properties. The optrodes were characterized in terms of their light transmission, and their luminescence properties both before and after exposure in the plant growth chamber. Although changes in the light transmission properties were observed, no definite link could be established to biofouling. The optrodes were found to retain the luminescence characteristics necessary for measuring oxygen concentrations in the plant growth chamber.

2.0 BIOFOULING ASSESSMENT

Our evaluation focused on determining the degree of biofouling inside the plant growth chamber. Two methods were used to evaluate the degree of biofouling:

1. Inspection of the optrodes under a microscope both before and after the biofouling tests

2. Testing the optical characteristics of the optrodes to their respective target analytes both before and after the biofouling tests.

In addition, arrangements were made with NASA Ames Research Center to evaluate biofilm generation on various substrates, including the optrodes. The following procedure was developed for the tests.

Test Procedure:

1. Optrodes were tested and inspected under a microscope before being sent to NASA Ames. All optrodes were made of Vycor (porous silica), and some were impregnated with ruthenium-based oxygen indicator. The optrodes were 5 mm long and 3 mm in diameter.

2. The optrodes were sent to NASA Ames in a sealed container. All optrodes underwent the same treatment at NASA Ames: They were placed close together inside a plant growth chamber. The optrodes were then removed from the chamber and shipped back to POC in separate sealed containers to prevent growth from spreading.

3. The optrodes were tested immediately upon their return to POC. They were put through the same tests as before they were sent to NASA, including post-test inspection.

Samples tested at POC:

Quantity	Ruthenium	Support Pieces	Housing
2	N	2	0
2	Y	2	0
2	N	2	2-40 µm brass
2	Y	2	2-40 µm brass
2	N	0	2-polymer
2	Y	0	2-polymer

Dr. Devendra Kumar was assisting POC in preparing optrodes for exposure in a plant growth chamber at NASA Ames. His departure from NASA and equipment failure problems led to an unexpected delays in executing the scheduled tests.

After the optrodes were returned to POC two tests were performed to evaluate the sensor characteristics.

1. Using the white light source of the Ando optical spectrum analyzer, the absorbance characteristics of the optrodes were recorded over the range from 400 nm to 1400 nm. Figures AA-1 through AA-5 (in the Appendix to this Addendum) show the spectra.

2. Using a UV light source to excite the optrodes, we recorded the emission characteristics of the optrodes over the range from 500 nm to 700 nm. Figures AA-6 through AA-10 show the emission spectra.

The optrodes labeled as Ames 1, Ames 2, Ames 7, Ames 8, and Ames 10 were sent back to NASA-Ames. They were in the plant growth chamber for about a month, and were than shipped back to POC, where they were tested again. Figures AA-11 through AA-15 represent the absorption spectra and Figures AA-16 through AA-20 the emission spectra.

2.1 Conclusion

Close scrutiny of their light transmission characteristics reveals that all five optrodes exhibit a pronounced change in intensity in the 500 nm to 700 nm range. Although the number of peaks remains the same in the 850 nm to 1400 nm region, the relative intensities of the peaks changed when the optrodes were incubated in the plant growth chamber. Some fouling has obviously taken place, although we cannot determine from our data whether the fouling is biological in nature. It could be predicted that deposition of biological materials would diminish light transmission in the UV-visible region. The spectral measurements show otherwise.

Comparison of the emission spectra is less meaningful, because the UV lamp was not equipped to generate a constant output. Visually, we did not observe any difference in the glow of the optrodes. The optrodes did exhibit their characteristic luminescence even after the biofouling experiments. Thus, we determine that the optrodes are still sensitive to oxygen. Resources did not allow us to explore the calibration parameters before and after the biofouling tests.

ADDENDUM APPENDIX AA
Biofouling Test Data

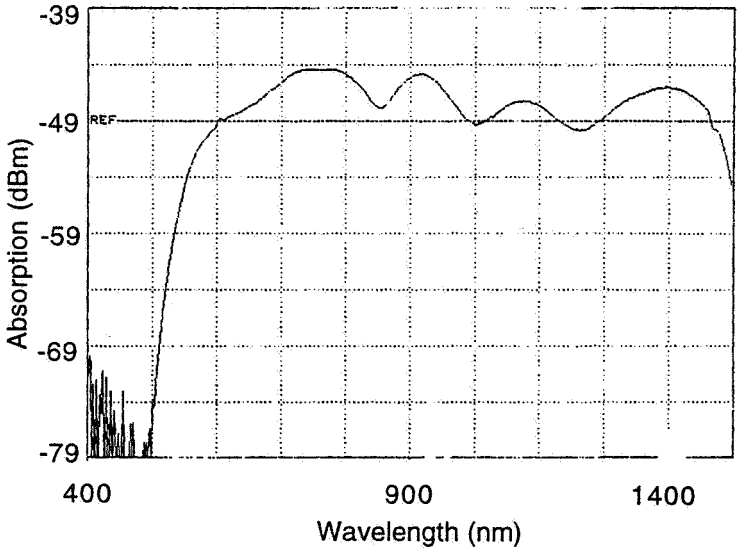

Figure AA-1
Absorption spectrum of the optrode labeled as Ames 1.

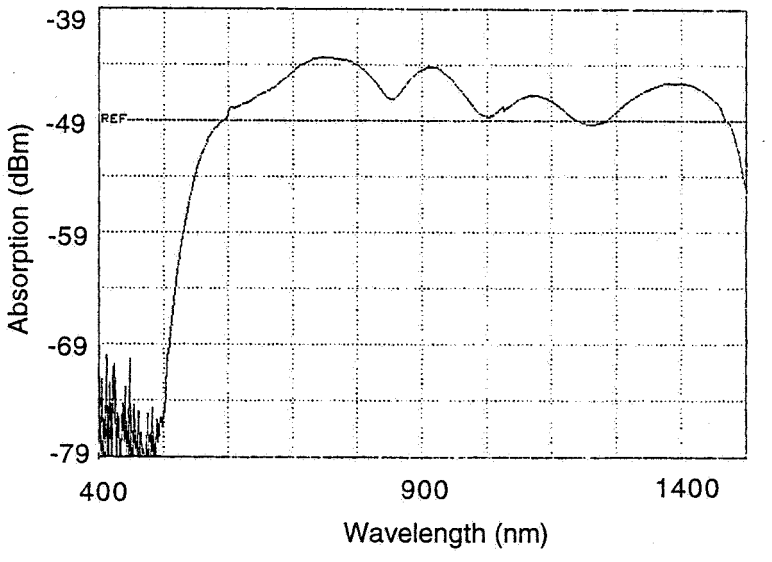

Figure AA-2
Absorption spectrum of the optrode labeled as Ames 2.

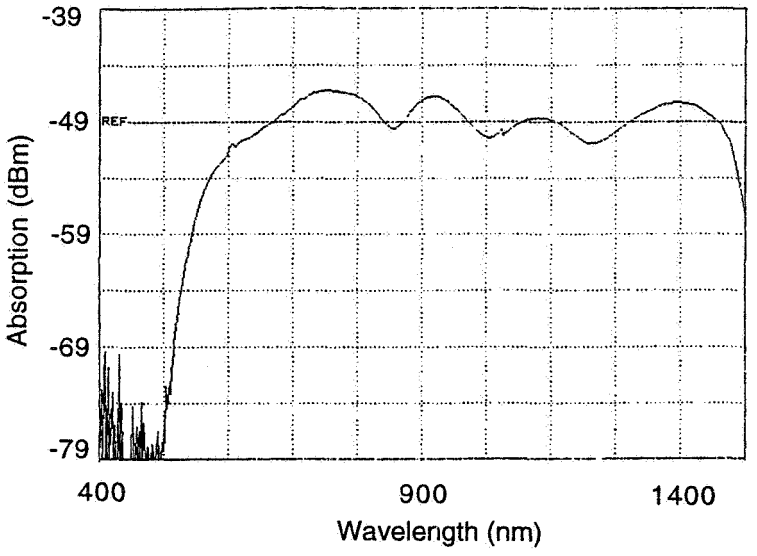

Figure AA-3
Absorption spectrum of the optrode labeled as Ames 7.

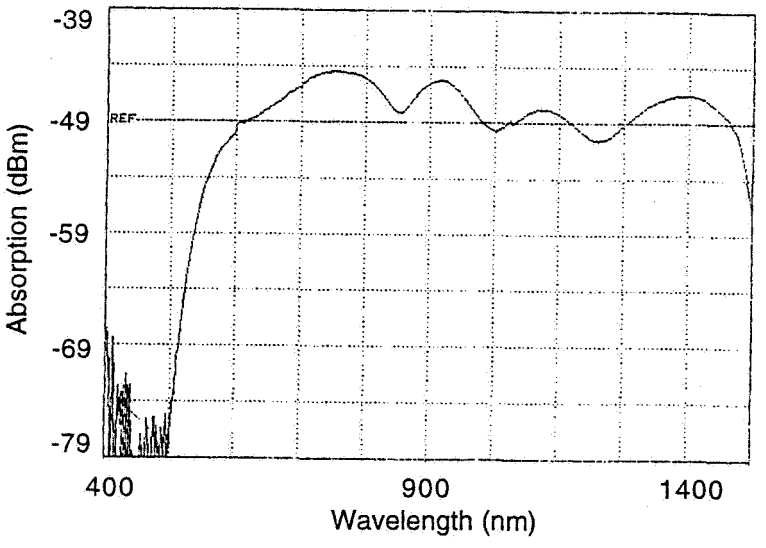

Figure AA-4
Absorption spectrum of the optrode labeled as Ames 8.

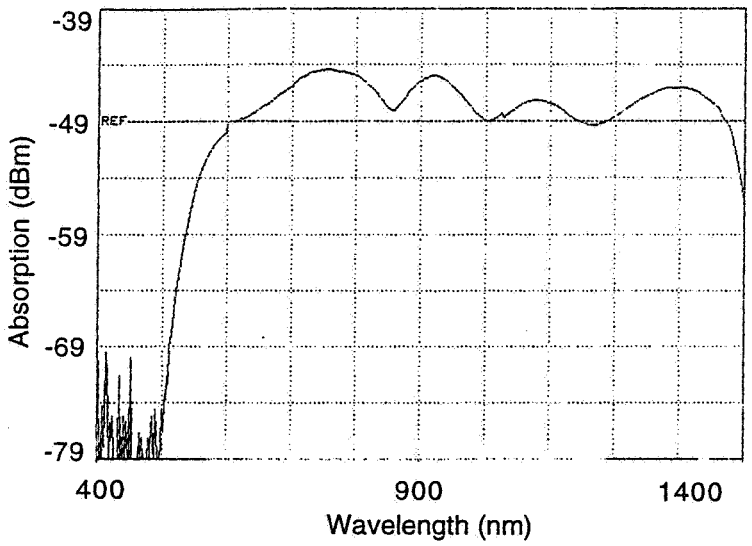

Figure AA-5
Absorption spectrum of the optrode labeled as Ames 10.

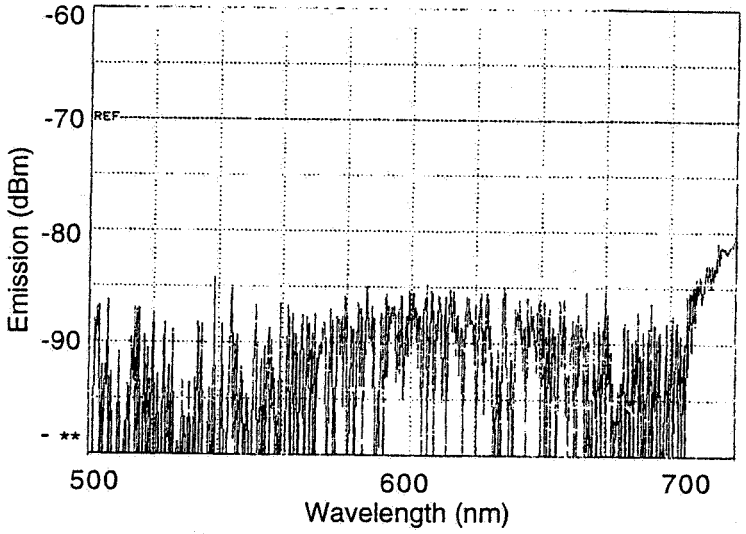

** Beyond range of instrument sensitivity

Figure AA-6
Absorption spectrum of the optrode labeled as Ames 1.

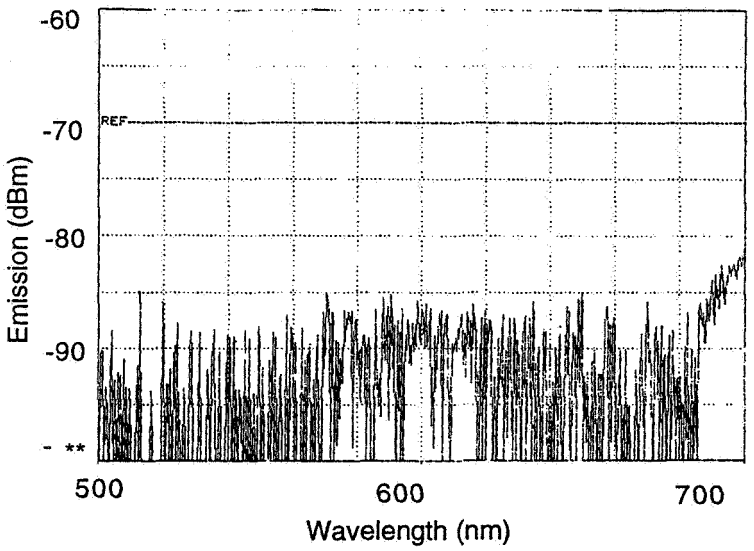

**Beyond range of instrument sensitivity

Figure AA-7
Emission spectrum of the optrode labeled as Ames 2.

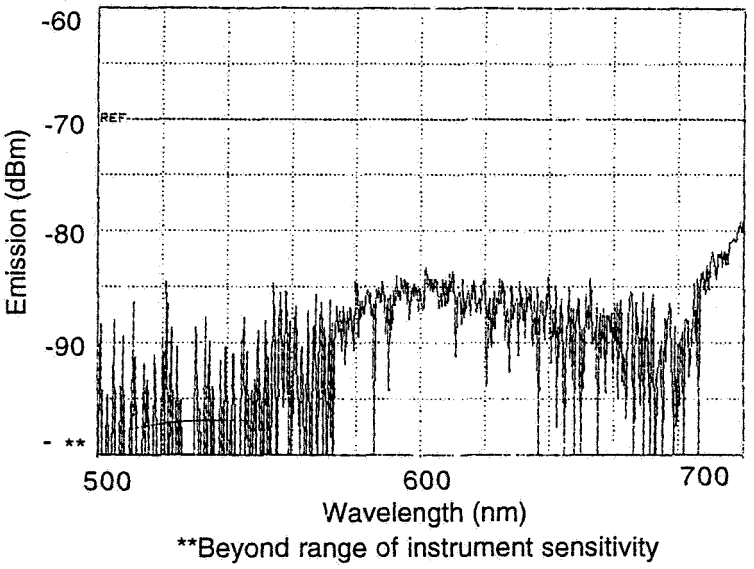

**Beyond range of instrument sensitivity

Figure AA-8
Emission spectrum of the optrode labeled as Ames 7.

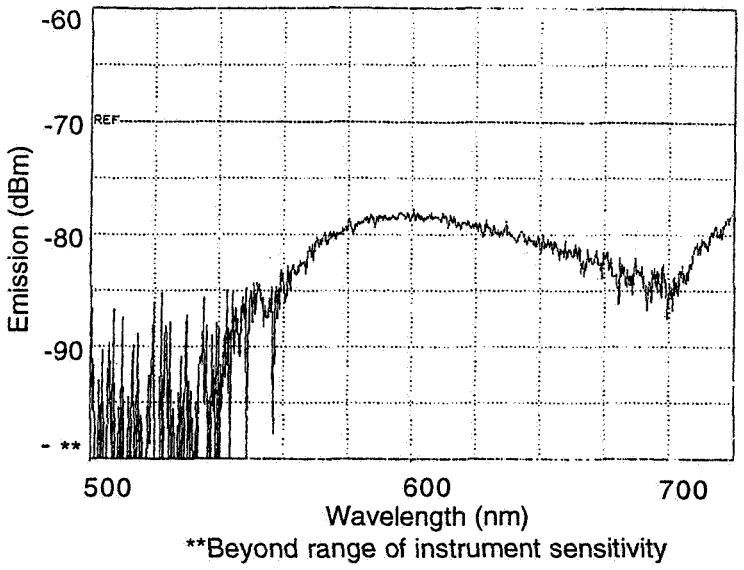

Figure AA-9
Emission spectrum of the optrode labeled as Ames 8.

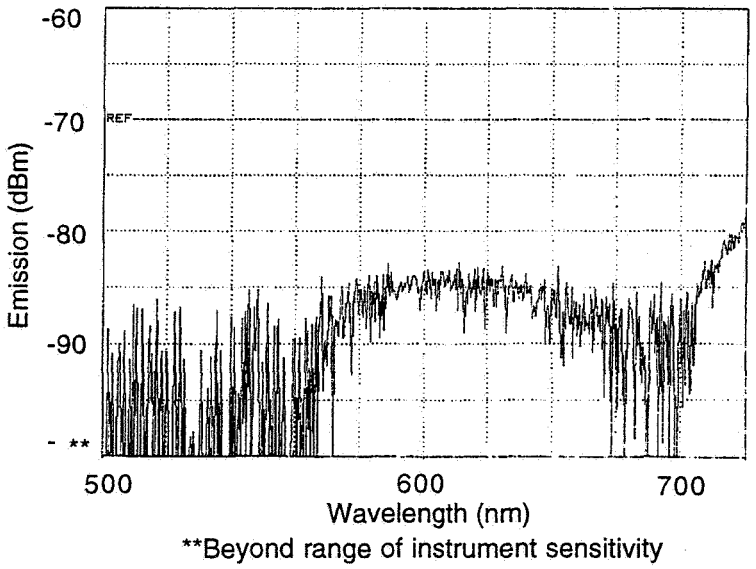

Figure AA-10
Emission spectrum of the optrode labeled as Ames 10.

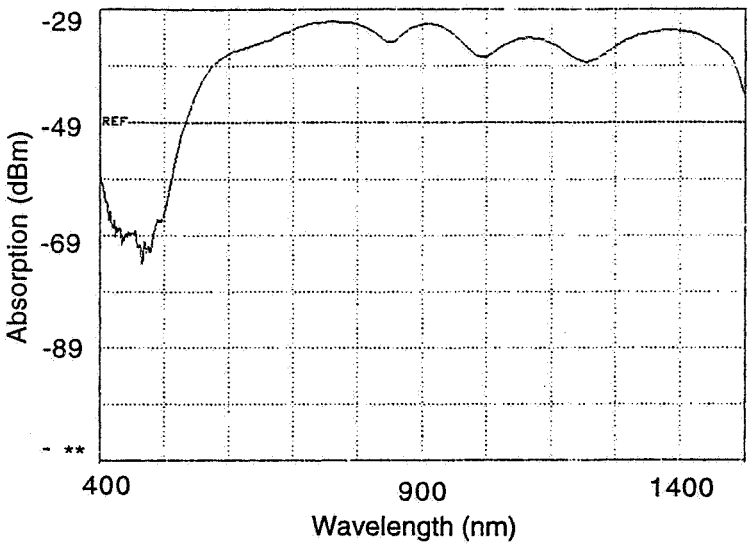

Figure AA-11
Absorption spectrum of the optrode labeled as Ames 1.

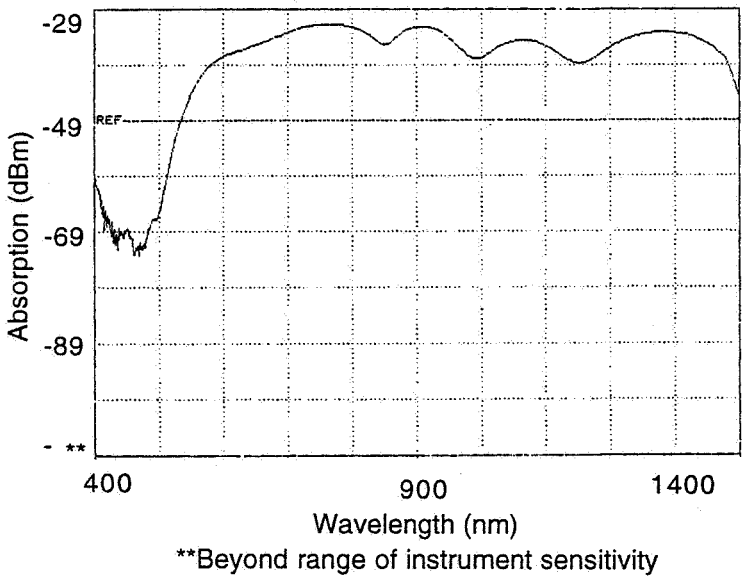

Figure AA-12
Absorption spectrum of the optrode labeled as Ames 2.

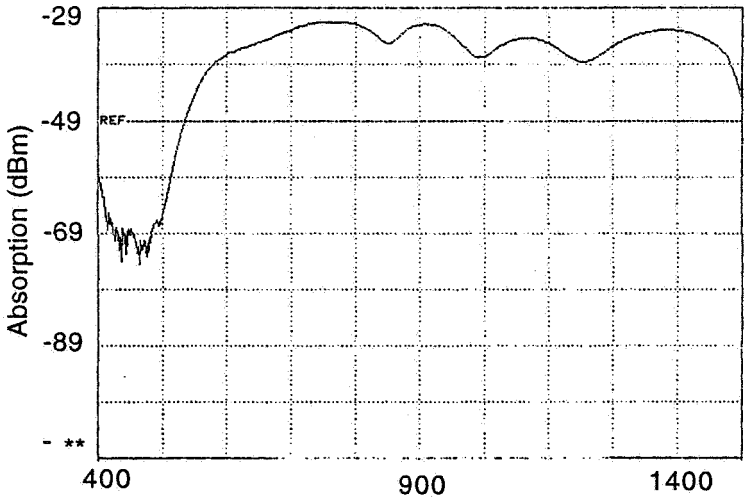

Figure AA-13
Absorption spectrum of the optrode labeled as Ames 7.

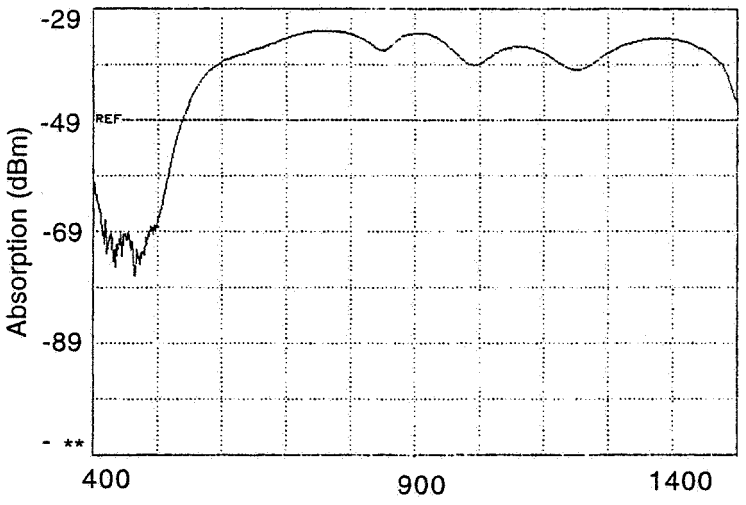

Figure AA-14
Absorption spectrum of the optrode labeled as Ames 8.

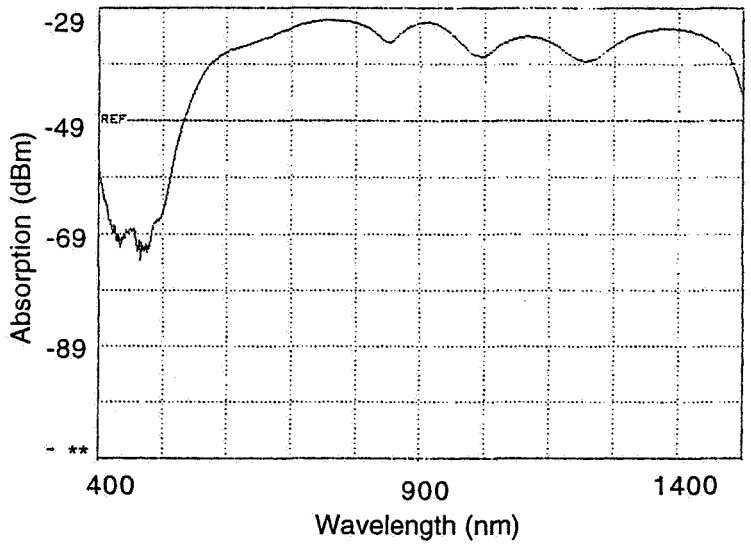

Figure AA-15
Absorption spectrum of the optrode labeled as Ames 10.

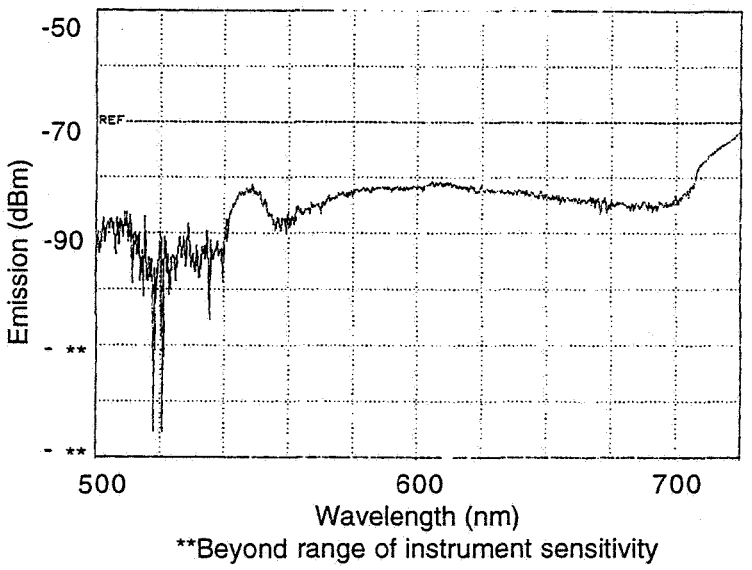

Figure AA-16
Emission spectrum of the optrode labeled as Ames 1.

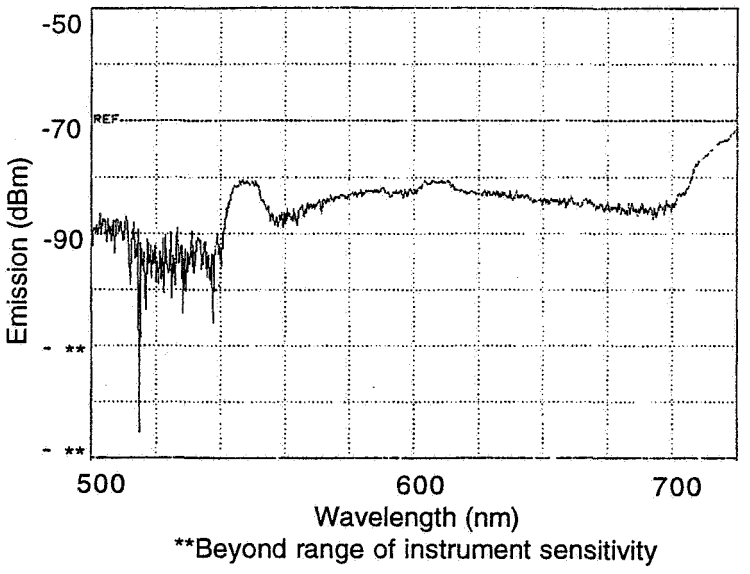

Figure AA-17
Emission spectrum of the optrode labeled as Ames 2.

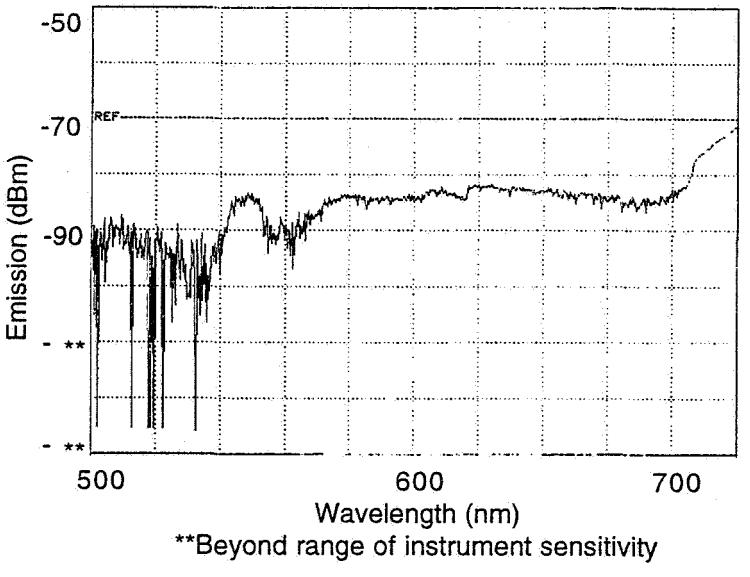

Figure AA-18
Emission spectrum of the optrode labeled as Ames 7.

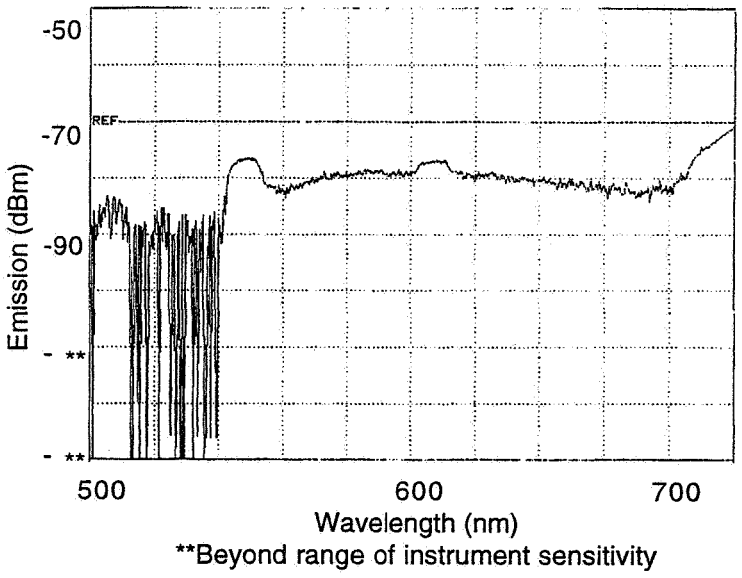

Figure AA-19
Emission spectrum of the optrode labeled as Ames 8.

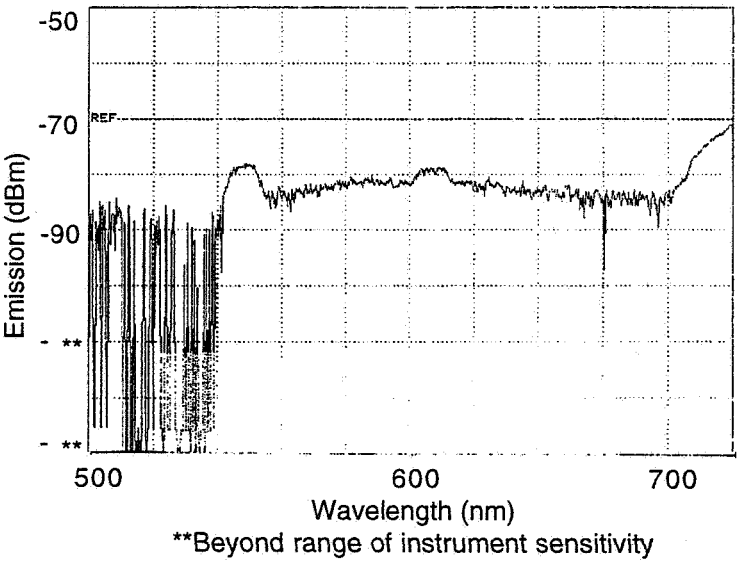

Figure AA-20
Emission spectrum of the optrode labeled as Ames 10.

NASA National Aeronautics and Space Administration

Report Documentation Page

1. Report No.	2. Government Accession No.	3. Recipient's Catalog No.

4. Title and Subtitle

Lightweight Fiber Optic Gas Sensor for Monitoring Regenerative Food Production

5. Report Date

December 18, 1995

6. Performing Organization Code

OAZ36

7. Author(s)

Edward Schmidlin, Kisholoy Goswami

8. Performing Organization Report No.

3238

10. Work Unit No.

9. Performing Organization Name and Address

Physical Optics Corporation, R&D Division
20600 Gramercy Place, Suite 103
Torrance, CA 90501

11. Contract or Grant No.

NAS2-13887

13. Type of Report and Period Covered

Final, 8/29/93 to 12/19/95

12. Sponsoring Agency Name and Address

NASA Ames Research Center
Moffett Field, CA 94035-1000

14. Sponsoring Agency Code

15. Supplementary Notes

N/A

16. Abstract

In this final report, Physical Optics Corporation (POC) describes its development of sensors for oxygen, carbon dioxide, and relative humidity. POC has constructed a phase fluorometer that can detect oxygen over the full concentration range from 0% to 100%. Phase-based measurements offer distinct advantages, such as immunity to source fluctuation, photobleaching, and leaching. All optics, optoelectronics, power supply, and the printed circuit board are included in a single box; the only external connections to the fluorometer are the optical fiber sensor and a power cord. The indicator-based carbon dioxide sensor is also suitable for short-term and discrete measurements over the concentration range from 0% to 100%. The optical fiber-based humidity sensor contains a porous core for direct interaction of the light beam with water vapor within fiber pores; the detection range for the humidity sensor is 10% to 100%, and response time is under five minutes. POC is currently pursuing the commercialization of these oxygen and carbon dioxide sensors for environmental applications.

17. Key Words (Suggested by Author(s))	18. Distribution Statement
Phase Fluorometer, Oxygen, Carbon Dioxide, Relative Humidity, Sol-Gel	Unlimited

19. Security Classif. (of this report)	20. Security Classif. (of this page)	21. No. of pages	22. Price
Unclassified	Unclassified	75	